Special Topics On Developed Miscibility

by

Nan Cheng, Msc

Dissertation

Presented to the Department of Petroleum Engineering and Applied Geophysics

Norwegian University of Science and Technology

in Partial Fulfillment

of the Requirements

for the Degree of

Doktor Ingeniør

Norwegian University of Science and Technology

October 2005

Special Topics On Developed Miscibility

Approved by
Dissertation Committee:

_____

_____

_____

_____

_____

To my parents who always encourage me throughout my life experience

Acknowledgments

It has been my good fortune to have had the opportunity of working with my supervisor Professor Curtis H. Whitson. I would like to express my sincerest gratitude to him for his excellent academic and professional guidance, stimulating discussions, and many invaluable suggestions and comments. It has been fascinating working with him.

I would like to thank Dr. Lars Hoier at Statoil Research Center in Trondhiem. He, together with Curtis, introduced me to the first research topic presented in this thesis. And the research results of his Ph.D work served as a starting point for me to carry out the research. During this research work, especially on the first topic, I have had many interesting and fruitful discussions with him. I greatly enjoyed working with him.

Sincere thanks to Professor Michael Golan for interesting discussions and valuable suggestions during my research. I also would like to thank the office staff at the Department of Petroleum Engineering and Applied Geophysics; they were always keen to help whenever needed.

Thanks to Pera staff engineers: Dr. Øivind Fevang, Dr. Tao Yang, Dr. Kameshwar Singh, Dr. Mohammad Faizul Hoda, and Dr. Knut G. Uleberg. I enjoyed and benefited a lot from working with them. It has been professionally rewarding to have worked with them.

I would like to acknowledge Norsk Hydro ASA for the financial support for three years and Pera AS for the last year funding for my Ph.D research.

Lackner Alf Sebastian and Sverre Gullikstad Johnsen have been my close friends at the department. I thank them for many interesting discussions and comments. I also

acknowledge their help on proof-reading of the thesis.

I would like to thank Logtek associate Robert Jorro for his help in proof-reading part of the thesis for improved readability.

Finally, I would like to thank my dear wife Youlin Yang and my son Larry Y. Cheng for their support. Without their understanding, support, and patience, it would not have been possible for me to accomplish.

NAN CHENG

Norwegian University of Science and Technology

October 2005

Contents

Special Topics On Developed Miscibility

Publication No. _____

Nan Cheng, Ph.D.

Norwegian University of Science and Technology, 2005

Supervisor: Curtis H. Whitson

This dissertation presents results of two closely related research topics on developed miscibility by gas injection in petroleum reservoirs. The first topic is a study on miscible gas injection in undersaturated compositionally grading gas-oil systems. The objective was to define a minimum miscibility pressure (MMP) for the fluid system as a whole – the *system* MMP. The results of this first topic are presented in Chapter 1. The second topic is a simulation study on modeling physical dispersion of one-dimensional (1D) multi-contact miscible processes by gas injection . The objective was to investigate the effect of oil saturation prior to gas injection on the development of miscibility in the presence of dispersion. Chapter 2 presents the research results of the second topic.

Each topic is summarized below.

Miscible Gas Injection in Undersaturated Gas-Oil Systems

A number of petroleum reservoirs exhibiting a compositional grading feature have been reported worldwide. The mole fraction of the lighter components decreases with depth, while the mole fractions of the heavier components increase from the top to the bottom of the reservoir. Some of these are saturated reservoirs with a distinct gas-oil contact (GOC)

separating the gas zone from the oil zone. Others are undersaturated reservoirs, of which the reservoir pressure is always higher than the saturation pressure of the fluid system at any depth. There exists no clearly-defined GOC in a normal sense in this type of reservoir. In this study, we decided to focus on miscible gas injection in undersaturated gas-oil reservoirs. Some of the results for conditions of reservoir pressure lower than fluid saturation pressure seem to have a general nature and are applicable to saturated fluid systems as well.

For an undersaturated compositional grading gas-oil reservoir, the fluid system exhibits a smooth and monotonic compositional variation with depth. From top to bottom, the reservoir fluids can vary from lean gases, rich gases, critical mixture, volatile oils, and black oils. The critical mixture marks the transition from reservoir gas to reservoir oil, thus defining the undersaturated "GOC". The saturation pressure of this mixture is a critical pressure at the reservoir temperature, which also is the maximum saturation pressure of the entire fluid system. A special feature of this type of reservoir is that the reservoir fluid is inherently first-contact miscible (FCM) with its neighboring fluids. For a one-dimensional flow, this implies that full pressure maintenance by up-structure gas injection should lead to miscibility throughout the system.

As is the case for miscible gas injection in constant composition petroleum reservoirs, MMP is one of the key operating parameters needed to be evaluated properly for miscible gas injection in undersaturated gas-oil reservoirs. Failure in predicting the system MMP for such a fluid system might lead to incorrect conclusions or incur unnecessary costs. Unlike the case for a constant composition system for which the MMP is constant for a specified injection gas at the reservoir temperature, the MMP varies with depth for an undersaturated reservoir and the MMP for the system as a whole is not obvious. Another complication occurs when the reservoir pressure has locally or entirely fallen below the saturation pressure. The MMP-depth relationship also will change as a function of the prevailing reservoir pressure. Though some reservoirs of this type have been produced by miscible or immiscible gas injection, no study exists addressing miscibility conditions for this type of reservoir on a generic scope. Therefore, a systematic study to define the system

MMP would be valuable.

Compositional reservoir simulation was used as the main tool in this study, assisted by a pressure-volume-temperature (PVT) program for the calculation of variations of fluid composition and MMP with depth. The data used in this study was based on the Smorbukk South field in the Norwegian Sea.

A step-by-step problem-solving approach was adopted in this research. We first studied the system MMP for full pressure maintenance. For partial pressure maintenance, we began with studying only part of the fluid system for MMP for simplicity and then extended for more complicated the entire fluid system.

In this study, we focused on defining the minimum miscibility pressure for the fluid system as a whole and the developed miscibility mechanisms. Extensive one-dimensional compositional simulations were performed to achieve the goal. Two-dimensional cross-sectional models also were simulated and analyzed to study the effects of layering and gravity segregation.

Results show that the system MMP for such a fluid system is limited between the shallowest condensing/vaporizing (C/V) MMP on the MMP-depth relationship and the maximum saturation pressure of the system when a condensing/vaporizing miscibility mechanism exists. This applies to injection gases somewhat enriched in intermediate components C_2 - C_5 or CO_2 so that the C/V mechanism can develop at some depth in the reservoir. When lean gas is injected and only a vaporizing gas drive (VGD) mechanism develops, the system MMP equals the maximum saturation pressure, the upper bound pressure for the system MMP.

For a 1D fluid system of this type, we also demonstrate that *any* injection gas can be used to achieve miscibility provided that the displacement pressure is maintained at or above the maximum saturation pressure of the fluid system (full pressure maintenance). It follows that the cheapest available injection gas is the optimum injection gas for full pressure maintenance. This might be rather different from what one usually expects for miscible gas injection in such an undersaturated gas-oil system.

Another key contribution has been the finding that once an injection gas develops a C/V mechanism and a miscible leading-edge oil bank, the oil bank will miscibly displace any downstream oil. We also found that the C/V oil bank can develop at low pressures but at a reduced scale at immiscible conditions, when the C/V mechanism exists. It is believed that these conclusions are general, not restricted to undersaturated gas-oil systems.

The combination of these two findings might represent a great potential for improving oil recovery by enriched gas injection for two-phase hydrocarbon reservoirs in general. With the help of gravity, the oil saturation, which is below the critical oil saturation prior to gas injection, will build up and the oil might gain mobility. Thus, the oil can be mobilized and recovered. In this process, the developed oil bank functions as an injected liquefied natural gas (LNG) slug, but developed at lower costs. This might particularly be favorable for high vertical permeability and high structural relief reservoirs.

Most of the results for the first topic have been presented in the following paper, included as Appendix A:

Hoier, L., Cheng, N. and Whitson, C.H.: "Miscible Gas Injection in Undersaturated Gas-oil Systems," paper SPE 90379 presented at the 2004 Annual Technical Conference and Exhibition, Houston, Texas, 26 – 29, September 2004.

Modeling Physical Dispersion of 1D Multi-Contact Miscible Processes

Physical dispersion represents one of the major concerns in miscible gas injection, chemical flooding, and tracer tests in petroleum reservoirs. It results in dilution of injectant concentrations and even the loss of the designed miscibility, thus potentially leading to the failure of the miscible gas injection project. For field-scale applications, the effect of physical dispersion might not be important because the dispersive front usually is small relative to the distance between the injector and the producer. For lab-scale gas floods, however, it can be crucial.

Under the influence of physical dispersion, the minimum miscibility pressure is no longer a pure thermodynamic property of the reservoir oil for the injection gas at the reser-

voir temperature. In addition, it will be affected by flow parameters such as fluid mobility or relative permeability. To what extent the minimum miscibility conditions are affected by the level of oil saturation which affects fluid mobility in the presence of dispersion is still an open question and has yet to be addressed in the literature. The effect might be important for designing miscible gas floods for gas condensate reservoirs and for oil reservoirs at the tertiary development phase, where the oil saturations usually are low prior to gas injection.

Based on analysis of Lantz's equation for quantifying numerical dispersion, we have proposed an equation for determining number of grid cells and time-step size to emulate physical dispersion by numerical dispersion for simulating first-contact miscible processes. The proposed method was verified by fine grid simulations and analytical calculations for 1D single phase flow. Simulation using the proposed method of selecting the grid cell and time-step sizes reproduces the results of fine grid simulations and analytical calculations and requires only one-tenth of the computing time of the fine grid simulation runs.

1D compositional simulations were conducted to study the effect of oil saturations prior to gas injection on the development of multi-contact miscibility with the presence of dispersion. Models were initialized with different levels of oil saturation with the presence of different degrees of emulated dispersion.

Through simulation, we have demonstrated that when dispersion is included, the miscibility conditions are affected by oil mobilities, besides the compositions of the oil and the injection gas and the reservoir temperature. Results show that, at a realistic dispersivity level, miscibility can be achieved when the oil saturation prior to gas injection is high but it might never develop at all if the oil saturation is too low.

Chapter 1

Miscible Gas Injection in Undersaturated Gas-Oil Systems

1.1 Introduction

A number of petroleum reservoirs have been reported [1–9] worldwide exhibiting continuous compositional variations with depth. The mole fraction of the lighter components decreases with depth, while the mole fractions of the heavier components increase from the top to the bottom of the reservoir. These reservoirs usually are called compositionally grading petroleum reservoirs. Compositionally grading gas-oil reservoirs can be either undersaturated or saturated, depending on the relationship between the reservoir pressure and the maximum saturation pressure of the reservoir fluids.

For a saturated compositionally grading gas-oil system, the reservoir pressure is equal to the saturation pressure of the fluid at the gas-oil contact.

For an undersaturated compositionally grading gas-oil reservoir, the reservoir pressure is greater than the saturation pressure of the fluid at any depth. The fluid at the GOC is neither an oil nor a gas, but a critical mixture. The saturation pressure of this mixture is the critical pressure at the reservoir temperature and also is the maximum saturation pressure of the entire fluid system. A special feature of this type of reservoir, first pointed out

by Schulte [1] in 1980, is that the reservoir fluids are initially first-contact miscible with their neighboring fluids for 1D flow. Therefore, up-structure gas injection in such a 1D system should lead to 100% oil recovery if the reservoir pressure is maintained above the maximum saturation pressure of the system.

Miscible gas flooding projects normally require extra investments if the reservoir pressure needs to be maintained or the injection gas needs to be enriched. Consequently, to optimize the economy of the project, miscible gas injection strategy will always be compared with less costly immiscible gas injection. It is therefore crucial to be able to quantify accurately the improved oil recovery potential by miscible gas flooding.

This chapter presents a study on miscible gas injection in an undersaturated compositionally grading gas-oil reservoir. The objective of this study was to define the miscibility conditions for the fluid system as a whole and to investigate the possibility of developing miscibility at pressures lower than the maximum saturation pressure by enriched gas injection. The fluid data used in this study was based on the Smorbukk South field in the Norwegian Sea.

Compositional reservoir simulation was the main tool used in this study. In addition, a PVT simulator was used to calculate fluid compositions and minimum miscibility pressure (MMP) values for a specified injection gas.

One-dimensional numerical models were built to simulate the miscibility conditions and the developed miscibility mechanisms. Numerical dispersion involved in the numerical simulations was eliminated following a conventional procedure [10] – linear extrapolation of recoveries at 1.2 hydrocarbon pore volumes (HCPV) injected for dispersion-free recovery estimates. The number of grid cells used in these simulations generally ranged from 500 to 5000. In some cases, 50000 grid cells were used.

Different injection gases were injected at different pressures. Particular effort was made to define system MMP for enriched gas (e.g. separator gas) injection, when the reservoir pressure has locally fallen below the maximum saturation pressure and a two-phase region has formed in the reservoir. For enriched gas injection, the predominant

miscibility mechanism is multi-contact condensing/vaporizing miscibility. It requires a very fine grid to model it properly.

Two-dimensional (2D) x-z cross-sectional models were used to investigate the effects of layering and gravity segregation on oil recoveries. Two- and eight-layer numerical models were created and used to simulate gas injection at pressures above the maximum saturation pressure of the fluid system. Production performance was analyzed.

Section 1.2 reviews important concepts such as miscibility and condensing/vaporizing mechanism relevant to this research. It also describes the variations of fluid composition and MMP with depth for the undersaturated gas-oil fluid system used in this study, which are typical variations for any undersaturated gas-oil reservoir.

Section 1.3 outlines the key problem investigated in this research: the determination of the system MMP and the possibility of achieving miscibility at pressures lower than the maximum saturation pressure by enriched gas injection. This problem needs to be addressed for gas injection in any undersaturated gas-oil system. Literature review indicated that this problem has not been addressed and studied systematically for this type of reservoir.

Section 1.4 describes the reservoir fluid model and presents the compositions of injection gases, separator conditions, a relative permeability model, and well constraints applied in the simulations.

Full pressure maintenance simulation results are presented in Section 1.5. Different injection gases were used in these simulations. We also studied the effect of formation dip angle on oil recovery for full pressure maintenance.

Section 1.6 presents simulation results for partial pressure maintenance by enriched gas injection, which represents another development scenario for miscible gas injection. This is the most important section addressing the problem outlined in Section 1.3. Different injection gases and different injection depths were simulated and analyzed in this section.

The dynamic nature of the system MMP is discussed in Section 1.7. MMP calculated by a PVT program offers a fast first-order approximation; the lower and the upper

limits of system MMP can be defined based on these calculations. To determine the system MMP, numerical simulation must be used to capture the dynamic change in miscibility pressures. Potential risk also is discussed particularly for reservoirs with a big gas cap and a small oil rim.

Section 1.8 presents simulation results for 2D x-z two- and eight-layer models. The effect of strong layer permeability contrast and the importance of gravity segregation is discussed in this section.

1.2 Background

This section presents necessary background knowledge for understanding miscible gas injection recovery processes and describes typical features of undersaturated gas-oil systems. The concept of minimum miscibility conditions is reviewed and the most common miscibility mechanism encountered in field operations is described. A brief review on the determination of MMP is also included.

As this study was conducted for an undersaturated gas-oil system, we felt it was necessary to present fluid characteristics of a typical undersaturated compositionally grading fluid system. Fluid composition variations with depth and the condition of reservoir pressure exceeding saturation pressures define an undersaturated gas-oil reservoir. MMP variations with depth are the direct consequences of composition variations with depth. For different injection gases, the variations of initial MMP with depth and miscibility mechanisms can be different.

1.2.1 Minimum Miscibility Conditions

The definition of minimum miscibility conditions can be defined as follows:

The minimum conditions at which the resulting mixture of two fluids mixed together at any proportion is homogeneous in compositions and identical in intensive properties (e.g. density and viscosity).

For reservoir engineering, as the reservoir temperature usually is assumed to be constant, the minimum miscibility conditions refer to either the minimum miscibility pressure (MMP) when compositions of the two fluids are fixed, or the minimum miscibility enrichment (MME) when the oil composition and the reservoir pressure are specified. In this thesis, the minimum miscibility conditions always refer to the minimum miscibility pressure as we have specified the compositions of reservoir fluids and injection gases at a constant reservoir temperature.

When two fluids are fully miscible, there exists no fluid interface between these two fluids and their interfacial tension (IFT) is zero. Consequently, capillary forces between them vanish. If a reservoir oil is fully miscible with an injection gas at the minimum miscibility conditions, in the absence of any dispersion, the residual oil saturation behind the injection gas front is expected to be zero and the microscopic oil recovery is expected to be 100%.

A number of parameters affect the minimum miscibility conditions: including chemical compositions of the oil and the injection gas, and the reservoir temperature. It is also believed that physical dispersion can locally have some impact on the minimum miscibility conditions. This might particularly be of concern for lab-scale studies.

The process of achieving miscibility at the minimum miscibility conditions can be different, depending on the compositions of the displacing and displaced fluids and the reservoir temperature. Some fluids may become miscible upon the first contact; the process is called first-contact miscible. Some fluids are not first-contact miscible, but can achieve miscibility through continuous contact by interphase mass transfer. These fluids are multi-contact miscible. For hydrocarbon reservoirs, the multi-contact miscible process usually is the common one occurring in actual field operations.

Different multi-contact miscible mechanisms have been proposed and studied in the literature [11, 12] based on the nature of compositions of the two fluids and pressure and temperature: vaporizing gas drive (VGD), condensing gas drive (CGD) and condensing/vaporizing gas drive (C/V). We decided not to discuss the VGD and CGD mechanisms

as those have been extensively discussed in the literature and the CGD mechanism might seldom happen [13] in actual petroleum reservoirs. Only the condensing/vaporizing mechanism is briefly reviewed as it is directly relevant to this research.

1.2.2 Condensing/Vaporizing Miscibility Mechanism

The condensing/vaporizing gas drive for enriched gas injection was first proposed and verified by experiments and numerical simulations by Zick [13] in 1986. Interphase mass transfer of the intermediate components is the key process of the mechanism. Later, analytical theory [14] for the combined condensing/vaporizing mechanism was developed. It can be argued that condensing/vaporizing gas drive is the most common mechanism developed in miscible gas injection field projects as injection gases usually contain somewhat light- and heavier-intermediate components.

A typical condensing/vaporizing gas drive shows the following characteristics:

1. Development of a miscible front characterized by converged phase densities and other intensive fluid properties. Interfacial tension at the front is extremely low and this is the direct indication of achieved miscibility.

2. Two regions identified on each side of the miscible front. The region upstream of the miscible front is dominated by strong vaporization of heavy components of the reservoir oil. The region downstream of the miscible front is strongly dominated by condensation of intermediate components of the injection gas.

3. Component K-values (ratio of composition of the component in vapor phase to the composition of the component in the liquid phase) tend to converge at the near miscible front and then diverge downstream.

It has been reported that miscible displacement of oils and/or gas condensates can develop through a condensing/vaporizing mechanism at a pressure far below saturation pressure if the injection gases are sufficiently rich in intermediate components [15] or

CO_2 [16]. For saturated oil reservoirs or depleted gas condensate reservoirs, if the C/V mechanism exists and an oil bank develops at and above the C/V minimum miscibility conditions, the oil saturation behind this front approaches zero. The formation and development of the oil bank was first demonstrated by Hoier and Whitson [17] through numerical simulations, and later proved by Jessen and Orr [18] based on method of characteristics (MOC). It also was found that the C/V MMP is dictated by the composition of the retrograde condensate [15] or the reservoir oil for a specified injection gas.

It is worth pointing out that the condensing/vaporizing mechanism can exist for enriched gas injection at pressures lower than the C/V MMP, though the fluids are not near-miscible. The oil bank will still develop but at a reduced scale. For a depleted gas condensate reservoir, this implies the retrograde condensate might gain enough mobility to flow to the producer due to the developed oil bank by enriched gas injection at low pressures. For a water-flooded oil reservoir, the residual oil might still be recoverable if a C/V oil bank can be developed by enriched gas injection. In this sense, the developed oil bank can function as a miscible (miscible with the downstream immobile oils) slug, which usually is required for miscible displacement by a liquefied natural gas (LNG) slug. Candidates for enriched gas injection at low pressures might be reservoirs (depleted gas condensate and oil reservoir) with high structure relief and high vertical permeability, making use of gravity and the developed oil bank.

1.2.3 Determination of MMP

A number of methods for determining MMP are available in the literature, such as slimtube experiment [19], multi-cell algorithm [20–22], single cell forward- and backward-contact algorithms [23], slimtube-type compositional numerical simulation, and analytical method based on method of characteristics [24, 25]. Rising bubble apparatus [26] has also been suggested as an alternative to slimtube experiment. Several investigators [12, 27] have expressed their skepticism about the capability of determining MMP of a condensing/vaporizing mechanism.

The slimtube experiment is considered to define an unbiased MMP if designed, conducted, and interpreted properly. This method usually is expensive and time-consuming. Alternatively, 1D slimtube-type numerical simulations can be used to evaluate MMP or MME. This method usually is faster but requires a properly tuned equation of state (EOS) model capable of modeling the important phase behavior, such as swelling test, forward- and/or backward-contact experiments and MMP experiment. In this study, MMP values were calculated either by a PVT program or by 1D numerical simulations using a fine-tuned EOS model.

An inherent problem with 1D numerical simulations for defining a MMP is numerical dispersion, which can have a strong influence on the development of miscibility, oil recovery, and thus on the MMP estimate. For gas condensate systems in particular, a large number of grid cells usually are required to provide recoveries that can be reliably extrapolated for a dispersion-free result [15]. The C/V mechanism might not be properly captured if too few grid cells are used in the simulations and the MMP might be erroneously overestimated.

Dispersion-free MMP is a thermodynamic property of the reservoir oil for a specified injection gas at a reservoir temperature and is independent of flow parameters such as fluid mobilities. In this chapter, MMP refers to dispersion-free MMP. When dispersion is included, we found that MMP also is affected by oil saturations prior to gas injection. Simulations, performed at the displacement pressure equal to the dispersion-free MMP, show that when the oil saturation prior to gas injection was too low and physical dispersion was included, the C/V mechanism might never develop during the displacement. This issue is addressed in Chapter 2.

1.2.4 Compositionally Grading Gas-Oil System

Due to various reasons, e.g. gravitational and thermal effects, some petroleum reservoirs, particularly those with thick pay zones, exhibit fluid compositional variations with depth [4, 28]. From the reservoir top to bottom, the molecular weight of the hydrocarbon fluids

increase with depth; the fluids are progressively heavier in density and lower in GOR. The top structure fluids may be reservoir gases and at some depth downward the reservoir fluids may exist as liquids. The reservoir can be either saturated with a clearly defined GOC or undersaturated transforming from reservoir gases, critical fluid, to reservoir oils without discontinuity in compositional grading.

For an undersaturated compositionally grading gas-oil reservoir, the "undersaturated GOC" describes the phase transition from dewpoint gases to bubblepoint oils at a depth where a "critical" mixture is located. The "critical" GOC mixture has a saturation pressure equal to its critical pressure at the reservoir temperature. The critical pressure also marks the maximum saturation pressure of the entire fluid system, but it is still lower than the reservoir pressure at the GOC depth for an undersaturated gas-oil system.

Fluids of this type of reservoir can often be modeled relatively accurately using an isothermal gravity/chemical equilibrium (GCE) model [4]; other potentially important effects such as thermal diffusion or thermal convection[1] might often be neglected. Chaback [29] argues that thermal effects are small relative to gravity/chemical effects in the vicinity of the critical point.

An undersaturated gas-oil system modeled by the isothermal GCE exhibits the following typical characteristics.

1. Monotonic and continuous changes in fluid compositions (e.g. C_{7+} content) and intrinsic properties such as density and viscosity, as shown in Figures 1.1 and 1.2.

2. Largest changes in fluid properties occur at the depth of the undersaturated GOC.

3. Dewpoint pressures of gases in the gas zone increase with deepening depth; bubblepoint pressures of oils in the oil zone decrease with deepening depth. The maximum saturation pressure is the critical pressure of the GOC mixture, shown in Figure 1.3.

4. Reservoir pressure at any depth is always higher than the saturation pressure of the

[1] Our experience has been that naturally fractured petroleum reservoirs have a much greater tendency to experience thermally-induced convection than conventional reservoirs.

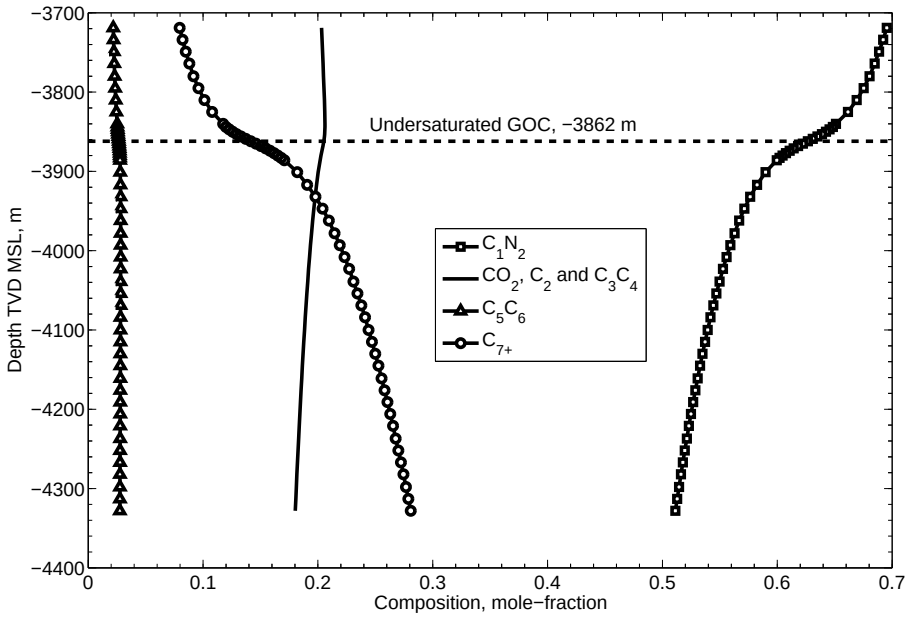

Figure 1.1: EOS calculated composition variations with depth for Smorbukk South field using isothermal gravity/chemical equilibrium (GCE) model. Greatest composition changes are in C_{7+} and C_1N_2 contents.

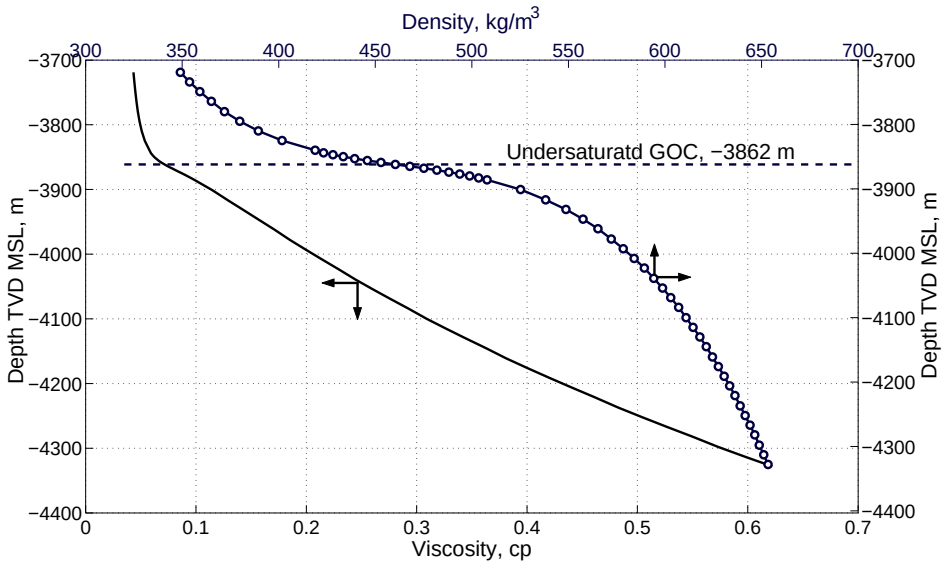

Figure 1.2: EOS calculated phase density and viscosity variations with depth at reservoir conditions using isothermal gravity/chemical equilibrium (GCE) model. Great changes in these properties occur in the vicinity of the undersaturated GOC depth.

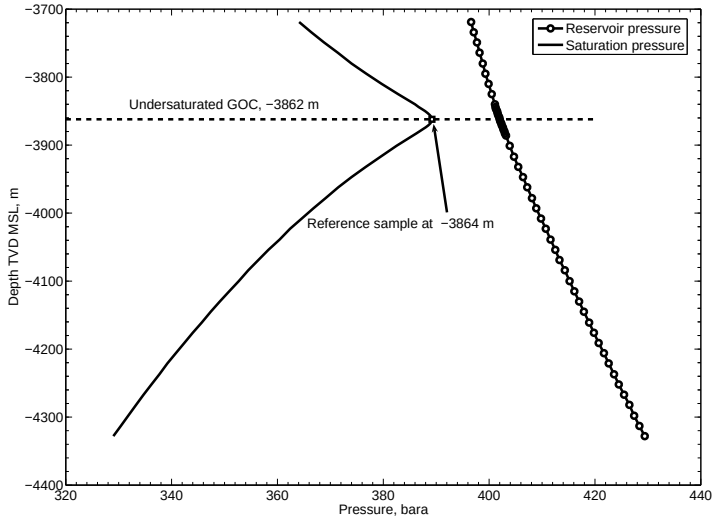

Figure 1.3: EOS calculated pressure and saturation pressure variations with depth using isothermal gravity/chemical equilibrium (GCE) model. Dewpoint pressures increase with depth in the gas zone; bubblepoint pressures decrease with depth. The maximum saturation pressure is the critical pressure of the GOC mixture. Reservoir pressure is greater than saturation pressure at any depth.

fluid at the same depth, as shown in Figure 1.3.

1.2.5 MMP Variations with Depth

MMP variations with depth[2] are the direct consequences of composition variations with depth. The MMP variations with depth can be calculated by combining the isothermal gravity/chemical equilibrium (GCE) gradient calculations and a robust MMP algorithm, e.g. Zick multicell algorithm [30]. For a fluid at a given depth, the isothermal gradient calculations provide the composition, reservoir pressure, and saturation pressure of the fluid. The MMP algorithm then makes use of the calculated composition and determines the MMP for a given injection gas at the reservoir temperature. These calculations are repeated for a series of fluids at different depths and injection gases, generating a static[3]

[2]Depth in this thesis always refers to true vertical depth (TVD) measured from the mean sea level (MSL).

[3]static means that the MMP is calculated assuming that the injection gas is directly in contact with the initial reservoir fluid at the local depth, neglecting any interference in composition from above/below fluids

map of MMP with depth [17].

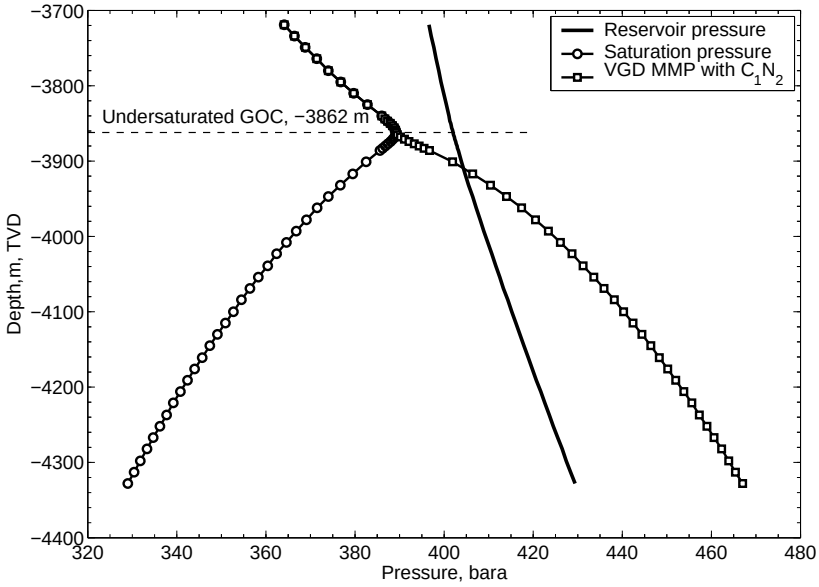

Figure 1.4: VGD MMP versus depth for C_1N_2 injection gas. MMP equals dewpoint pressure in the gas zone, and greater than bubblepoint pressure in the oil zone.

This methodology was applied to calculate MMP variations with depth for the undersaturated gas-oil system shown in Figure 1.3 and used in this study. Gravity and capillary forces were neglected for the MMP calculations.

Figure 1.4 shows MMP calculation results for a dry injection gas C_1N_2. For this injection gas, the miscibility was developed by a pure vaporizing gas drive (VGD) mechanism at all depths. The VGD MMP equals the dewpoint pressure of the gas in the gas cap, and exceeds the bubblepoint pressure of the oil in the oil zone.

For an enriched injection gas, the VGD miscibility mechanism might exist *only* in the upper part of the gas zone. Approaching the undersaturated GOC, as the reservoir gases become richer in intermediate and heavier components, the C/V mechanism might develop. Figure 1.5 shows the calculated MMP values for the fluid system used in this study for a separator gas (denoted by SepGas, with composition shown in Table 1.6). A condensing/Vaporizing mechanism started to develop for a reservoir gas at the depth of

during flow.

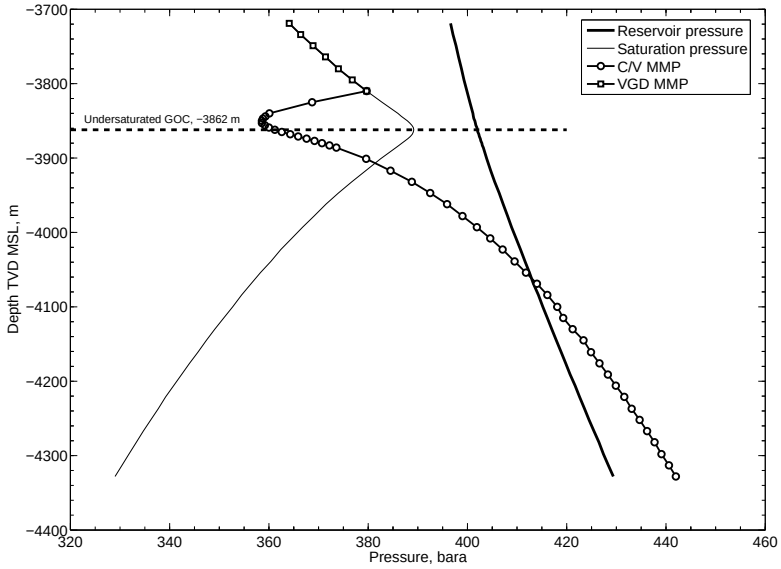

Figure 1.5: MMP versus depth for the separator gas (SepGas) calculated using an EOS-based PVT simulator. In the upper part of the gas zone, VGD MMP exists. In the lower part of the gas zone and in the oil zone, C/V MMP presents. Lowest C/V MMP is found close to the undersaturated GOC.

-3810 m. C/V MMP for the separator gas increases gradually with depth in the oil zone. If the injection gas is further enriched, VGD mechanism might disappear and only C/V mechanism exists for all the fluids. For an undersaturated gas-oil system predicted with the isothermal GCE model, it is found that this is characteristic for MMP variations with depth [17]. If the C/V MMP exists in part of the gas cap, the *minimum* C/V MMP usually is found close to (at or slightly above) the undersaturated GOC. Note that C/V MMP of fluids in the vicinity of the undersaturated GOC can be lower than the saturation pressure.

1.3 Problem Statement

For a given injection gas, the minimum miscibility pressure needed for a miscible displacement is one of the key parameters in designing a miscible flood. MMP is directly related to the added costs and the profits of the project. Failure in predicting the minimum reservoir

pressure required for miscible displacement might lead to the failure of the project or incur unnecessary costs.

MMP for an oil reservoir of constant composition can be determined by different methods as mentioned in Subsection 1.2.3. A PVT simulator using a well-tuned EOS model can usually define a fairly accurate MMP for an injection gas. For miscible gas injection in an undersaturated compositionally grading fluid system, however, the MMP for the system as a whole is not obvious. Neither the maximum MMP nor the minimum MMP of the fluid column is necessarily the system MMP.

For designing a miscible gas flood for a reservoir showing a significant compositional gradient, one of the most important questions is:

What should be the minimum miscibility pressure for the success of a miscible flood for a given injection gas?

As mentioned in Subsection 1.2.5, static MMP values of the reservoir fluids can be readily determined by combining GCE gradient calculations and an MMP algorithm. The calculated MMP values are based on the assumption that the injection gas is directly in contact with the initial reservoir fluid at a specified depth, neglecting any possible interference in composition from up- and/or down-structure fluids. In fact, this assumption might not hold as all the fluids are firstly in contact with their neighboring fluids and the fluid at a depth might potentially be altered in composition by its upstream neighboring fluid due to pressure change and flow. Consequently, this will result in change in MMP. Therefore, the system MMP cannot be defined solely based on the calculated initial MMP versus depth.

Numerous reservoirs exhibiting compositional gradient at undersaturated conditions have been reported in the literature. To our knowledge, no systematic study on determining the system MMP for this type of reservoir exists. The difficulty of defining the system MMP lies in the fact that the MMP of reservoir fluids change with both depth and *pressure*. In this research work, we focused on the system MMP conditions and in particular on the possibility of developing a fully miscible displacement at pressures lower than the GOC saturation pressure by enriched gas injection.

The approach to this problem has been numerical compositional simulation assisted by a PVT program for calculating static MMP values for a specific injection gas. Sensor [31] , a generalized three-dimensional (3D) numerical reservoir simulator was used in this study. PhazeComp [30], an EOS-based PVT simulator, was used to calculate variations of fluid composition and MMP with depth. Extensive compositional simulations were conducted for 1D slimtube type models and the key focus was on system MMP and the developed miscibility mechanisms. We believe that the results from 1D simulations are general and applicable to any reservoir of this fluid type for 1D flow, as the 1D slimtube type models did not bear any case-dependent features.

1.4 Description of Simulation Models

This section describes the reservoir simulation models used in this study. The reservoir fluid model, the composition of injection gases, the relative permeability model, and the well constraints are presented in each subsection.

Table 1.1: PARAMETERS OF THE NINE-COMPONENT SRK EOS MODEL.

N_c	P_c bara	Tc °K	MW	Z_c	AF	V-SHIFT	PCHOR	Ω_a	Ω_b
CO_2	73.74	304.12	44.01	0.27433	0.2250	0.2175	70.00	0.427480	0.08664
C_1N_2	45.80	189.54	16.15	0.28615	0.0114	-0.0929	76.67	0.430146	0.08649
C_2	48.72	305.32	30.07	0.27924	0.0990	-0.0473	108.00	0.427480	0.08664
C_3C_4	40.38	390.88	49.08	0.27847	0.1704	0.0989	163.46	0.416082	0.08579
C_5C_6	33.76	488.34	76.69	0.27011	0.2403	0.1221	247.40	0.425933	0.08568
C_7C_9	32.99	553.69	105.88	0.26700	0.2589	0.0116	328.73	0.427480	0.08664
$C_{10}C_{13}$	25.92	636.75	151.74	0.2600	0.3782	0.0517	450.87	0.427480	0.08664
$C_{14}C_{29}$	19.55	739.70	247.89	0.28594	0.5734	0.0095	672.77	0.422410	0.08607
C_{30+}	10.16	918.17	483.14	0.35542	1.1570	0.2299	1058.41	0.427480	0.08664

Table 1.2: BINARY INTERACTION PARAMETERS OF THE SRK EOS MODEL.

	CO_2	C_1N_2	C_2	C_3C_4	C_5C_6	C_7C_9	$C_{10}C_{13}$	$C_{14}C_{29}$	C_{30+}
CO_2	0.00000	0.18110	0.15000	0.15000	0.15000	0.15000	0.15000	0.15000	0.15000
C_1N_2	0.18110	0.00000	-0.00152	-0.00947	-0.02057	0.00150	0.00160	0.00173	0.03510
C_2	0.15000	-0.00152	0.00000	0.00000	0.00000	0.00000	0.00000	0.00000	0.12766
C_3C_4	0.15000	-0.00947	0.00000	0.00000	0.00000	0.00000	0.00000	0.00000	0.09202
C_5C_6	0.15000	-0.02057	0.00000	0.00000	0.00000	0.00000	0.00000	0.00000	0.06236
C_7C_9	0.15000	0.00150	0.00000	0.00000	0.00000	0.00000	0.00000	0.00000	0.05223
$C_{10}C_{13}$	0.15000	0.00160	0.00000	0.00000	0.00000	0.00000	0.00000	0.00000	0.04350
$C_{14}C_{29}$	0.15000	0.00173	0.00000	0.00000	0.00000	0.00000	0.00000	0.00000	-0.03296
C_{30+}	0.15000	0.03551	0.12766	0.09202	0.06236	0.05223	0.04350	-0.03296	0.00000

Table 1.3: COEFFICIENTS OF THE LBC VISCOSITY MODEL.

a_0	a_1	a_2	a_3	a_4
0.1	0.023364	0.0250939	-0.0081516	0.00186648

1.4.1 Reservoir Fluid Model

The reservoir fluid model[4] used in this study was a nine-component Soave-Redlich-Kwong (SRK) [32] equation of state fluid characterization and a Lohrenz-Bray-Clark (LBC) [33] viscosity model. C_{7+} heavy components were split into four pseudo-components. Tables 1.1 and 1.2 give the nine-component EOS fluid characterization and Table 1.3 shows the coefficients of the LBC viscosity model used in study.

First, a detailed 15-component EOS model was developed for characterizing the reservoir fluids of the Garn formation of Smorbukk South field. It was tuned to match key PVT data from more than 30 PVT reports from the field, ranging from measurements on lean gas condensates, near-critical fluids, to volatile oils sampled at different depths. The PVT data was mainly from conventional depletion type PVT experiments, such as constant composition expansion (CCE), differential liberation expansion (DLE), and constant volume depletion (CVD) tests. It also included viscosity measurements, four multi-stage separator experiments, one MMP experiment, and one revaporization experiment.

The 15-component EOS model was pseudoized to nine components following the

[4]This fluid model was the result of an independent study for Smorbukk South field performed by Pera in 2003.

techniques given by Hearn and Whitson [34]. The resulting nine-component EOS model provided a satisfactory description of all the important PVT data, including saturation type and volumetric behavior in the near-critical region.

Table 1.4: REFERENCE OIL SAMPLE CONDITIONS.

N_c	Composition mole-fraction
CO_2	0.033518
C_1N_2	0.624082
C_2	0.088604
C_3C_4	0.082830
C_5C_6	0.026788
C_7C_9	0.050294
$C_{10}C_{13}$	0.032021
$C_{14}C_{29}$	0.050599
C_{30+}	0.011263
Depth, TVD, m	-3864
Pressure, bara	402.1
Saturation pressure, bara	389.2
Temperature,°C	141.0

Table 1.5: FOUR-STAGE SEPARATOR CONDITIONS.

Stage #	Pressure bara	Temperature °C
1	86.2	90.6
2	24.1	98.9
3	2.3	71.1
4	1.0	15.6

The initial fluid compositions and saturation pressures, shown in Figures 1.1 and 1.3, were calculated by PhazeComp, using the nine-component EOS model and the isothermal gravity/chemical equilibrium (GCE) model. A reference oil sample in the critical region was chosen for the calculations. The sample conditions are given in Table 1.4. The initial reservoir pressure at the reference sample depth -3864 m was 402 bara. The reservoir temperature was 141 °C. The four-stage separator conditions are given in Table 1.5.

Table 1.6: CHEMICAL MOLE COMPOSITION OF INJECTION GASES, FRACTION.

N_c	SepGas	SMS Gas	CO_2-enriched SMS Gas
CO_2	0.03956	0.04599	0.19599
C_1N_2	0.73799	0.75696	0.60696
C_2	0.10375	0.10041	0.10041
C_3C_4	0.08911	0.08484	0.08484
C_5C_6	0.01509	0.01095	0.01095
C_7C_9	0.01294	0.00085	0.00085
$C_{10}C_{13}$	0.00147	0.00000	0.00000
$C_{14}C_{29}$	0.00009	0.00000	0.00000
C_{30+}	0.00000	0.00000	0.00000
Sum	1.0	1.0	1.0

1.4.2 Injection Gases

Injection gases with different compositions may result in different system MMP values and different miscibility mechanisms for the fluid system. Four injection gases[5] were considered in this study. The compositions of three of these gases are give in Table 1.6. The forth injection gas was dry gas, made up of C_1N_2 only.

1.4.3 Relative Permeability Model

Figure 1.6 shows a set of immiscible relative permeability curves (rock curves) used in the simulations. The initial water saturation was 0.26; the residual oil saturation to gas was 0.227, and the critical gas saturation was 0.02. At near-miscible conditions, the gas-oil interfacial tensions were expected to be low in the two-phase region. For evaluating the effect of interfacial tensions on oil recoveries, a set of straight line curves were also applied. Sensor can internally scale relative permeabilities based on the calculated interfacial tensions and the input threshold value of IFT.

[5]Separator gas and SepGas are used interchangeably; dry gas and C_1N_2 are used interchangeably in this thesis.

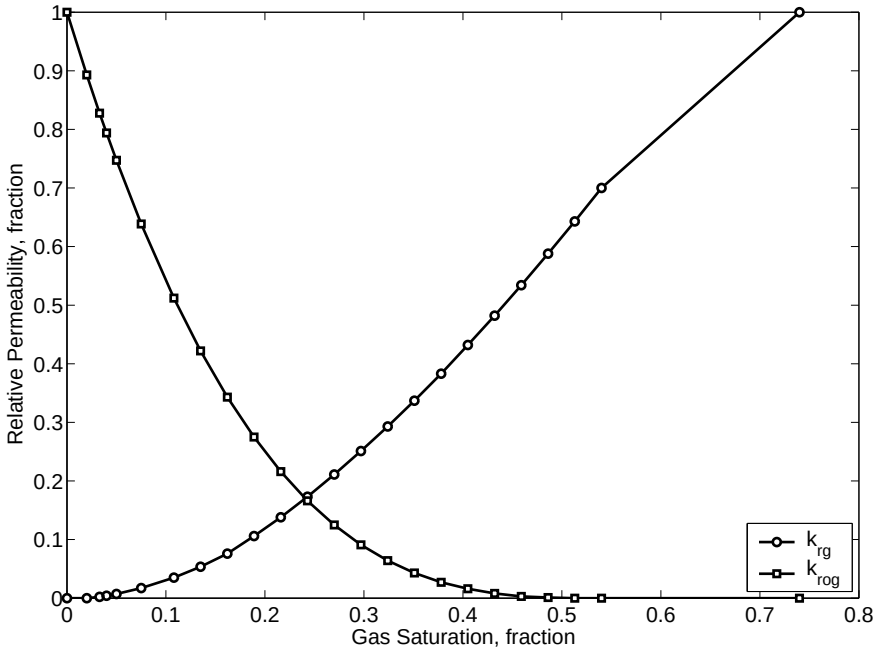

Figure 1.6: Gas-oil relative permeability curves (rock curves) used in simulations.

1.4.4 Well Constraints

All the simulation models consisted of two wells: one gas injector and one oil producer. The gas injection well was located in the first grid cell in x-direction, up-dip if a dip angle exists. This well was always on injection rate control – injecting at a constant volumetric rate. The producer was completed in the last grid cell in x-direction, down-dip if a dip angle exists. This well was controlled by the bottomhole flowing pressure (BHFP). The BHFP of the producer was used to control the reservoir pressure during the displacement. The pressure drop across the 1D model was kept negligible.

1.5 Full Pressure Maintenance

This section presents 1D simulation results for full pressure maintenance by gas injection. We investigated the system MMP for different injection gases and the effect of dip angles on oil recoveries and on MMP. A separate subsection summarizes the results for full pressure maintenance.

Full pressure maintenance represents one of the injection strategies for miscible gas flooding of this type of reservoir. The advantage of full pressure maintenance is that the reservoir fluids will not be altered in composition when dispersion effect is negligible. Consequently, the first-contact miscible nature of the fluids will be preserved and this will lead to miscible (near-100%) recovery efficiency for a 1D the displacement. MMP of the reservoir fluid changes only with depth, independent of reservoir pressure.

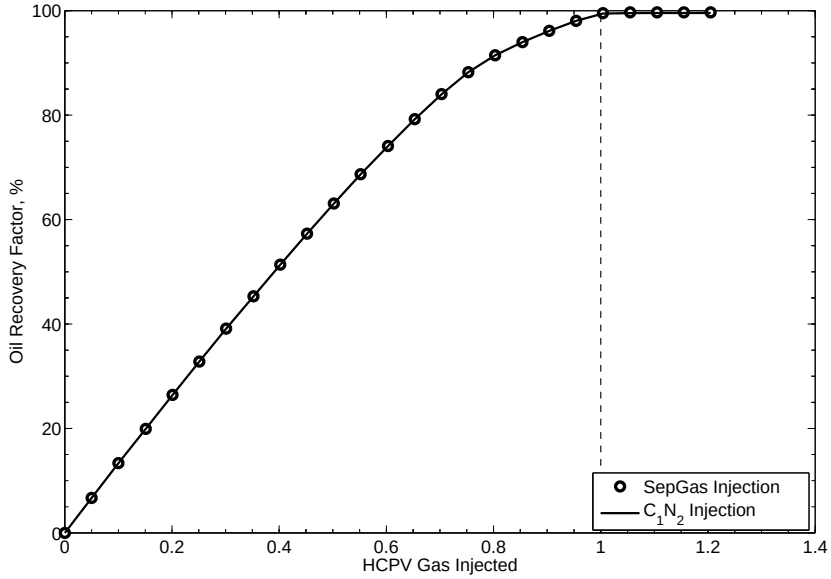

Figure 1.7: Oil recovery performance for 1D horizontal model initialized with compositional variations with depth from isothermal GCE gradient calculations. Displacement pressure p = 393 bara, 4 bar higher than the maximum saturation pressure of the fluid system; number of grid cells N = 1000, Δx = 0.61 m.

1.5.1 Recovery Independence of Injection Gases

This subsection presents simulation results for full pressure maintenance by dry gas and separator gas injection.

Figure 1.7 shows the simulated oil recoveries at different hydrocarbon pore volumes (HCPV) of separator gas and dry gas injected. The model was initialized with the undersaturated grading fluid system and 1000 grid cells were used. The reservoir pressure was 393

bara, 4 bar higher than the maximum saturation pressure of the fluid system. Performance of oil recovery and producing gas-oil ratio (GOR) by dry (C_1N_2) gas injection was practically identical to those by separator gas (SepGas) injection when reservoir pressure was above the saturation pressure of the GOC mixture. Oil recovery curves flattened at about 1.0 HCPV injected, indicating first-contact miscible displacements were achieved in both cases.

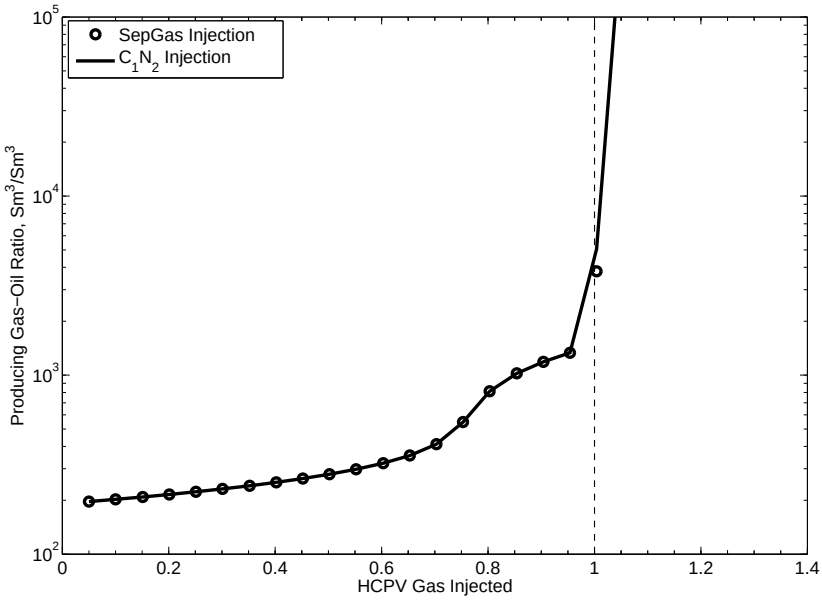

Figure 1.8: GOR performance for 1D horizontal model initialized with compositional variations with depth from isothermal GCE gradient calculations. Displacement pressure p = 393 bara, 4 bar higher than the maximum saturation pressure of the fluid system; number of grid cells N = 1000, Δx = 0.61 m.

Figure 1.8 compares GOR performance of the two cases, showing no difference in GOR development. Gradual increase in GOR was due to the fact that the produced fluids were progressively leaner. Smooth and monotonic change in GOR also indicates that no two-phase region existed in the model and first-contact miscibility was obtained.

It is clear, from the above figures, that oil recoveries and GOR development are independent of composition of injection gases, when the reservoir pressure is kept above the saturation pressure of the undersaturated GOC fluid.

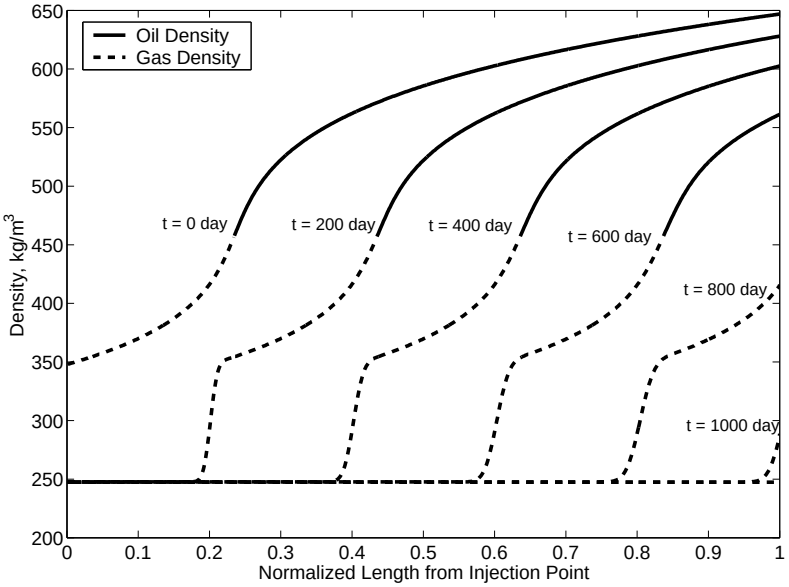

Figure 1.9: Snapshots of phase densities at different simulation times during the 1D horizontal displacement for the separator gas injection case. Displacement pressure p = 393 bara, 4 bar higher than the maximum saturation pressure of the fluid system; number of grid cells N = 1000, Δx = 0.61 m.

Fluid movements in the 1D model can be further visualized in Figure 1.9, the snapshots of phase densities for the separator gas injection case. Fluid densities of the reservoir oil and gas were taken at different simulation times (with 100 days corresponding to 0.1 HCPV injected). It shows that the phase density profiles at different times were practically identical, just shifted along the flow direction.

1.5.2 Recovery Independence of Reservoir Dip Angles

Recovery performance and producing GOR development of simulation runs with different dip angles were almost identical when the reservoir pressure was kept above the maximum saturation pressure. Figures 1.10 and 1.11 show oil recovery and producing GOR versus HCPV injected for the separator gas injection in 1D horizontal, vertical, and 45° angle models. The displacement pressure was 393 bara, 4 bar higher than the maximum saturation pressure of the undersaturated GOC fluid. A total of 1000 grid cells were used in these runs. All the three models predicted almost the same oil recovery and GOR performance,

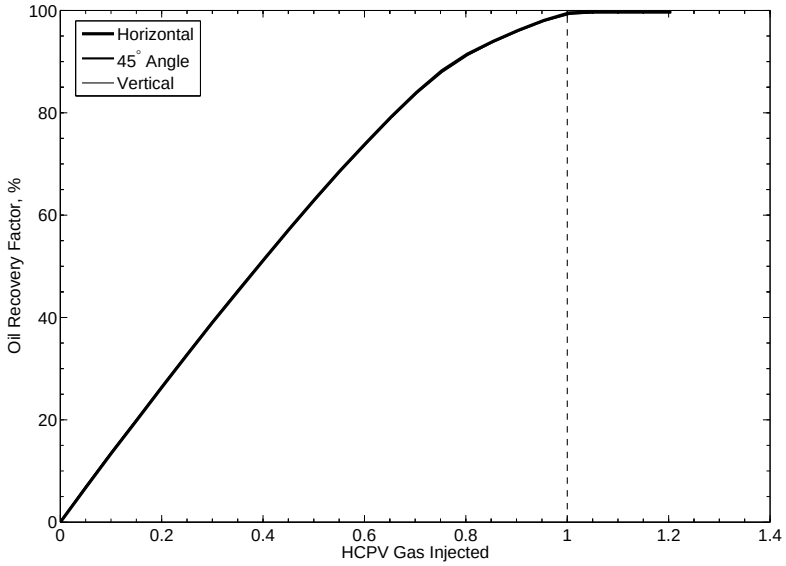

Figure 1.10: Recovery performance for 1D models initialized with compositional variations with depth from isothermal GCE gradient calculations for the separator gas injection case. Displacement pressure p = 393 bara, 4 bar higher than the maximum saturation pressure of the fluid system; number of grid cells N = 1000, Δx = 0.61 m.

indicating that the oil recovery is practically independent of formation dip angles.

In all of the simulations shown in Figures 1.7 to 1.11, the injection gas developed miscibility with the first fluid it met (top structure gas) through first-contact miscible or multi-contact miscible processes. Figure 1.12 shows results of swelling tests on the top structure gas with the two injection gases. At the displacement pressure 393 bara, for the dry gas injection, miscibility was achieved through a multi-contact process at the injection point. For the separator gas injection, the miscibility was achieved by a first-contact miscible process. All the other fluids downstream were displaced by their neighbors in a first-contact miscible manner. For a stable (e.g. by gravity) 1D displacement, it is clear that oil recovery is near 100%, independent of composition of injection gases and formation dip angles, when the reservoir pressure is kept above the saturation pressure of GOC fluid.

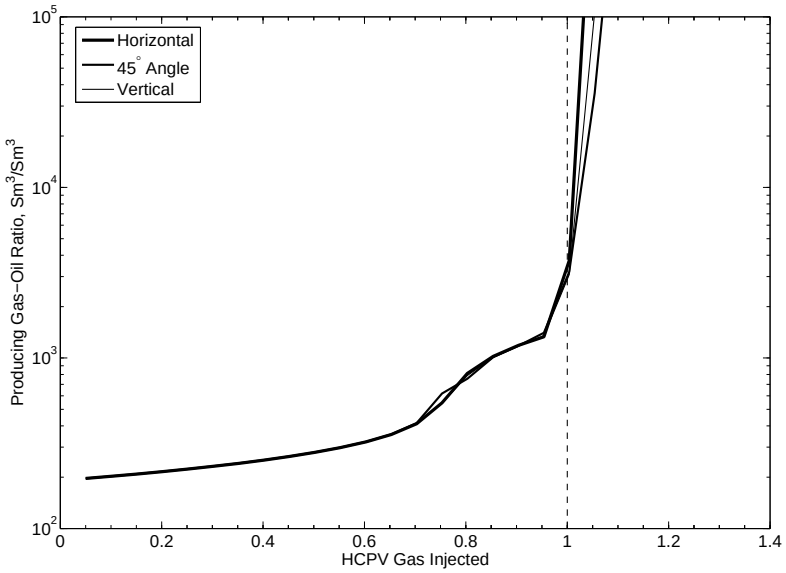

Figure 1.11: GOR performance for 1D models initialized with compositional variations with depth from isothermal GCE gradient calculations for the separator gas injection case. Displacement pressure p = 393 bara, 4 bar higher than the maximum saturation pressure of the fluid system; number of grid cells N = 1000, Δx = 0.61 m.

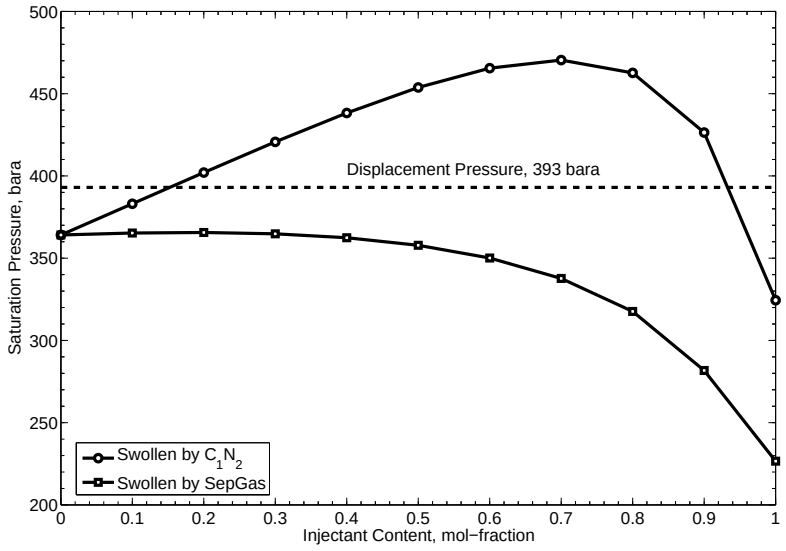

Figure 1.12: Results of swelling test for the top structure gas with the dry (C_1N_2) and separator gases. At the displacement pressure, for the dry gas injection, miscibility was achieved by a multi-contact process. For the separator gas injection, miscibility was achieved by a first-contact miscible process.

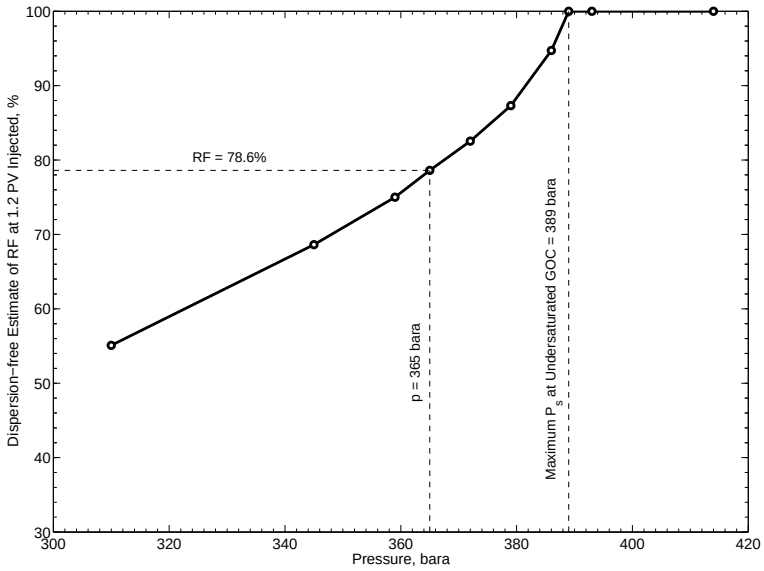

Figure 1.13: Dispersion-free 1D recovery estimate versus pressure indicating a system MMP of 389 bara for C_1N_2 gas injection. System initialized with compositional variations with depth from isothermal GCE gradient calculation.

1.5.3 Dry Gas Injection

Using a dry injection gas (C_1N_2), multi-contact VGD miscibility develops at the point of injection for displacement pressures at/above the saturation pressure of the GOC mixture. The developed miscible fluid front displaces the downstream neighboring fluid; this fluid miscibly displaces its downstream neighboring fluid, and so on. Neighboring fluids displace downstream neighboring fluids first-contact miscibly; the injection gas displaces (only) the first fluid through a multi-contact vaporization process.

Figure 1.13 shows the dispersion-free recovery versus displacement pressure for the dry gas injection. Dispersion-free recoveries at 1.2 HCPV were estimated based on linear extrapolation of simulated recoveries of runs using different numbers of grid cells. The recovery-pressure curve indicates that the system MMP was the saturation pressure (also the VGD MMP) of the GOC fluid, lower than the local VGD MMP of the down structure heavier oils as shown in Figure 1.4. Recall that the oils below the GOC were displaced by

their upstream oil neighbors, not directly by the injection gas.

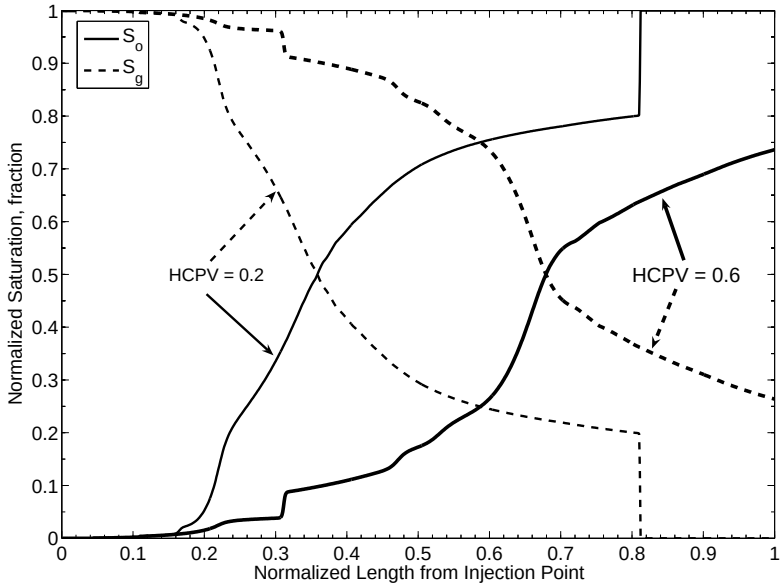

Figure 1.14: Phase saturation distribution at 0.2 and 0.6 HCPV along the 1D model initialized with compositional variations with depth from isothermal GCE gradient calculations. Displacement pressure p = 365 bara; N = 1000, Δx = 0.61 m; dry gas injection.

One might ask, why isn't the system MMP equal to the VGD MMP of the first-displaced reservoir gas? Figure 1.13 shows that the system oil recovery at 1.2 HCPV was only about 80% for a displacement pressure of 365 bara, the VGD MMP (also the dewpoint pressure) of the top reservoir gas (1^{st} cell in the 1D model). Figures 1.14 and 1.15 show the snapshots of normalized saturations[6] and phase densities at 0.2 and 0.6 HCPVs injected. At the displacement pressure of 365 bara, only heavier oils at deeper locations would stay undersaturated. At 0.2 HCPVs injected, the single phase oils had not been fully produced, thus resulting unity normalized oil saturations close to the producer. Large two-phase region and large difference in phase densities also indicate that the displacement was in fact immiscible. The immiscible recoveries under these conditions resulted because the downstream reservoir gases were below their dewpoints, and retrograde condensate had developed at the displacement pressure. When the injection gas moved ahead it met the

[6]Normalized gas and oil saturations refer to gas and oil saturations normalized with respect to hydrocarbon saturations.

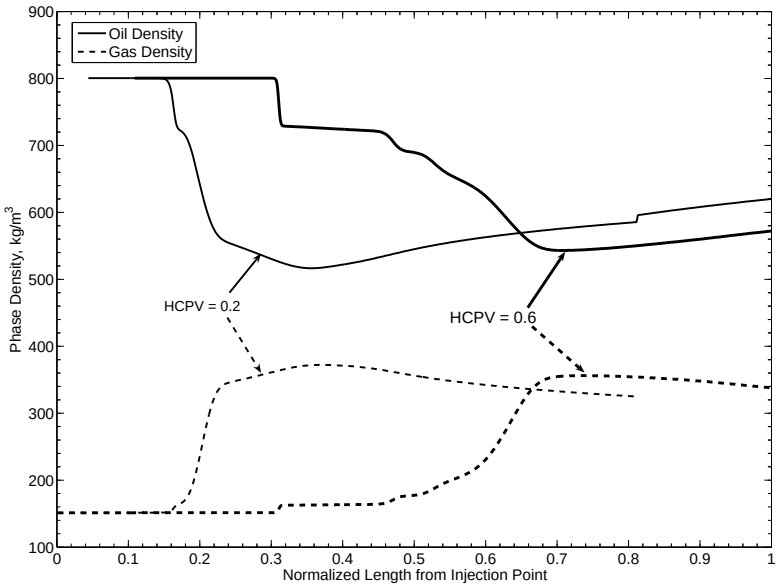

Figure 1.15: Phase density at 0.2 and 0.6 HCPV along the 1D model initialized with compositional variations with depth from isothermal GCE gradient calculations. Displacement pressure p = 365 bara; N = 1000, Δx = 0.61 m; dry gas injection.

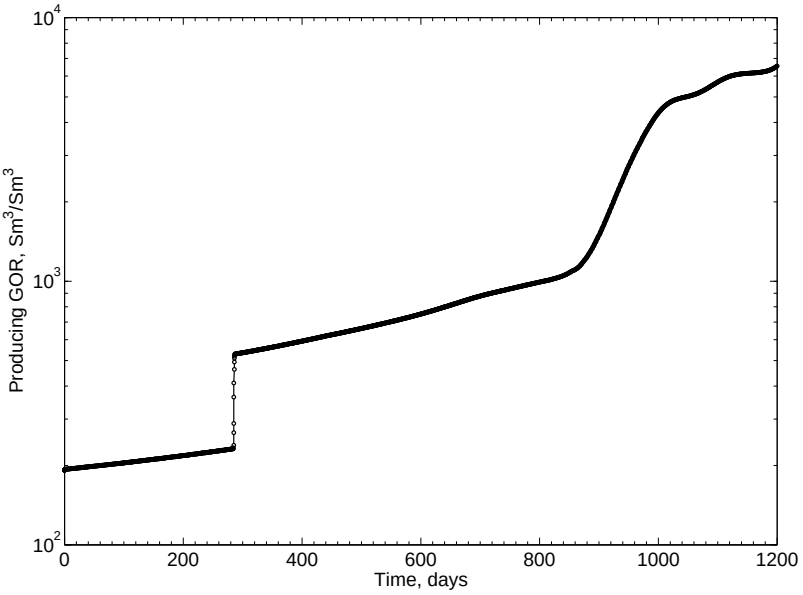

Figure 1.16: GOR development of the 1D model initialized with compositional variations with depth from isothermal GCE gradient calculations, displacement pressure p = 365 bara, N = 1000, dry gas injection.

residual retrograde condensate with which it was not miscible. A two-phase immiscible region existed downstream to the point of injection, resulting in a system recovery less than 100%.

Figure 1.16 shows the development of the producing GOR for the same simulation run. Up to about 300 days, only single phase oils of different compositions were produced. Then, the two-phase front arrived at the producer as indicated by a sudden increase in GOR. Producing GOR continued to increase as the oil saturations at the producer decreased and the produced gases phase became leaner. At about 900 days, a considerable fraction of injection gas was produced as indicated by another increase in producing GOR.

1.5.4 Summary

In summary, the system MMP for full pressure maintenance is the critical pressure of the GOC mixture of the fluid system. Oil recoveries are independent of the composition of the injection gases and the formation dip angles. We believe that these conclusions are general for 1D flow of any undersaturated compositional grading gas-oil reservoir undergoing gas injection for full pressure maintenance.

Full pressure maintenance by gas injection offers flexibility in selecting available injection gases. The optimal injection gas is apparently the most economical gas available for injection. In addition, production by full pressure maintenance might require less demanding surface processing facility, as the producing GOR will increase only smoothly and gas breakthrough occurs at about 1.0 HCPV, at which point gas injection might be stopped.

The disadvantage is that the minimum reservoir pressure (or the maximum saturation pressure of the fluid system) is usually high, implying that high compression costs might be expected. In some cases, partial pressure maintenance by enriched gas injection might be more economically viable.

1.6 Partial Pressure Maintenance

This section presents 1D simulation results for partial pressure maintenance by enriched gas injection, which represents an alternative to full pressure maintenance for miscible gas flooding. The necessity for enriched gas injection to achieve miscibility is because the reservoir pressure has locally (or entirely) fallen below the saturation pressure of the fluids and a two-phase region has formed in the reservoir.

Key focus was on estimating the system MMP and studying the C/V mechanism developed in such a reservoir, when the injection gas was enriched with intermediate components. The difficulty in defining the system MMP for enriched gas injection is that the MMP of the fluids not only changes with depth but also with the prevailing reservoir pressure. Different injection gases and different initializations (injecting at different depths and excluding the reservoir zone up-structure from the injection point in the model) were simulated to evaluate the system MMP, the displacement mechanisms, and the oil recovery efficiencies.

For injection gases containing intermediate C_2 - C_5 or CO_2 components in sufficient quantity, the C/V MMP can exist in some regions or throughout the entire reservoir. The C/V MMP may be lower or higher than the saturation pressure; but it is always lower than the saturation pressure for a reservoir gas. For the fluid system used in this study, shown in Figure 1.3, injecting the separator gas (SepGas) yielded local C/V MMP for the rich reservoir gases, the GOC mixture, and all the reservoir oils, shown in Figure 1.5. The shallowest C/V MMP on the initial MMP versus depth curve was 380 bara for the gas at a depth of -3810 m. The minimum C/V MMP was 359 bara for a near-critical mixture at a depth of -3850 m, slightly above the undersaturated GOC.

Dispersion-free recoveries at 1.2 HCPV were estimated based on linear extrapolation of the simulated recoveries of runs using different numbers of grid cells. At some pressures (e.g. 359 and 380 bara), the dispersion-free recovery estimates were obtained based on the results of runs with even larger number of grid cells (e.g. 5000 and up to 50000 grid cells).

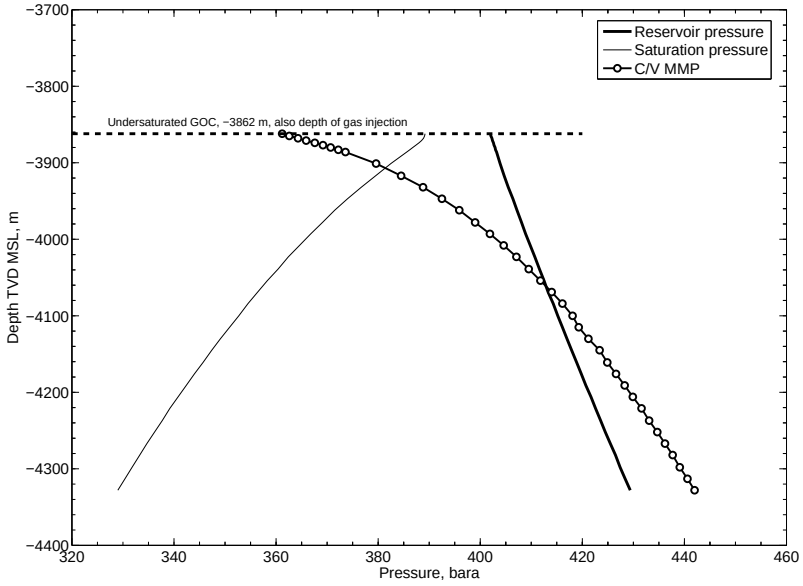

Figure 1.17: Reservoir pressure, saturation pressure, and C/V MMP for SepGas of a compositionally grading oil system, which is the lower portion of the fluid system ranging from GOC fluid to black oil shown in Figure 1.3.

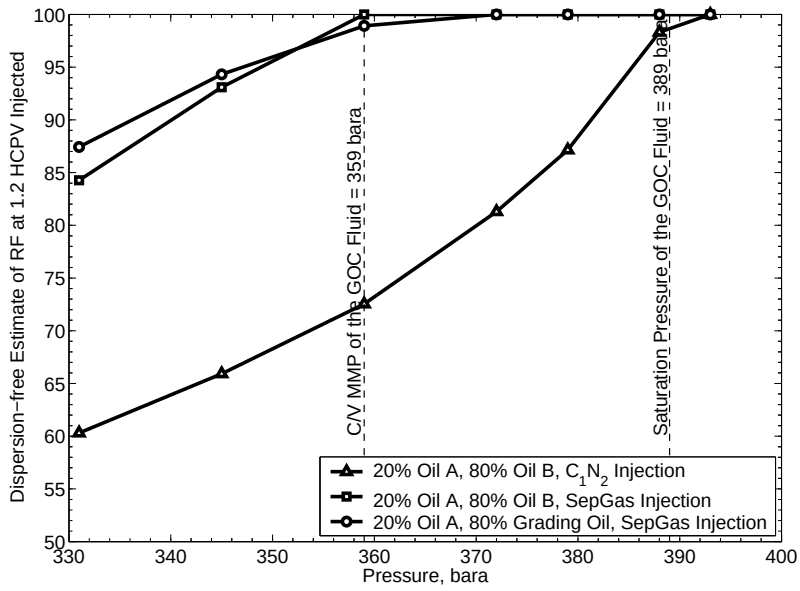

Figure 1.18: Dispersion-free recovery estimate at 1.2 HCPV versus pressure for a 1D model initialized with different oils in composition, indicating the system MMP for the separator gas injection was the C/V MMP of the reservoir fluid at the injection depth.

1.6.1 Injection at Undersaturated GOC

As part of a step-by-step problem-solving approach, we isolated and studied the oil zone shown in Figure 1.3 for the separator gas injection case. The 1D model contained only the grading oils and the critical mixture located at the top. The reservoir gas zone was excluded. The objective was to determine the system MMP for a relatively simple grading oil system. The pressure, saturation pressure and C/V MMP of this fluid system is shown in Figure 1.17. One can see that the C/V MMP for the separator gas increased monotonically from top to bottom for this fluid system. The C/V MMP of the critical mixture at the top was the minimum MMP of this fluid system.

One simulation model was initialized with the equilibrium liquid (oil A) of the GOC fluid for the first 20% of grid cells; the remaining grid cells were filled (to S_o = 100%) with equilibrium oils resulting from flash calculations of the initial grading reservoir oils at the current displacement pressure. Note that oil A had a C/V MMP of 359 bara for the separator gas. In Figure 1.18 the line with open circles shows the dispersion-free recovery estimates at 1.2 HCPV, indicating a system MMP of 359 bara, equal to the C/V MMP of the critical mixture at the top for this initialization.

Another initialization was made to study the issue whether a miscible oil bank will miscibly displace any downstream oil that itself has a much higher MMP with the injection gas. The first 20% of the grid cells of the model was initialized with the GOC fluid (oil A); the remaining grid cells were filled completely (to So = 100%) with the heaviest reservoir oil (oil B) at a depth of -4328 m, having a local C/V MMP of 442 bara with the separator gas. The line with open squares in Figure 1.18 shows the simulation results for this initialization, indicating a system MMP of 359 bara.

C_1N_2 gas injection was simulated for the second initialization. The line with open triangles in Figure 1.18 indicates that the system MMP was 389 bara for this dry gas injection, equal to the VGD MMP of the GOC mixture for the injection gas.

All the simulation results presented in this subsection consistently showed that the system MMP of a grading oil reservoir equals the C/V MMP of fluid at the injection depth.

The advantage of a grading oil reservoir for enriched gas injection is that the system MMP is the minimum C/V MMP of the fluid system, i.e. the C/V MMP of the fluid at the injection point. A critical mixture, if present, offers the most advantage for achieving miscibility at a lowered reservoir pressure.

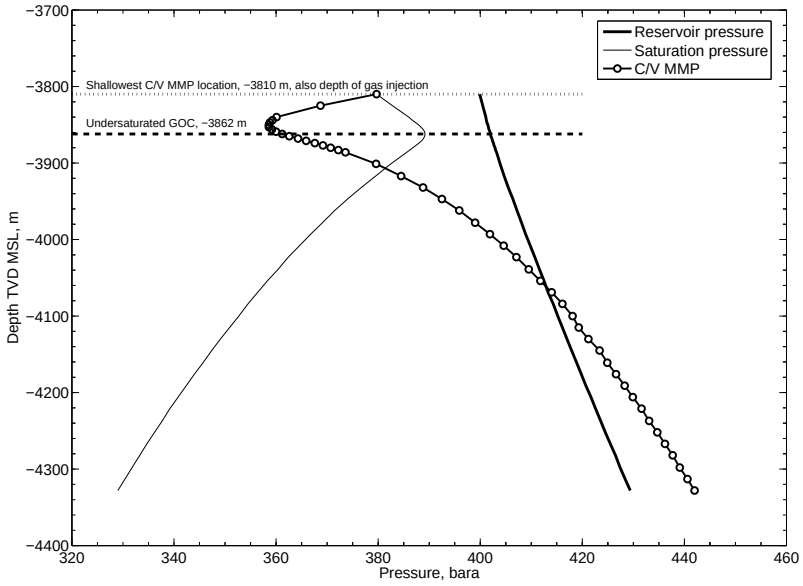

Figure 1.19: Reservoir pressure, saturation pressure, and C/V MMP for SepGas of a compositionally grading system, which is the lower portion of the fluid system ranging from the shallowest rich gas having C/V MMP with SepGas to black oil shown in Figure 1.3.

1.6.2 Injection at Shallowest C/V MMP Depth

This subsection presents simulation results for the separator gas injection at the shallowest C/V MMP depth (-3810 m), shown in Figure 1.19, where the injection gas can develop a multi-contact C/V miscibility with the initial reservoir gas at that depth based on PhazeComp calculations. The 1D horizontal model was initialized with the compositionally grading fluids from -3810 to -4328 m as shown in Figure 1.3; reservoir gases up-structure to the injection depth were excluded in the model.

The dispersion-free oil recovery estimates of the simulation results are shown in

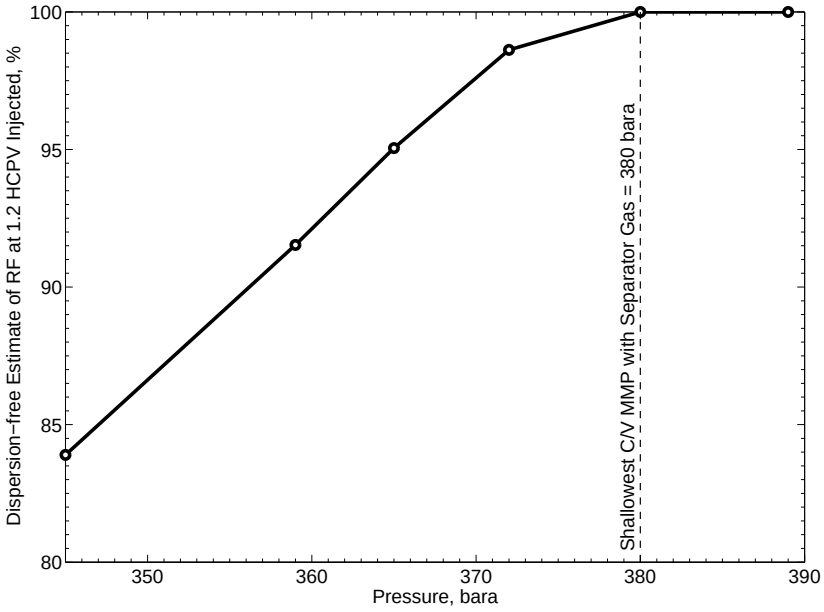

Figure 1.20: Dispersion-free recovery estimates at 1.2 HCPV for separator gas injection at depth of -3810 m, the shallowest C/V MMP location. Linear extrapolation based on simulated results of N = 500, 1000, and 5000.

Figure 1.20, indicating the system MMP of 380 bara, equal to the C/V MMP and the dewpoint pressure of the reservoir gas at the injection depth.

Experience has been that gas condensate systems, near-critical systems in particular, are more sensitive to numerical dispersion. We therefore run simulations, for some cases, using larger ($>$ 1000) number of grid cells to minimize numerical dispersion effect.

Figure 1.21 shows oil saturation distributions in the 1D model for a run using 5000 grid cells (Δx = 0.12 m). The displacement pressure was equal to the estimated system MMP of 380 bara. We found that the C/V miscible front formed, as expected, creating an oil bank. The oil bank also built in size. Figure 1.22 shows the snapshots of IFT at different HCPVs injected for the same run. The C/V front remained miscible throughout the displacement indicated by the increasingly low IFT values at the front.

Figures 1.23 and 1.24 show the recovery and producing GOR performance for the same run, respectively. The oil recovery curve tended to flatten out at about 1.2 HCPV,

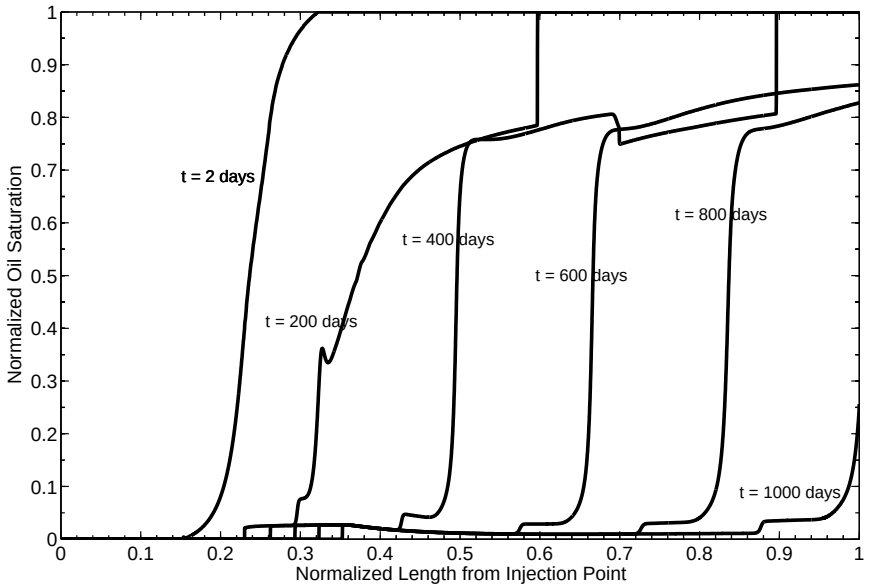

Figure 1.21: Oil saturation profiles at different times during a 1D displacement by separator gas, 100 days roughly corresponding to 0.1 HCPV injected. Injection at depth of -3810 m. System initialized with compositional variations from isothermal GCE gradient calculation, p = 380 bara, N= 5000.

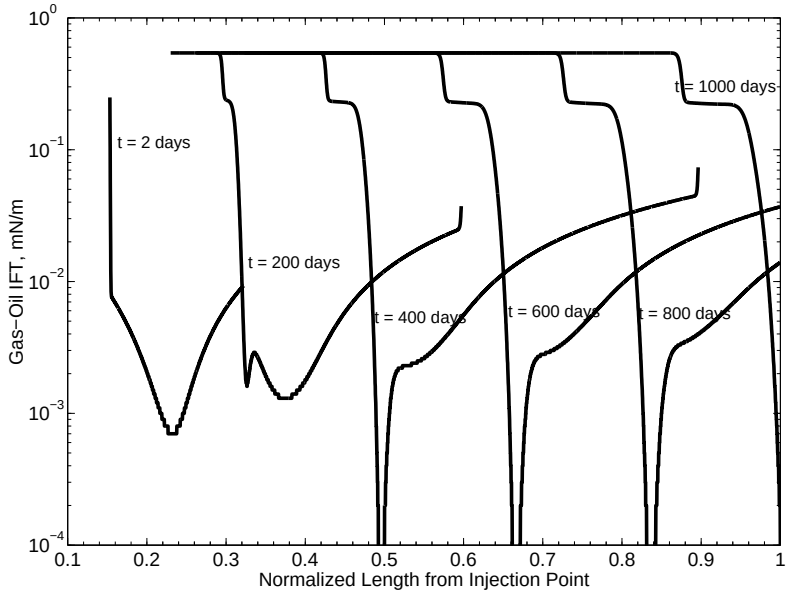

Figure 1.22: Gas-oil IFT profiles at different times during a 1D displacement by separator gas, 100 days roughly corresponding to 0.1 HCPV injected. Injection at depth of -3810 m. System initialized with compositional variations from isothermal GCE gradient calculation, p = 380 bara, N= 5000.

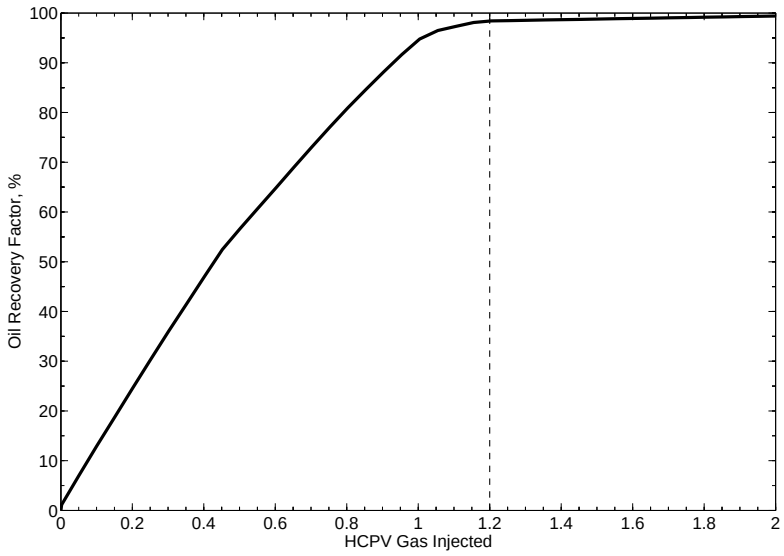

Figure 1.23: Recovery performance versus HCPV injected. Separator gas injection at depth of -3810 m. System initialized with compositional variations from isothermal GCE gradient calculation, p = 380 bara, N= 5000.

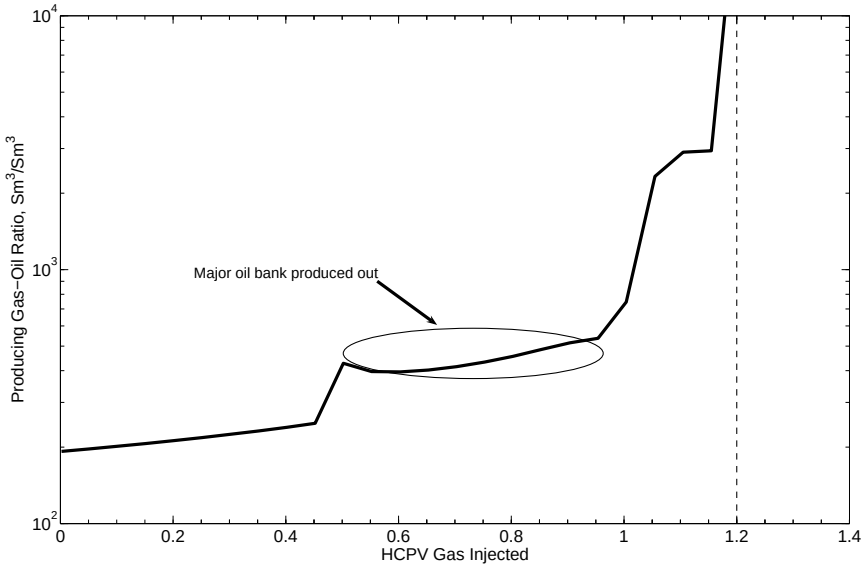

Figure 1.24: Producing GOR performance versus HCPV injected. Separator gas injection at depth of -3810 m. System initialized with compositional variation from isothermal GCE gradient calculation, p = 380 bara, N= 5000.

indicating a multi-contact near-miscible process. The GOR performance reflected when the oil bank was produced.

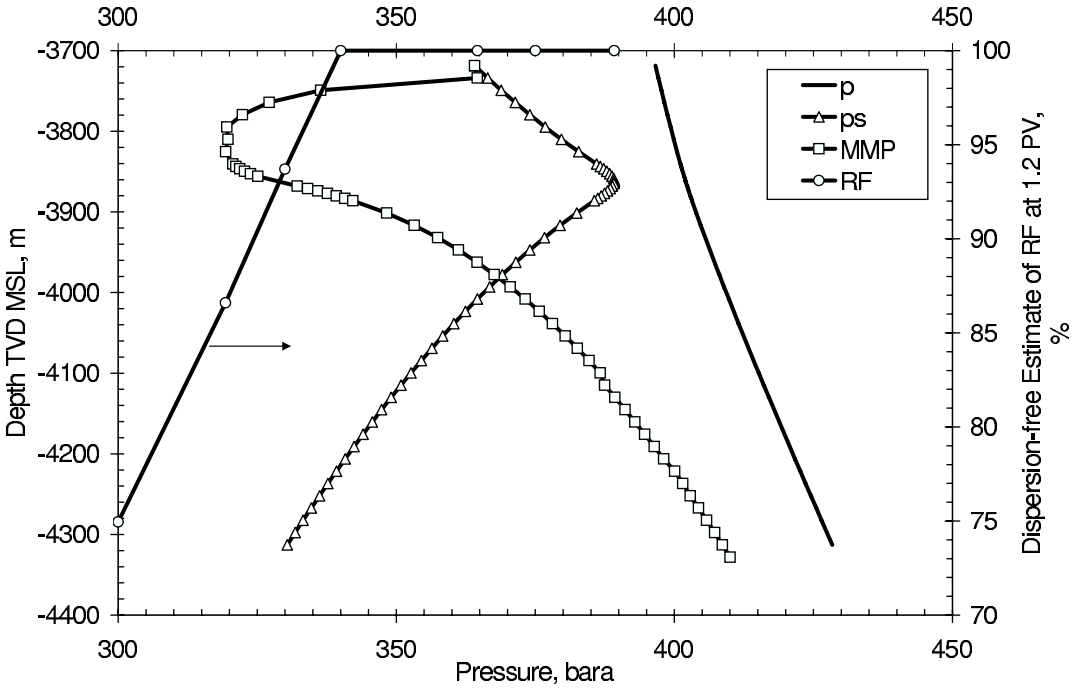

Figure 1.25: Reservoir pressure, saturation pressure, C/V MMP versus depth for CO2-enriched SMS gas injection, and resulting dispersion-free recovery estimate versus pressure for the system initialized with compositional variation from isothermal GCE gradient calculation. The system MMP was estimated to be 340 bara.

1.6.3 CO_2-enriched Gas Injection at Top

Simulation results for CO_2-enriched SMS gas injection in a 1D model is presented in this subsection. The model was initialized with the entire fluid column as shown in Figure 1.3 and the injection gas was injected at the reservoir top -3719 m. The injection gas, composition shown in Table 1.6, was enriched with CO_2 by 15 mol-%, lowering methane-nitrogen (C_1N_2) content by the same amount based on the composition of the SMS gas. This gas was found to have a C/V MMP equal to the dewpoint (365 bara) of the top reservoir gas at -3719 m.

Figure 1.25 depicts the reservoir pressure, saturation pressure, and MMP versus

depth; it also shows the relationship between the dispersion-free recovery estimates and the displacement pressure. The line with open squares shows the MMP versus depth for the injection gas. Only the C/V mechanism existed throughout the reservoir and the lowest C/V MMP being 320 bara was found for a reservoir gas located at a depth of -3795 m, slightly above the undersaturated GOC.

The line with open circles in Figure 1.25 shows the dispersion-free oil recovery estimate at 1.2 HCPV injected versus the displacement pressure. Linear extrapolation for dispersion-free recovery estimates was based on simulated recoveries using 500, 1000, and 5000 grid cells. The system MMP appeared to be 340 bara for this injection gas, the breakover point at 100% recovery. This pressure was between the C/V MMP at the point of injection and the minimum C/V MMP for a fluid at -3795 m.

The reason why the system MMP was between the first C/V MMP and the minimum MMP of the entire fluid system is not clear. We suspect that the reservoir gas at the depth of injection might be too lean and the oil saturation might be too low to develop the oil bank at its C/V MMP. At somewhat lower pressures, the reservoir gases at some depth below the injection point might be rich enough to allow the oil bank to develop and thus the development of miscibility. Further discussion on the effect of oil saturation on the development of miscibility is presented in Chapter 2.

1.6.4 Separator Gas Injection at Top

This subsection presents 1D simulation results for the separator gas injection at the top. The model was initialized with composition variations with depth of the entire fluid system as shown in Figure 1.3. The separator gas was injected in the first grid cell at an equivalent depth of -3719 m, the top of the reservoir. Different relative permeability treatments were applied as a two-phase region evidenced in the reservoir.

Figure 1.26 shows the simulation results for the separator gas injection. The line with open circles represents a horizontal displacement with IFT-corrected relative permeability (RP) curves. The system MMP was about 359 bara, close to the C/V MMP of the

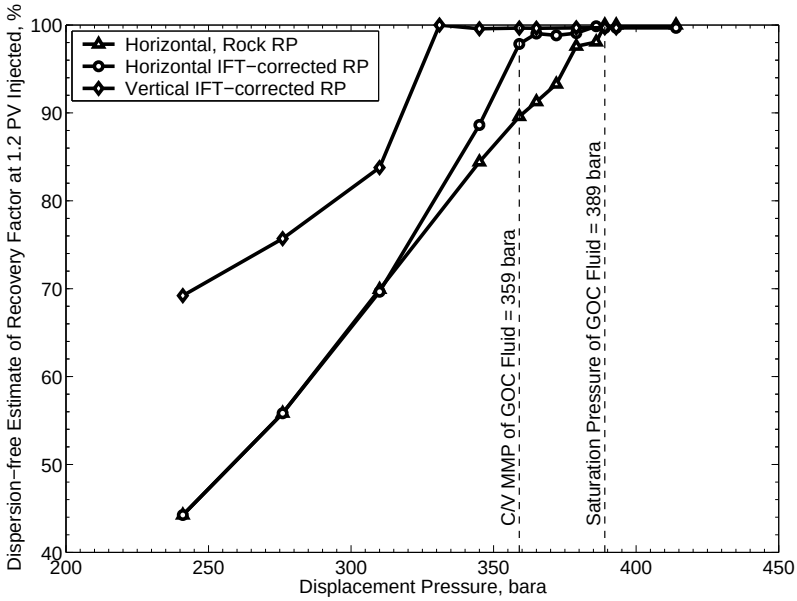

Figure 1.26: Dispersion-free 1D recovery estimate versus pressure for separator gas injection using different relative permeability treatments. System initialized with compositional variations with depth from isothermal GCE gradient calculations.

GOC fluid with the injection gas. The line with open triangles in Figure 1.26 represent a horizontal displacement with rock relative permeability curves – i.e. no IFT correction. The system MMP was close to 380 bara, the shallowest C/V MMP at the depth of -3810 m. The IFT correction has two effects on relative permeability – straightening the curves and reducing the residual oil saturation, both leading to improved oil recoveries. These effects were significant when the displacement was near miscible and negligible when the displacement was immiscible.

Figure 1.27 shows oil saturation snapshots taken at different times (with 100 days corresponding to 0.1 HCPV injected) for a run using 5000 grid cells at the pressure of 380 bara. A clear development of an oil bank can be seen after 500 days of gas injection. The oil bank also grew in size as displacement proceeded.

Figure 1.28 shows the oil recovery and producing GOR versus HCPV injected. The oil recovery curve tended to flatten out and GOR tended to reach its maximum at about 1.25 HCPV gas injected. The first sharp increase in GOR at 0.35 HCPV injected resulted

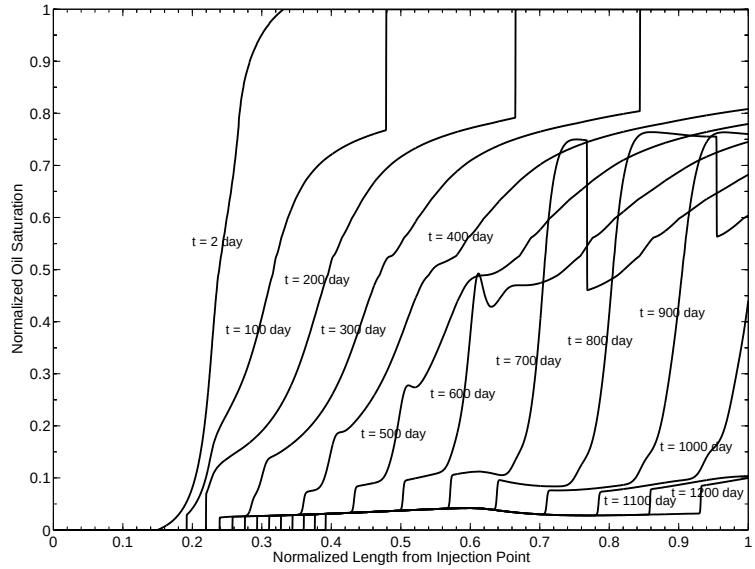

Figure 1.27: Oil saturation snapshots for a run using rock curve and N = 5000. Displacement pressure was 380 bara, and system initialized with compositional variations with depth from isothermal GCE gradient calculations. 100 days corresponding to 0.1 HCPV injected.

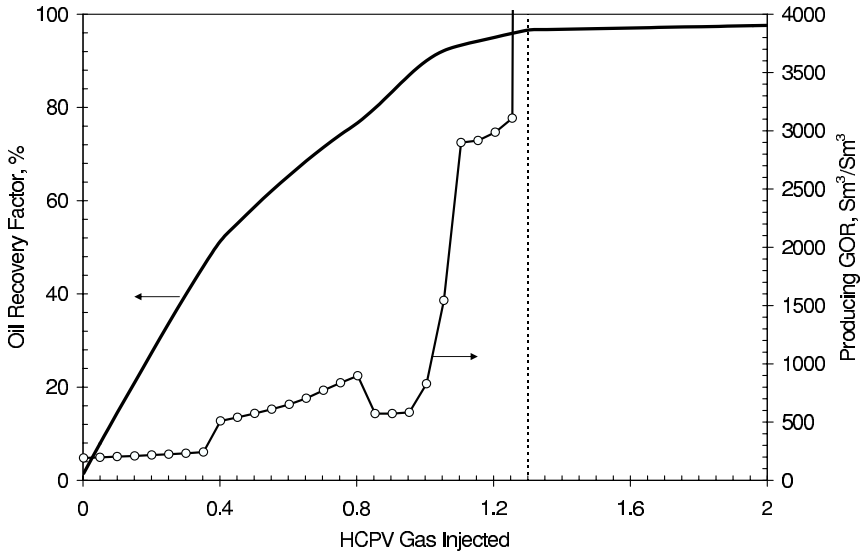

Figure 1.28: Recovery and GOR performance for a run using rock curve and N = 5000. Displacement pressure was 380 bara, and system initialized with compositional variations with depth from isothermal GCE gradient calculations.

from the arrival of the two-phase front at the producer. Drop in GOR at about 0.8 HCPV injected was due to the production of the developed C/V oil bank. Increase in GOR slowed down at 1.1 HCPV injected when the secondary oil bank was produced, and was followed by sharp increase in GOR because of the massive breakthrough of the injection gas at 1.25 HCPV injected.

Using the same number of grid blocks at the same pressure of 380 bara, injecting the separator gas from the top (-3719 m) resulted in 2 – 3% lower recovery for runs using 5000 and 50,000 grid cells. Compared with the case of injection at the shallowest C/V MMP depth (Figures 1.23 and 1.24), the displacement was less efficient.

The gases from -3719 to -3810 m should be miscibly displaced at 380 bara because this pressure exceeded their dewpoint pressures. The difference resulted in the change in compositions of the oil at -3810 m of which the saturation pressure was 380 bara. As the displacement proceeded, the oil was vaporized by continuous contact with non-equilibrium reservoir gases passing over it. When the injection gas arrived, the residual oil at this depth had become slightly heavier than originally found at that depth, thus resulting in less efficient displacement and $<$ 100% recoveries.

It might be expected that the system MMP could be somewhat higher than the shallowest C/V MMP as the composition of the oil at -3810 m could have been altered in composition to some extent by the upstream flowing gases. How much the system MMP will increase with respect to the original value of the shallowest C/V MMP depends on how much the oil at -3810 m has changed in composition.

When the displacement pressures were further reduced, the oil recovery curves showed several “regions” before it finally flattened out at about 1.6 HCPV injected, shown in Figures 1.29 and 1.30. The performance of producing GOR at these pressures shows the same characteristics as described for the run at the pressure of 380 bara shown in Figure 1.28, but the oil banks were produced at delayed times. Only at a displacement pressure of 389 bara, which was the critical pressure of the GOC mixture, did the oil recovery curve flatten out at 100% at about 1 HCPV injected, shown in Figure 1.31. This resulted in a

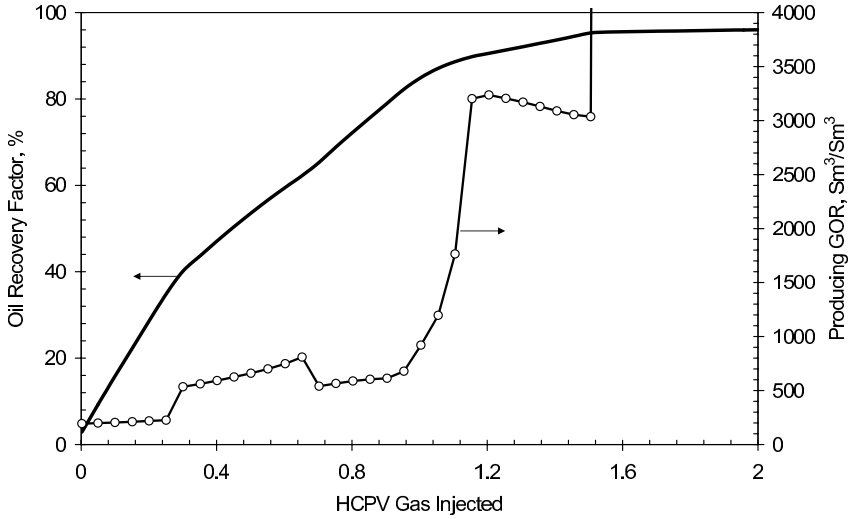

Figure 1.29: Recovery and GOR performance for a run using rock curve and N = 5000. Displacement pressure was 365 bara, and system initialized with compositional variations with depth from isothermal GCE gradient calculations.

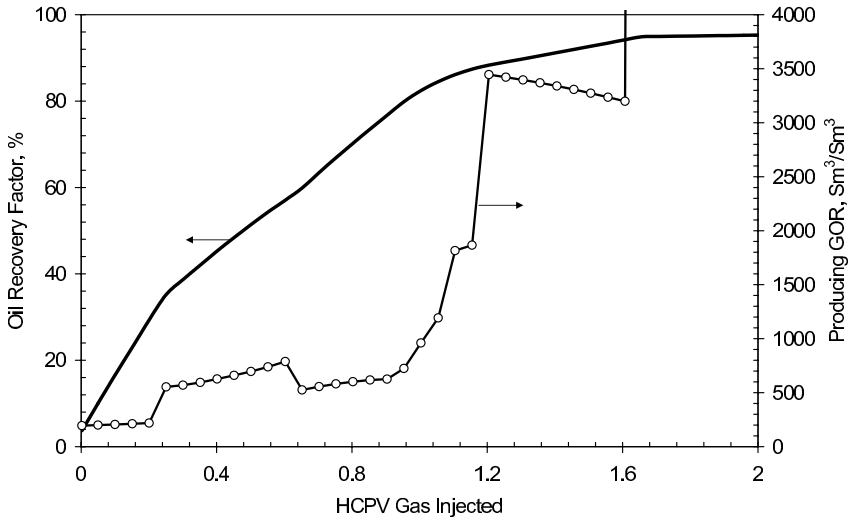

Figure 1.30: Recovery and GOR performance for a run using rock curve and N = 5000. Displacement pressure was 359 bara, and system initialized with compositional variations with depth from isothermal GCE gradient calculations.

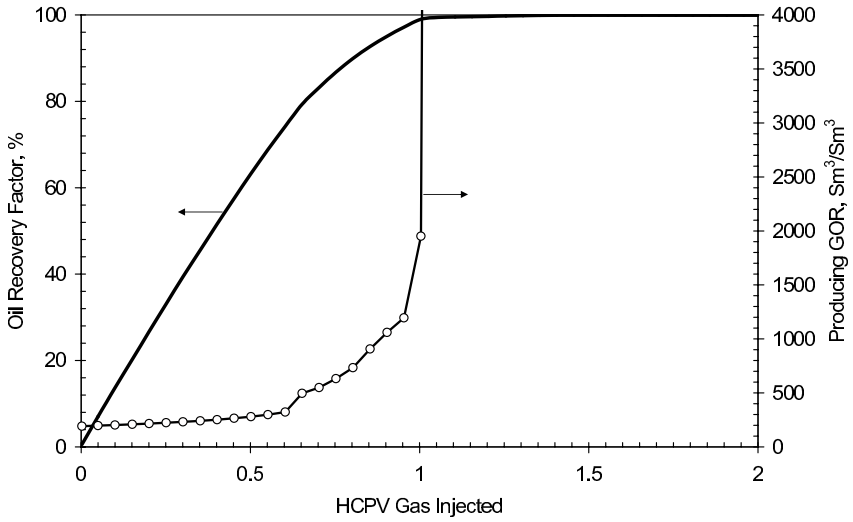

Figure 1.31: Recovery and GOR performance for a run using rock curve and N = 5000. Displacement pressure is 389 bara, and system initialized with compositional variations with depth from isothermal GCE gradient calculations.

first-contact miscible displacement.

When the reservoir pressure is less than the maximum saturation pressure, two equilibrium phases will develop in parts of the reservoir before the injection gas front arrives. As reservoir gases flow over the deeper equilibrium oils, these oils will change in composition prior to the arrival of the injection gas front and become heavier due to vaporization effect. Consequently, the C/V MMP values for these oils will also increase.

We studied the change in oil composition at the GOC depth for a displacement at 359 bara. Figure 1.32 shows that the oil compositions changed only marginally until the separator gas front arrived. After the separator gas front had arrived, the oil quickly became heavier and stabilized as a heavy residual oil at low oil saturations.

We also studied the change in C/V MMP of the oil at the initial GOC position with the injection gas before the arrival of the injection gas front. Figure 1.33 shows that as a consequence of the change in oil composition, the C/V MMP of the oil also increased from the initial value of 359 bara to about 385 bara before the *injection* gas contacted the oil at the initial GOC depth. This might partly explain why the dispersion-free recovery estimate at the displacement pressure of 359 bara was fairly low in comparison with the miscible

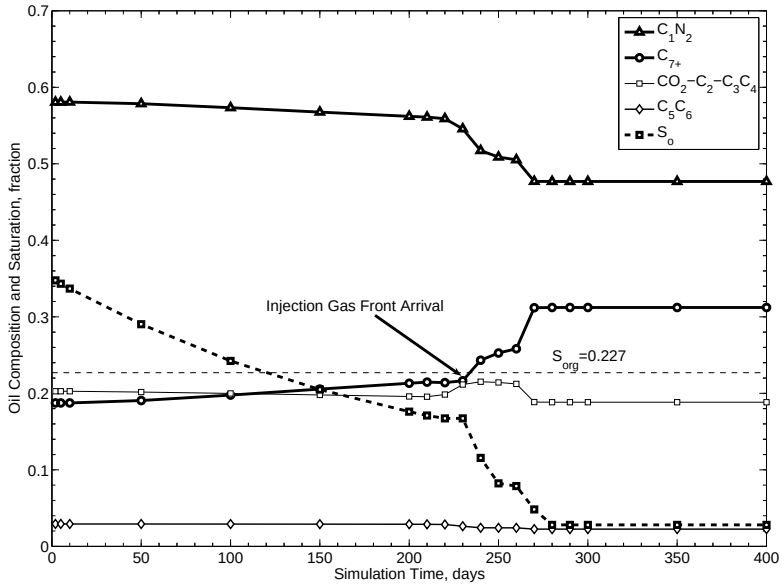

Figure 1.32: Composition and saturation change of the equilibrium oil at the initial GOC depth for a 1D displacement at p = 359 bara by the separator gas injection. System initialized with compositional variations with depth from isothermal GCE gradient calculations.

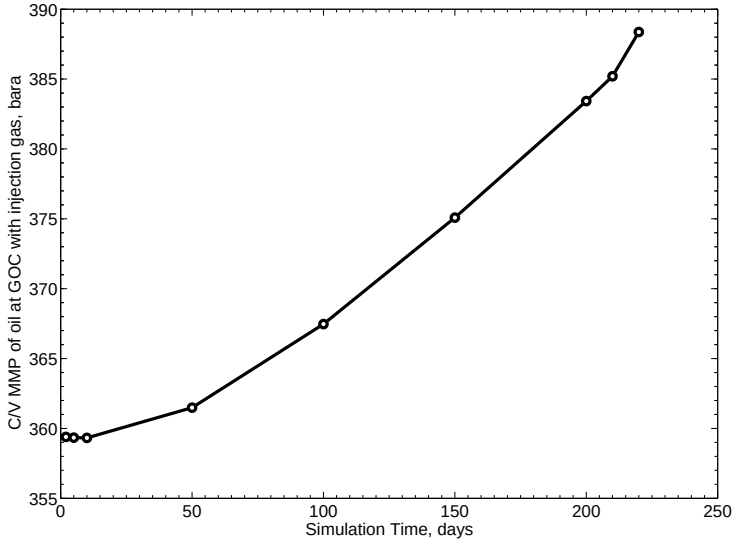

Figure 1.33: Change in C/V MMP of the oil at the initial GOC location with time for a 1D displacement at p = 359 bara by the separator gas injection. System initialized with compositional variations with depth from isothermal GCE gradient calculations.

recovery, shown in Figure 1.26.

It might be expected that the C/V MMP of the oil just before the injection gas arrival will increase to a higher value if the gas zone is bigger.

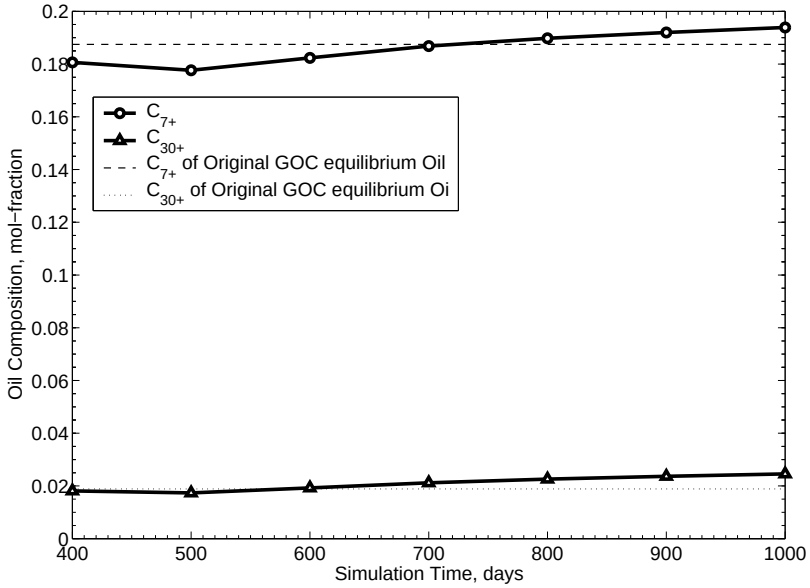

Figure 1.34: Oil composition change versus time at the C/V front during a 1D displacement at p = 359 bara by separator gas injection. System initialized with compositional variations with depth from isothermal GCE gradient calculations; N = 5000.

Figure 1.34 shows the oil compositions at the moving C/V front (open symbols) for the same run. The composition was quite similar to the original GOC equilibrium oil at 359 bara (dash and dotted lines), though it slowly became heavier and slightly less critical.

Figure 1.35 shows the development of oil saturation with time for a displacement at pressure of 359 bara. After 400 days, an oil bank developed just downstream to the near-miscible C/V front (marked with open circles); the front was defined by a clear minimum in gas-oil IFT shown in Figure 1.36. The leading-edge (relative to the position of the miscible front) oil bank grew significantly as the displacement moved into the oil zone below the original GOC. A smaller but still-significant secondary oil bank developed upstream to the C/V front. This bank also increased in size during the displacement, and resulted in a “late” recovery after the gas breakthrough, indicated by the producing GOR development shown in Figure 1.30.

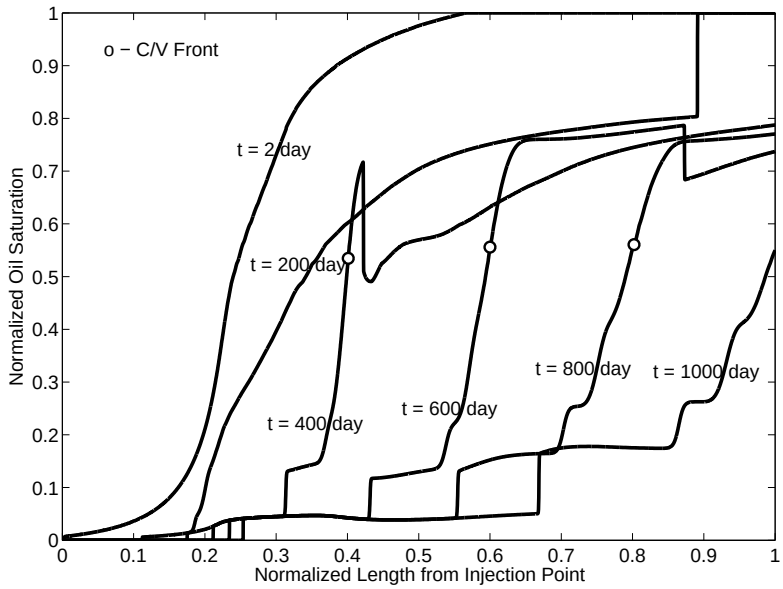

Figure 1.35: Snapshot of oil saturation profile change with time. C/V oil bank has developed just before 400 days. System initialized with compositional variations from isothermal GCE gradient calculation, p = 359 bara, N = 5000, separator gas injection.

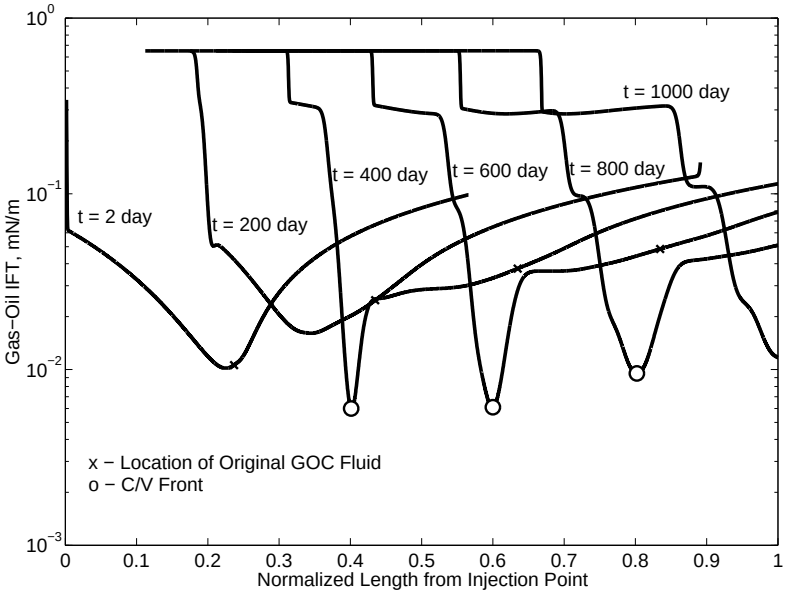

Figure 1.36: Gas-oil IFT profiles at different times during a 1D displacement with separator gas. System initialized with compositional variations from isothermal GCE gradient calculation, p = 359 bara, N = 5000.

Vertical Displacement

The line with open diamonds in Figure 1.26 shows the simulation results from a 1D vertical displacement with IFT-corrected relative permeabilities. The *apparent* MMP was about 330 bara, lower than any initial local MMP of the fluid system. Gravity effect for vertical displacement yields a much more favorable fractional flow curve so that oil recoveries can be high even at immiscible conditions. Therefore, we felt that it was not appropriate to evaluate thermodynamic system miscibility conditions using vertical displacements, though in reality fluid compositions vary with depth.

It was observed that an oil bank still will develop at immiscible conditions if the C/V mechanism exists, but at a reduced size. The magnitude and the size of the C/V oil bank is closely related to the displacement pressure. We found this is general for enriched gas injection when C/V mechanism exists.

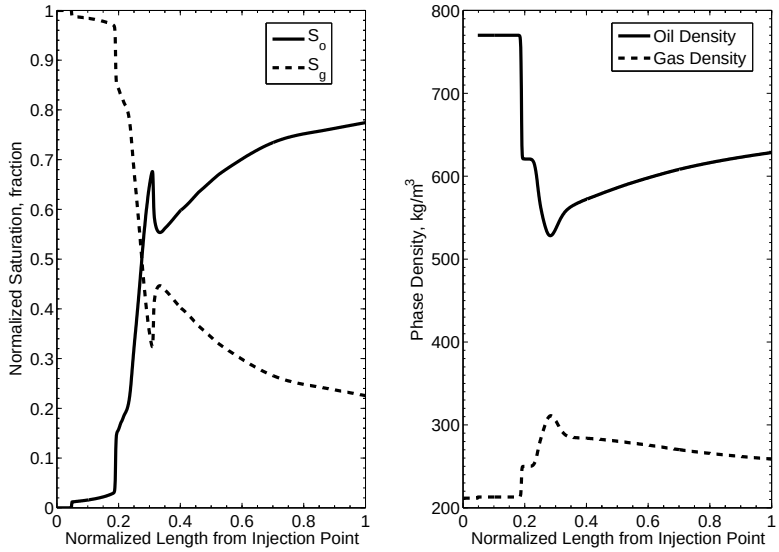

Figure 1.37: Snapshots of phase saturation (left) and densities (right) at 300 days (0.3 HCPV injected) for a 1D horizontal displacement at an immiscible displacement pressure of 310 bara by separator gas injection, N = 1000.

Figure 1.37 shows the development of the oil bank for a 1D horizontal flow simulated with 1000 grid cells at pressure of 310 bara. The difference in phase densities re-

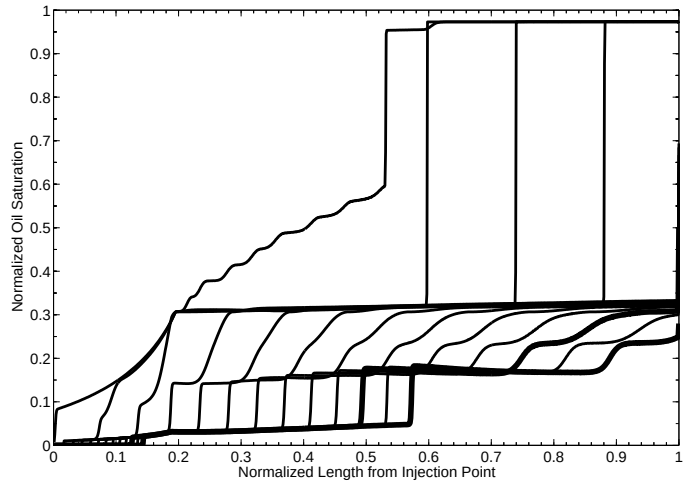

Figure 1.38: Snapshots of oil saturation at different times (HCPVs) for a 1D vertical displacement at an immiscible displacement pressure of 310 bara by separator gas injection, N = 1000. The first line to the left represents the initial state of saturation distribution at the displacement pressure; the rest lines represent saturation change at 0.1 HCPV increment. The thicker lines are snapshots at 1.0 and 1.2 HCPV injected.

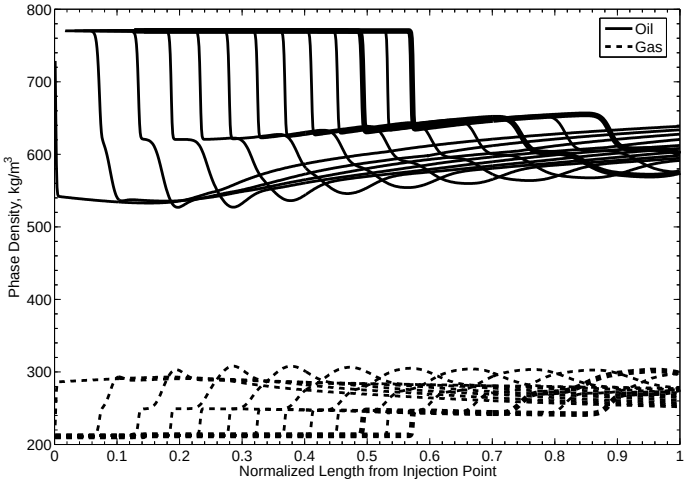

Figure 1.39: Snapshots of phase densities at different times (HCPVs) for a 1D vertical displacement at an immiscible displacement pressure of 310 bara by separator gas injection, N = 1000. The first line to the left represents the initial state of phase densities at the displacement pressure; the rest lines represent change in densities at 0.1 HCPV increment. The thicker lines are snapshots at 1.0 and 1.2 HCPV injected.

mained large but the oil bank still developed at 300 days. For comparison, Figures 1.38 and 1.39 show the change in oil saturation and phase densities respectively for a 1D vertical displacement simulated with 1000 grid cells at the same pressure. The displacement also remained immiscible but the oil saturation close to the producer was much higher in this case due to gravity segregation effect.

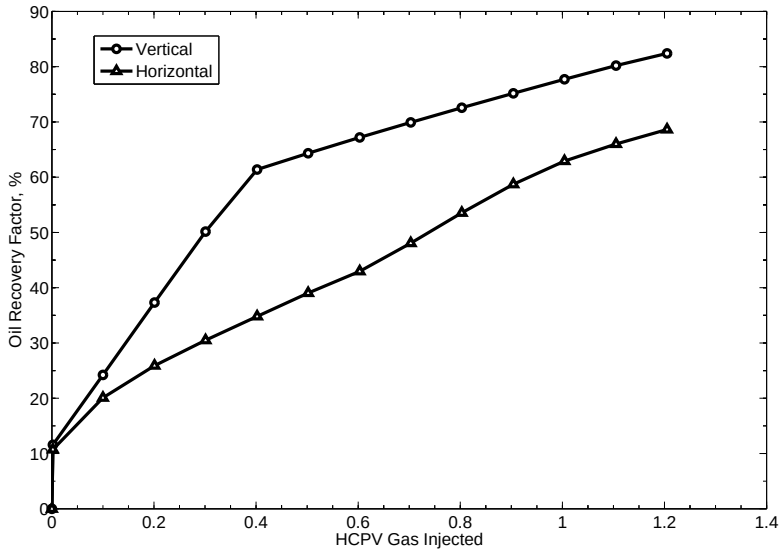

Figure 1.40: Comparison of oil recoveries of a 1D horizontal displacement with a 1D vertical displacement at the same immiscible pressure and used the same number of grid cells (N = 1000). System initialized with compositional variations from isothermal GCE gradient calculation.

Figures 1.40 and 1.41 compare the performance of oil recovery and producing GOR for the 1D horizontal and vertical displacements. The oil recovery at 1.2 HCPV for the vertical displacement was 12% higher than that for the horizontal flow. The combined effects of gravity segregation and the developed C/V oil bank were believed to be responsible for the high oil recoveries for the vertical displacement at low pressure immiscible conditions. The producing GOR performance also is significantly differently.

The combined effects of the developed oil bank and gravity might find general applications to depleted reservoirs (oil and gas condensate) for enriched gas injection. At low pressures, the injection gas still will develop a C/V oil bank at immiscible conditions. With

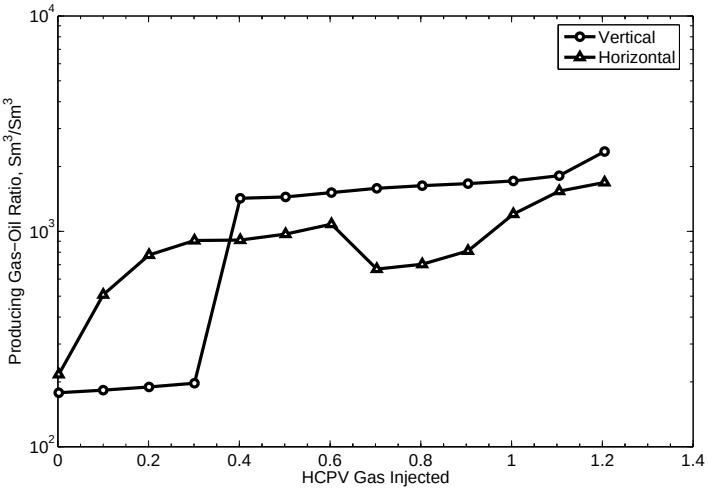

Figure 1.41: Comparison of GOR of a 1D horizontal displacement with a 1D vertical displacement at the same immiscible pressure and used the same number of grid cells (N = 1000). System initialized with compositional variations from isothermal GCE gradient calculation.

the help of gravity, the oil saturation might build up and the oil mobility might increase. The oil could thus be mobilized and recovered. In this process, the developed oil bank could function as an injected LNG slug, but developed at lower costs.

For a saturated gas-oil system, CO_2 might be an ideal injection gas for this process as it can develop C/V mechanism at low pressures and its density is high. If an oil bank is created in the gas cap, it will grow due to gravity and miscibly displace down-structure oil in the oil zone. Therefore, the combined effects of the C/V oil bank and gravity might represent a great potential for improved oil recoveries for reservoirs where the injection gas (continuous or gas slug) can develop C/V mechanism in the gas cap at some low pressures.

1.6.5 Slug Injection

As is already shown in Section 1.5 that dry gas injection and separator gas injection give the same recovery for full pressure maintenance. In this subsection, we show that slug injection of enriched gas might still be an alternative to continuous gas injection for partial pressure maintenance. We recommend that it always be assessed for viability with respect

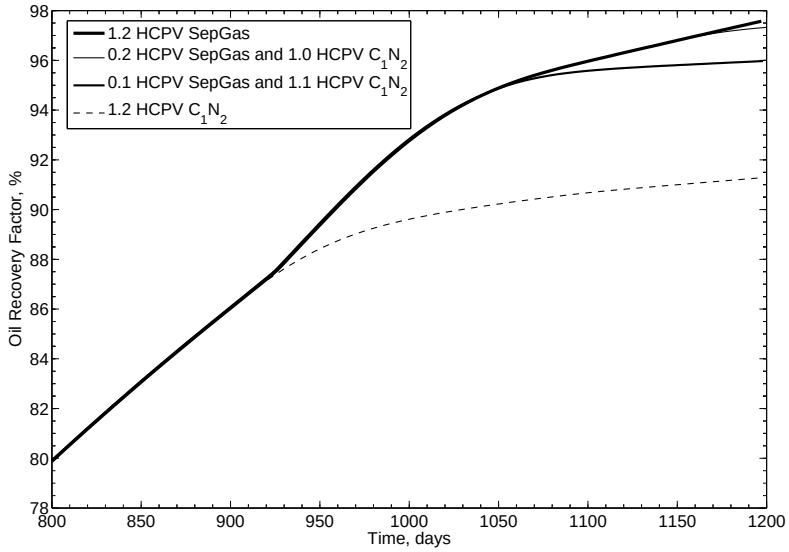

Figure 1.42: Recovery factors for cases with different slug sizes of separator gas injection. p = 359 bara, N = 1000, and liner relative permeability curves with S_{org} = 0. 100 days roughly corresponding 0.1 HCPV injected. System initialized with compositional variations from isothermal GCE gradient calculation.

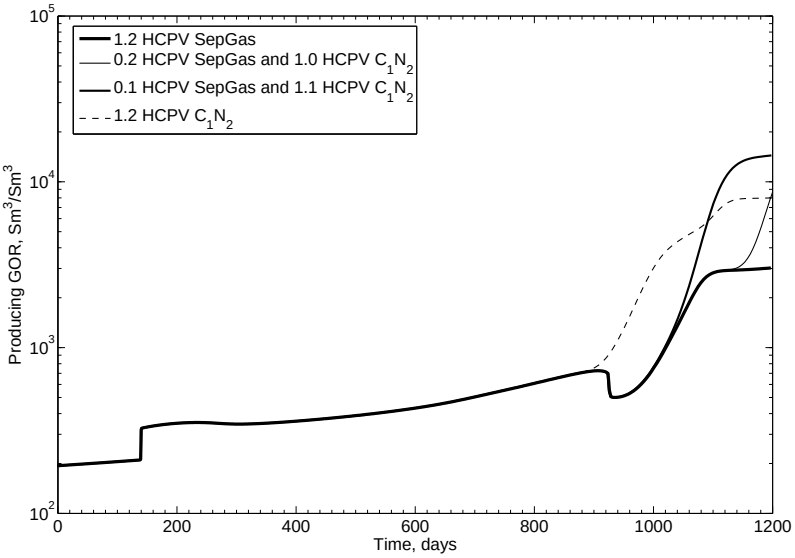

Figure 1.43: Development of producing GOR for cases with different slug sizes of separator gas injection. p = 359 bara, N = 1000, and liner relative permeability curves with S_{org} = 0. System initialized with compositional variations from isothermal GCE gradient calculation.

to continuous injection. We also are aware that multi-dimensional (2D and 3D) simulation models should be used to rigorously determine the size of the gas slug.

Figures 1.42 and 1.43 show comparison of performance of oil recoveries and producing GOR for four 1D horizontal simulation runs at a displacement pressure of 359 bara. All the parameters of these runs were the same except that the injection gases were different at different times. Simulation run with 0.2 HCPV separator injection gas driven by dry gas achieved effectively the same recovery as for continuous separator gas injection. For practical purpose, 0.1 – 0.2 HCPV of separator gas slug driven by the dry injection gas would result in the same oil recovery for this 1D fluid system. GOR development also showed that smaller slug size resulted in a slightly earlier breakthrough of dry gas, but it happened after 1.0 HCPV (1000 days of the simulation time) of gas injected.

1.7 System MMP

The maximum saturation pressure of the fluid system modeled by an isothermal GCE model defines the upper bound pressure for the system MMP. At this pressure, a predominant first-contact miscible displacement can be expected and the injection gas composition has no impact on oil recoveries for a 1D flow. This pressure can readily be determined by a PVT simulator without the involvement of numerical reservoir simulations. The calculation of saturation pressure variations with depth (saturation pressure map) is suffice to define the upper bound pressure for the system MMP of the fluid system.

The relationship between MMP and depth (MMP-depth curve) of the initial reservoir fluids calculated by a PVT program also defines the lower bound for the system MMP – the Shallowest C/V MMP if the C/V mechanism exists. This pressure is a function of the injection gas composition for a specified fluid system. When only the VGD mechanism exists for the entire fluid system, the lower bound and the upper bound pressures for the system MMP collapse at the maximum saturation pressure, i.e. the critical pressure of the GOC fluid.

MMP of a depth-specific fluid, dictated by the equilibrium oil composition shown in Chapter 2, tends to increase as the oil becomes heavier due to interphase mass transfer with the upstream non-equilibrium gases passing over it. The magnitude of the increase in MMP will be affected by the amount of the non-equilibrium gases. Therefore, it is difficult (if possible) to determine a definite MMP for the entire system only based on the calculated MMP by the PVT program . To capture the dynamic change in MMP and determine the MMP for the system as a whole, one must resort to numerical reservoir simulation.

If the reservoir only contains compositionally grading oils and the C/V mechanism exists for these oils, the system MMP is the C/V MMP of the oil at the top, also the lowest C/V MMP found on the initial C/V MMP-depth curve. The presence of a critical (or near-critical) mixture at the undersaturated GOC offers the most favorable situation for miscible displacement by enriched gas injection, as this mixture has the minimum C/V MMP with the injection gas, defining the system MMP for the grading oil reservoir .

If the compositionally grading gas-oil system has a small gas zone and a large oil zone, as the fluid system used in this study, the system MMP might be approximated by the shallowest C/V MMP. On the other hand, if the reservoir has a large gas cap and small oil rim, we suspect that the system MMP will increase toward the upper bound pressure (i.e. the maximum saturation pressure of the fluid system). How much the system MMP will increase will depend on the size of the gas zone where the C/V mechanism does not exist and the reservoir pressure.

1.8 2D Cross-Section Modeling

The 1D models were intended to investigate the system MMP, the miscibility mechanisms and the microscopic recovery efficiencies. However, no ideal slimtube type reservoir exists in reality. Geological features also must be incorporated in a multi-dimensional model to reflect heterogeneities for field studies. Layering with strong permeability contrast and effect of gravity are important factors to be taken into account.

In this Section, we present simulation results for 2D x-z cross-sectional models exhibiting strong permeability contrast. A two-geological-layer conceptual model and a more detailed eight-geological-layer model initialized with the compositional grading fluids shown in Figure 1.3 were constructed to study the effect of gravity segregation and volumetric sweep. These two models had a formation dip angle of 3.8°.

All the simulation runs were performed at the reservoir pressure of 393 bara, a few bar higher than the maximum saturation pressure of the original fluid system and for 18250 days (50 years). One year of gas injection in model was roughly equivalent to 0.03 HCPV of gas injected.

1.8.1 Two-Geological-Layer Model

A two-geological-layer x-z cross section model (1000 x 6.6 m) was built with each geologic layer 3.28 m thick, one layer with 50 md permeability and the other with 500 md. Vertical permeabilities were set to one-tenth of the value of horizontal permeabilities. Both layers were fully perforated at the injector and the producer. As expected, the reservoir performance was dominated by the high permeability layer of the model. Vertical grid refinement from 500x1x2 to 500x1x8 were simulated. The impact of vertical grid refinement on oil recovery was found to be negligible. Various cases were run to study the order of permeability distribution and the degree of vertical communication between these layers.

High-Permeability-Layer Order

The location of high permeability (high-k) layer was found to be important for the two-geological-layer model. Results of two simulation cases are presented to show the effect of the order of the high permeability layer. In one case, the high permeability layer was placed at the top; in the other case, the high permeability layer was located at the bottom. Full pressure communication between the two geological layers was enabled.

Figure 1.44 shows the oil recovery and the GOR development for these two cases. Efficient gravity segregation resulted for the high-permeability layer at the bottom, with

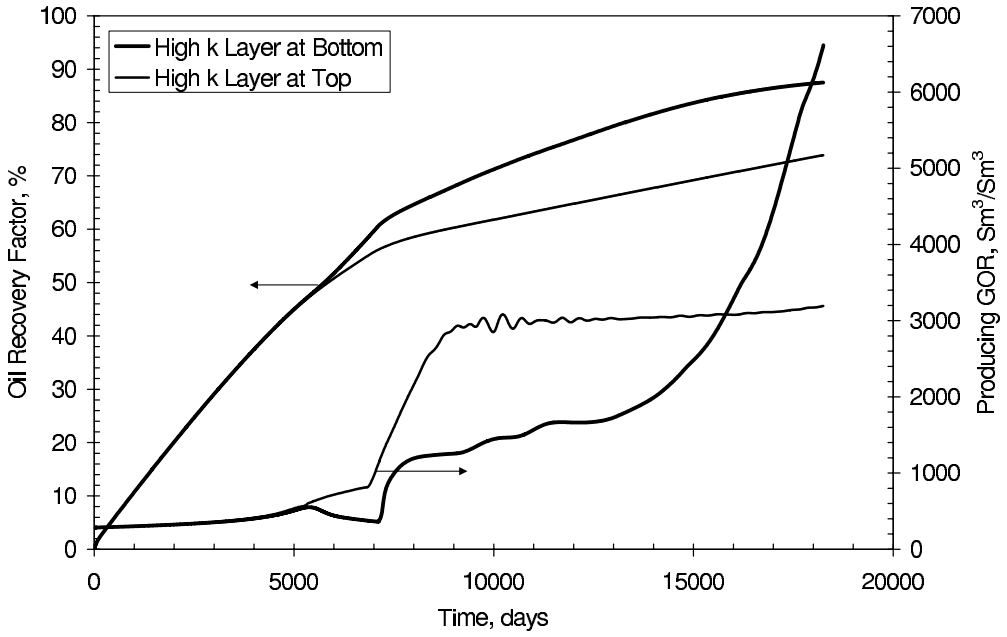

Figure 1.44: Recovery and GOR performance for runs with high permeability layer located at top and bottom. p = 393 bara, SMS gas injection, and 3650 days corresponding to approximately 0.3 HCPV injected.

the ultimate oil recovery 13% higher than with the high-k layer at the top. The GOR development also was substantially different, with a prolonged lower GOR period for high-k layer at the bottom. Drop in GOR after 5000 days for the run that high permeability layer was placed at bottom indicated that the oil in the upper low permeability layer segregated to the lower high permeability layer due to gravity effect.

Figures 1.45 to 1.48 show oil saturation distributions at different times for the run where high permeability layer was located at bottom. At 1095 days, shown in Figure 1.45, no significant segregation of the oil from the upper layer into the bottom layer was observed because the difference in phase densities was not large enough. At 1460, 1825 and 2190 days, the oil in the upper layer segregated into the bottom layer and the distance between the two moving fronts in these layers tended to decrease.

In contrast, Figures 1.49 to 1.52 show oil saturation maps of the run where the high-k layer was located at the top. No gravity effect was observed. This is consistent with the performance of producing GOR as shown in Figure 1.44.

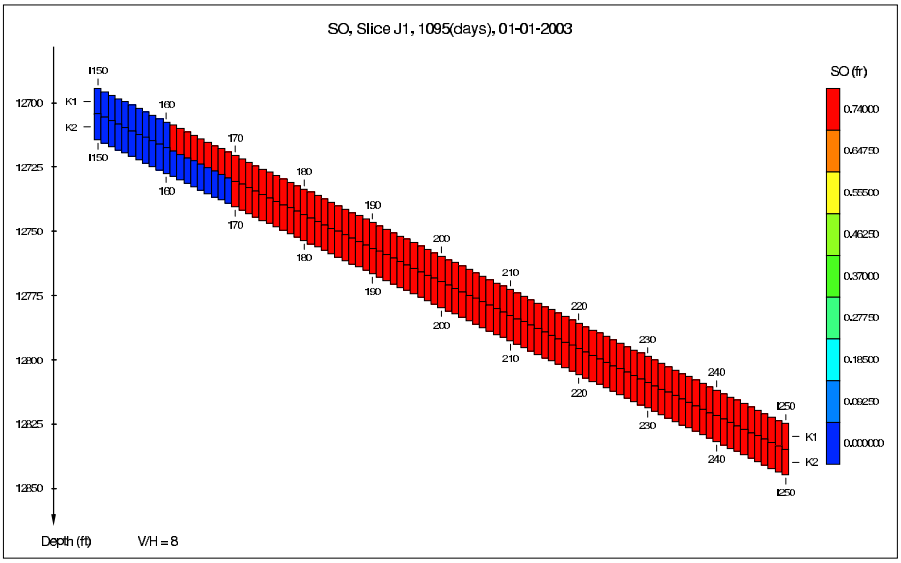

Figure 1.45: Oil saturation map at 1095 days of the run where high permeability layer was located at bottom. p = 393 bara, SMS gas injection.

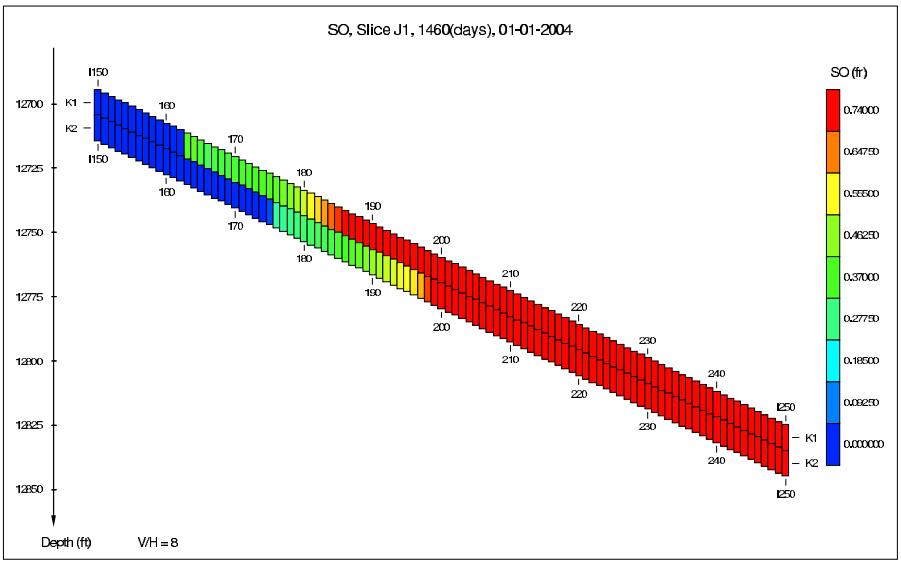

Figure 1.46: Oil saturation map at 1460 days of the run where high permeability layer was located at bottom. p = 393 bara, SMS gas injection.

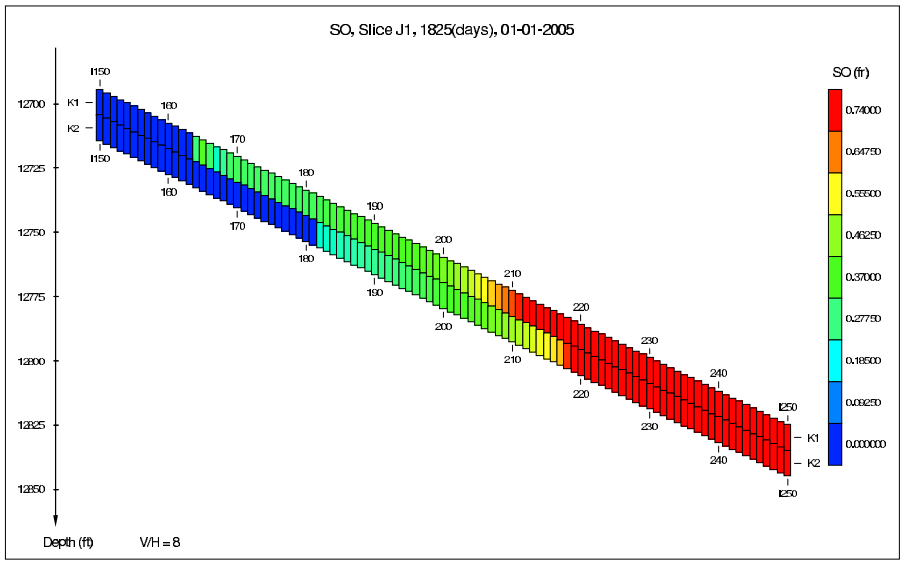

Figure 1.47: Oil saturation map at 1825 days of the run where high permeability layer was located at bottom. p = 393 bara, SMS gas injection.

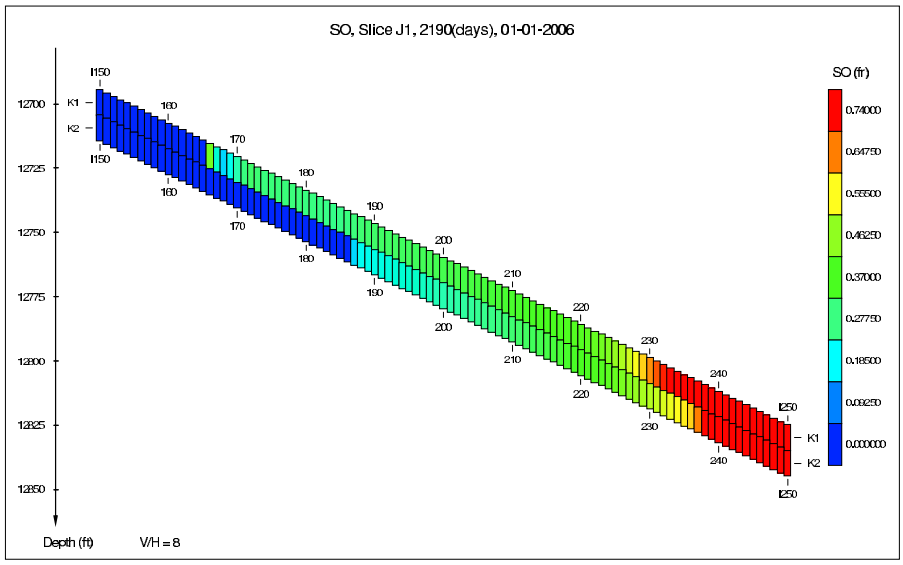

Figure 1.48: Oil saturation map at 2190 days of the run where high permeability layer was located at bottom. p = 393 bara, SMS gas injection.

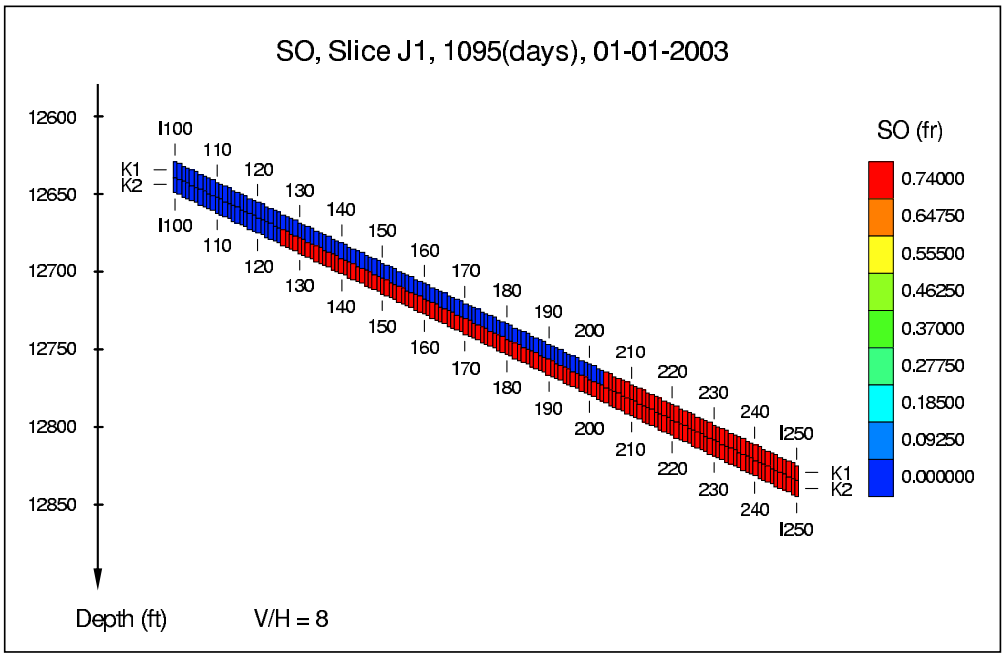

Figure 1.49: Oil saturation map at 1095 days of the run where high permeability layer was located at top. p = 393 bara, SMS gas injection.

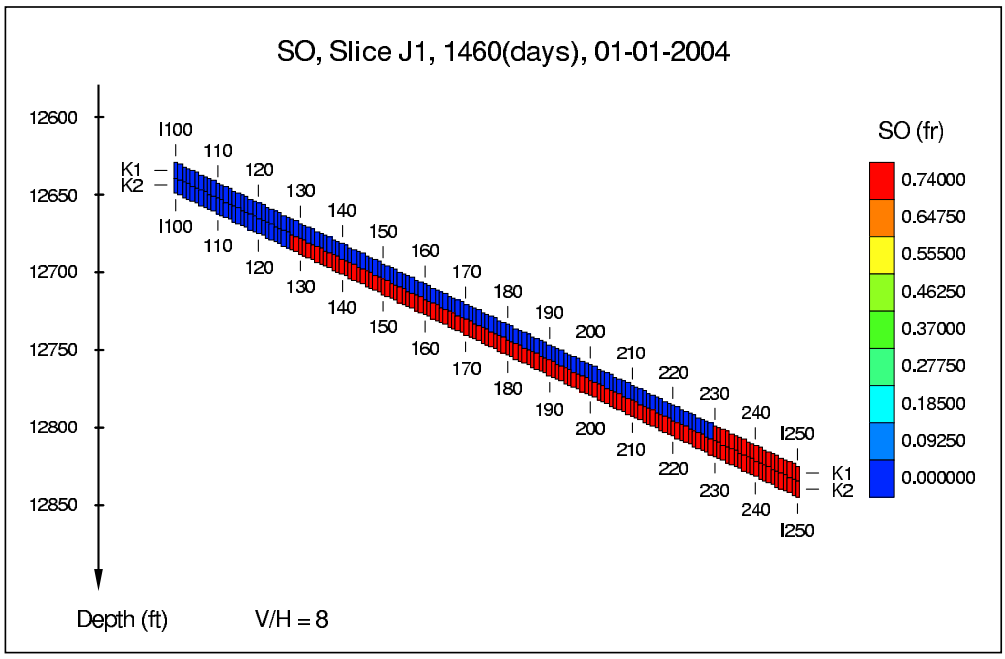

Figure 1.50: Oil saturation map at 1460 days of the run where high permeability layer was located at top. p = 393 bara, SMS gas injection.

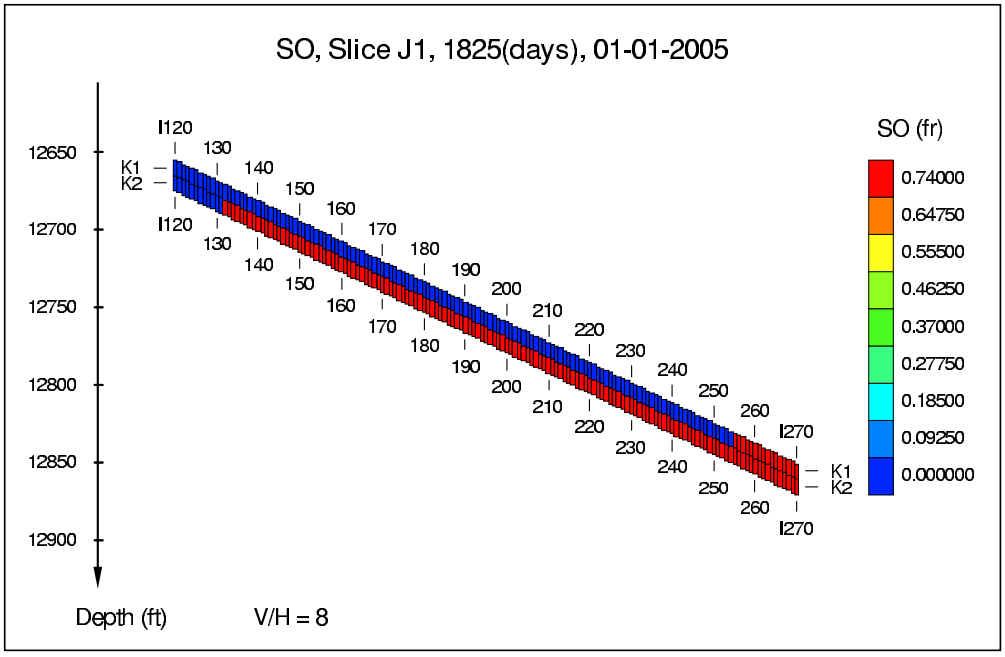

Figure 1.51: Oil saturation map at 1825 days of the run where high permeability layer was located at top. p = 393 bara, SMS gas injection.

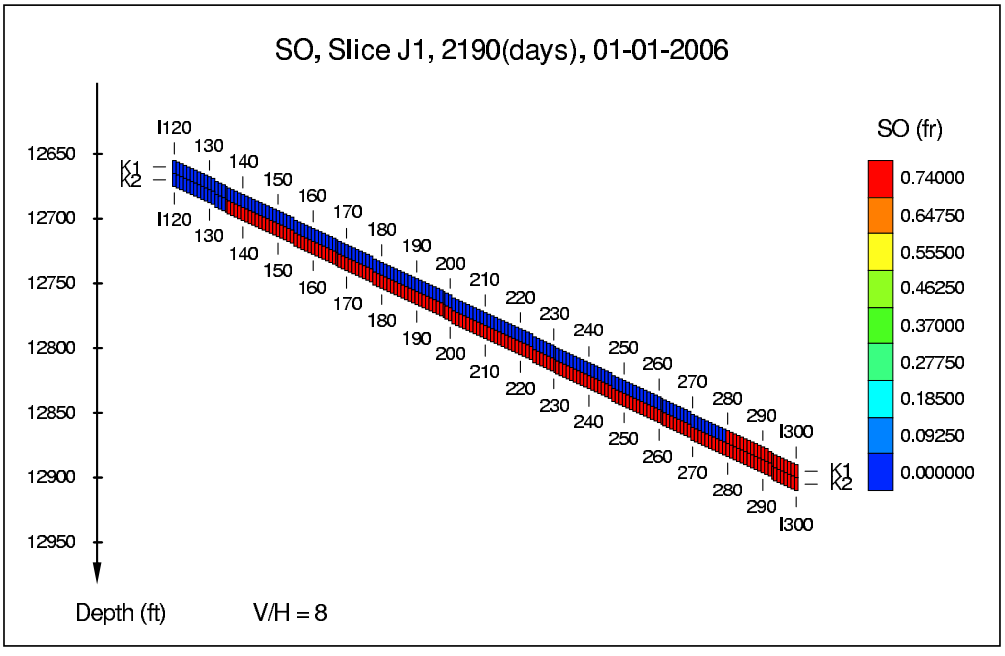

Figure 1.52: Oil saturation map at 2190 days of the run where high permeability layer was located at top. p = 393 bara, SMS gas injection.

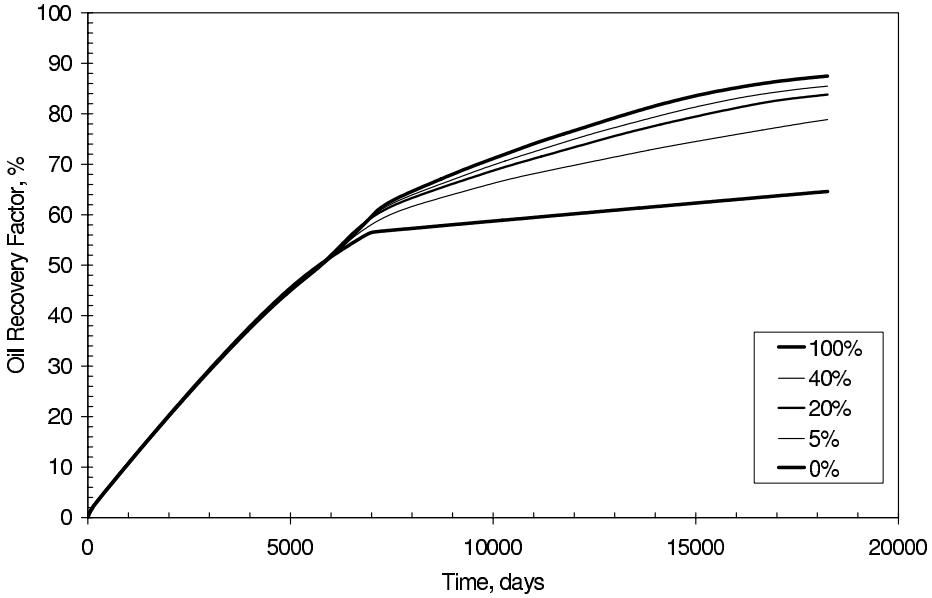

Figure 1.53: Comparison of oil recovery performance for runs with different degrees of vertical communication between the two layers. High permeability layer was located at the bottom. p = 393 bara, SMS gas injection, and 3650 days corresponding to approximately 0.3 HCPV injected.

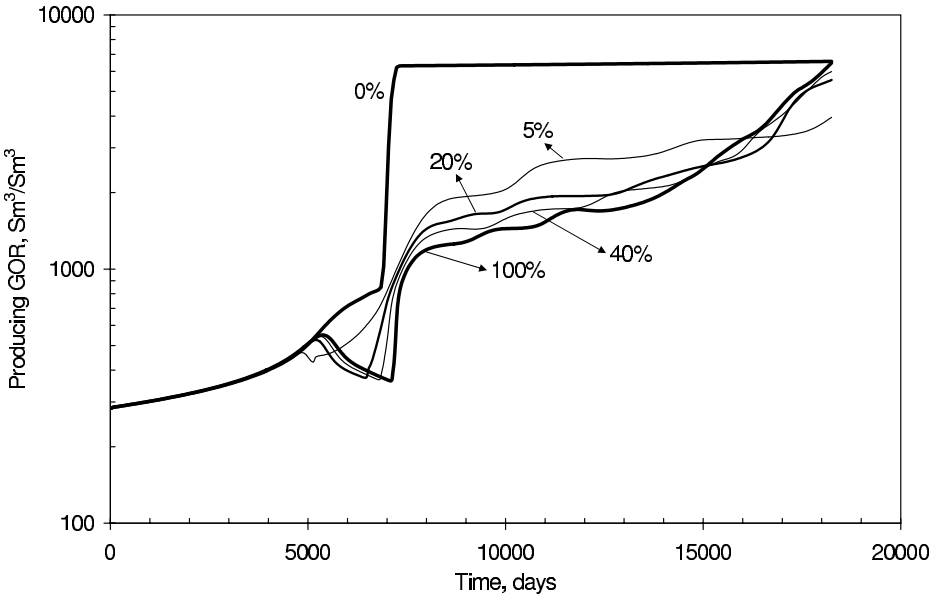

Figure 1.54: Comparison of producing GOR performance for runs with different degrees of vertical communication between the two layers. High permeability layer at the bottom. p = 393 bara, SMS gas injection, and 3650 days corresponding to approximately 0.3 HCPV injected.

Vertical Communication

We also introduced partial barriers between the two geological layers by modifying z-direction transmissibilities (TZ). We found that vertical communication between these two layers showed different sensitivities for different model configurations.

Figure 1.53 shows oil recovery performance for runs having different degrees of vertical communication between the two layers for the model that the high permeability layer was located at the bottom. With increased degree of vertical communication, the oil recovery also increased. It also is observed that the ultimate oil recovery was more sensitive to the existence of vertical communication rather than the degree of vertical communication. For example, when there was no vertical communication, the ultimate oil recovery was 65%. When the degree of vertical communication was increased only by 5%, the ultimate oil recovery increased by 14%. Further increase in the degree of vertical communication did not result in that significant increase in the ultimate oil recoveries. When vertical communication was fully enabled, the ultimate oil recovery reached 87.5%.

Producing GOR development is shown in Figure 1.54 for the same simulation runs as presented in Figure 1.53. It may be expected that GOR performance of the model was dominated by the high permeability layer as the flow capacity (kh) of the layer is ten times higher than that of the other layer. Drop in producing GOR resulted from the production of low GOR oils that had been pushed down from the upper layer to the lower layer as gas segregated. With no vertical communication, GOR performance changed the character dramatically.

Figures 1.55 and 1.56 show the impact of layer communication for the model that the high permeability layer was located at top. Less impact of vertical communication on oil recoveries and producing GOR performance was found. For example, drop in GOR in Figure 1.54 for the cases that the high permeability layer located at bottom was not observed for these cases. Even with only 5% vertical communication, oil recovery and GOR performance was almost identical to the case of 100% vertical communication. As expected, performance was identical for the non-communication cases, regardless the high

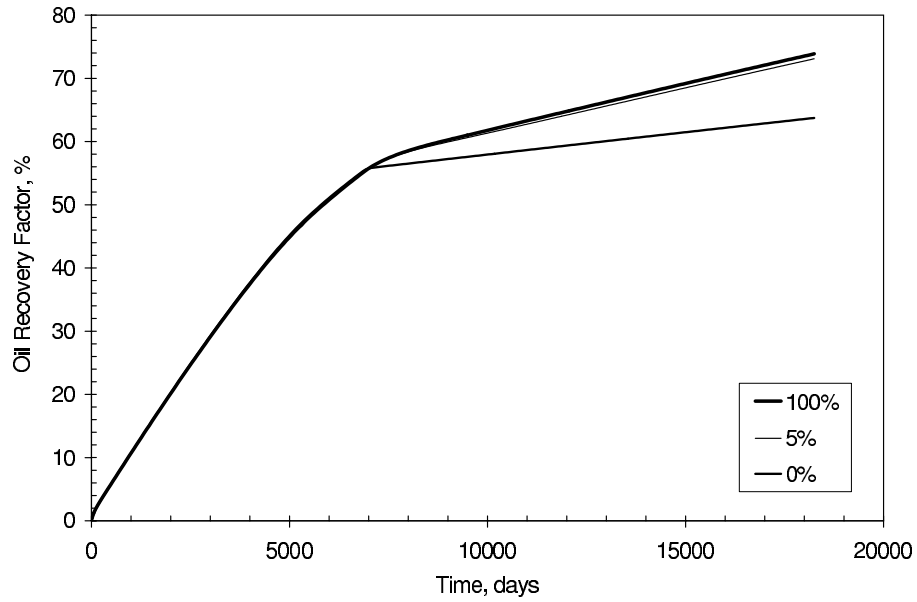

Figure 1.55: Comparison of oil recovery performance for runs with different degrees of vertical communication. High permeability layer at the top. p = 393 bara, SMS gas injection. 3650 days corresponding to approximately 0.3 HCPV injected.

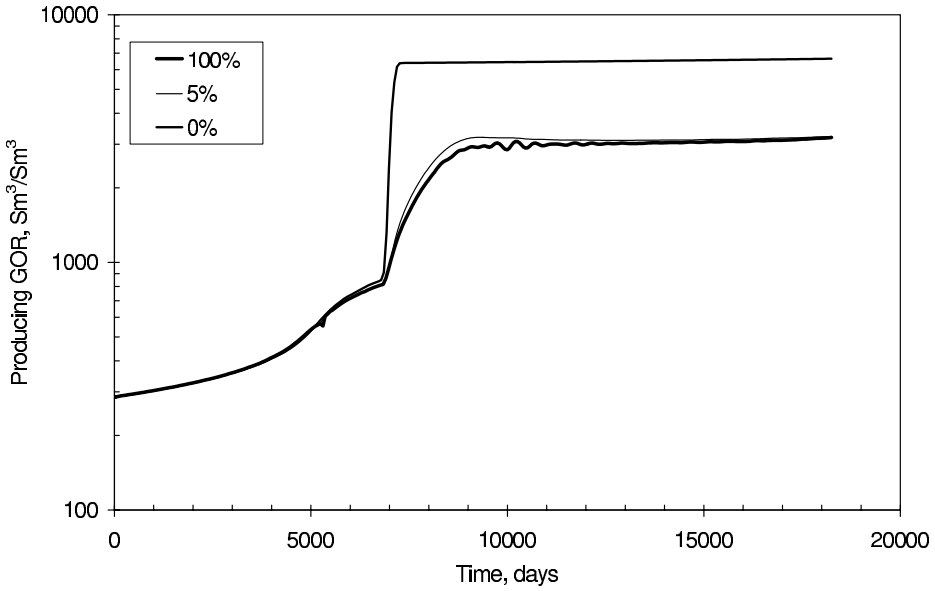

Figure 1.56: Comparison of producing GOR performance for runs with different degrees of vertical communication. High permeability layer at the top. p = 393 bara, SMS gas injection. 3650 days corresponding to approximately 0.3 HCPV injected.

permeability layer was located at top or at bottom.

1.8.2 Eight-Geological-Layer Model

This subsection presents simulation results for an eight-geological-layer x-z cross-sectional model (3000 x 52 m). Layer properties such as permeability, thickness, and porosity were assigned based on the Smorbukk South field data and given in Table 1.7. The first four geological layers represented the Garn formation unit 2 (Garn2) and the last four layers represent the Garn formation unit 1 (Garn1). Vertical permeabilities were 0.7 times of horizontal permeabilities for all the layers. Note that layer No. 5 had the highest flow capacity.

Though this model was still over-simplified compared with actual geological description and the heterogeneities of the field, it did capture important features of layer permeability distribution and communication between the two Garn units. All cases shown here maintained the reservoir pressure at 393 bara, a few bar higher than the maximum GOC saturation pressure of 389 bara. Most simulations used a 500x1x8 grid. Little increase (by about 3%) in the ultimate oil recovery was found when the model was simulated using a 500x1x80 grid.

Table 1.7: LAYER PROPERTIES OF THE EIGHT-LAYER MODEL.

Layer #	k_h md	Thickness m	porosity %
1	60	5.2	0.12
2	65	5.2	0.12
3	65	5.2	0.12
4	65	5.2	0.11
5	500	5.2	0.14
6	165	5.2	0.14
7	80	9.1	0.12
8	30	12.2	0.12

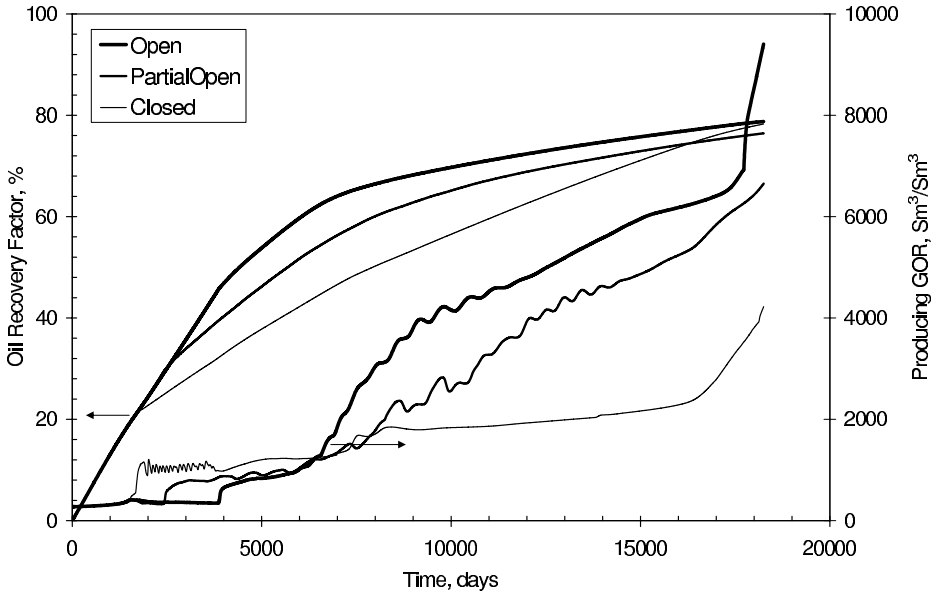

Figure 1.57: Oil recovery and GOR performance for the eight-layer dipping reservoir with varying permeabilities and degree of vertical communication. p = 393 bara, N = 500. SMS gas injection, and 3650 days corresponding to approximately 0.3 HCPV injected.

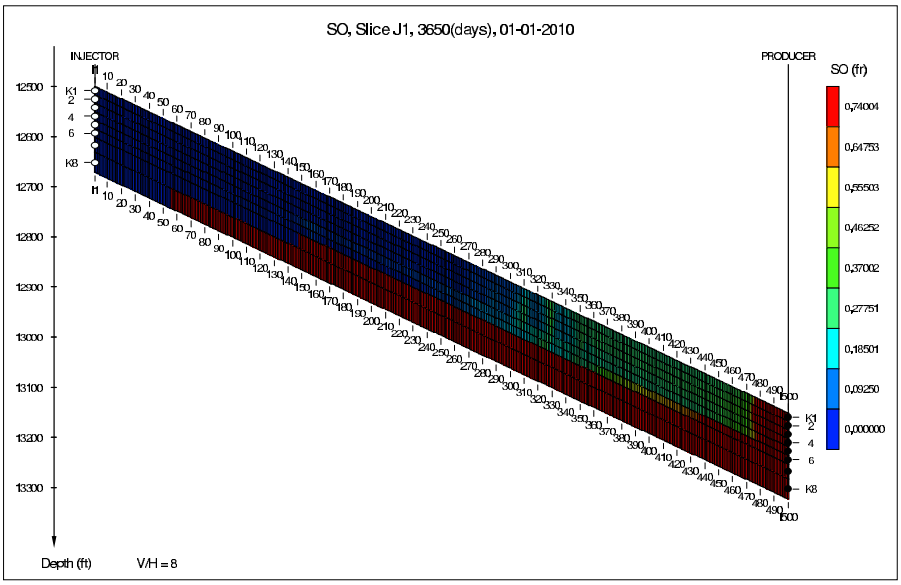

Figure 1.58: Oil saturation map at 3650 days for the eight-layer dipping reservoir with varying permeabilities and complete (100%) vertical communication, p = 393 bara, N = 500, SMS gas injection, and 3650 days corresponding to 0.3 HCPV injected.

Layer Communication

Figure 1.57 shows the recovery and GOR performance for the eight-layer model for varying degrees of vertical communication between the layers 4 and 5 (between Garn1 and Garn2). Recovery was accelerated with increasing degree of vertical communication, though the ultimate recoveries were not significantly affected. Gas breakthrough also was delayed when the degree of communication was increased.

Figure 1.58 shows a snapshot of oil saturation distribution for the case of full vertical communication after 10 years production when recovery factor was about 43%. Gas had yet to break through at the producer. In this case, the eight-layer model might be perceived as a two-layer model with the highest kh layer (layer 5) separating the two 'apparent' layers.

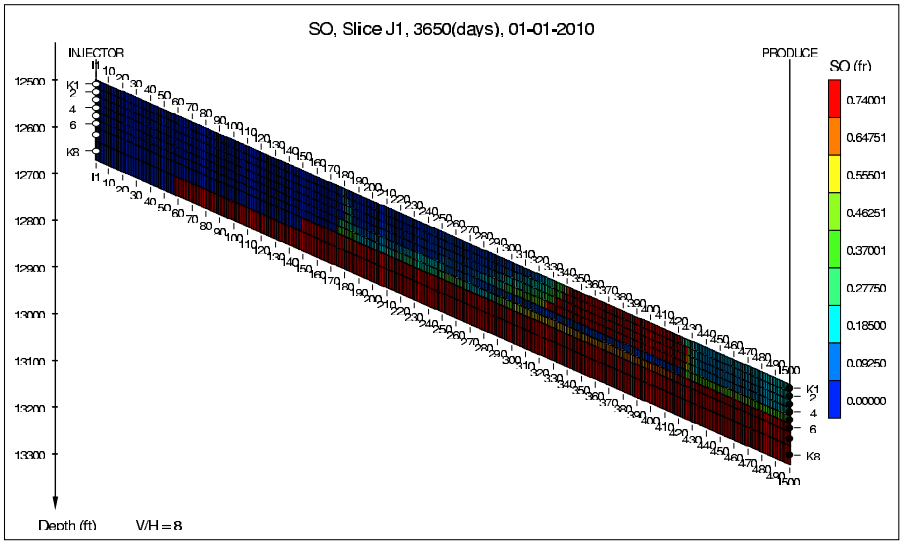

Figure 1.59: Oil saturation map at 10 years for the eight-layer dipping reservoir with varying permeabilities and partial vertical communication, p = 393 bara, N = 500, SMS gas injection.

Partial vertical communication between layers of Garn unit 1 and 2 was introduced by zeroing out 70% of TZ values of layer 4. This was supported by the geological feature of the Smorbukk South field, which a potentially partly open shale barrier exists between Garn1 and Garn2 due to the presence of faults. The first 35% grid cells close to the injector had no communication, followed by 15% being open, followed by 35% being closed, and

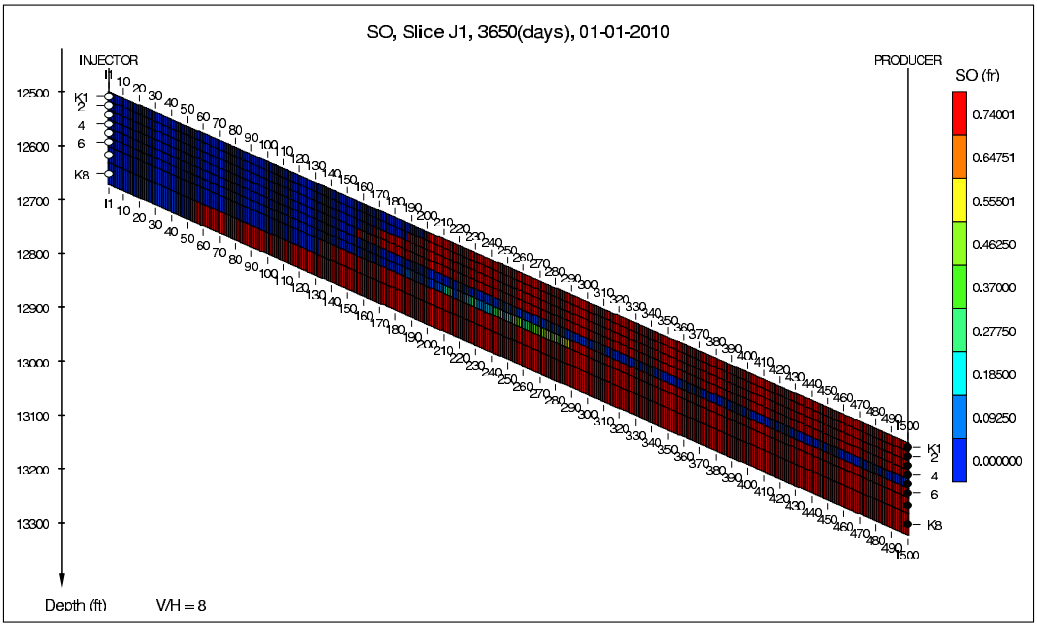

Figure 1.60: Oil saturation map at 10 years for the eight-layer dipping reservoir with varying permeabilities and no vertical communication, p = 393 bara, N = 500, SMS gas injection.

followed by the last 15% being open. Figure 1.59 shows a snapshot of oil saturation for the case of partial communication after 10 years production when recovery factor was about 38%. Gas had already broken through at the producer and GOR increased slowly.

For comparison, Figure 1.60 shows the oil saturation distribution for the case of no vertical communication between Garn1 and Garn2 after 10 years production. In this case, the eight-layer model might be regarded as a three-layer model. Layers on top of the highest kh layer (layer 5) might be seen as one ‘apparent’ layer; layers below the highest kh layer might be roughly regarded as another ‘apparent’ layer; and the highest kh layer itself might be considered as one ‘apparent’ layer.

2D simulations showed that gravity segregation was an efficient recovery process. GOR performance showed a strong link to the degree of vertical communication between Garn units 1 and 2, higher degree of vertical communication resulting in later increase in GOR. This might be used as a key history matching parameter in field-scale simulation studies.

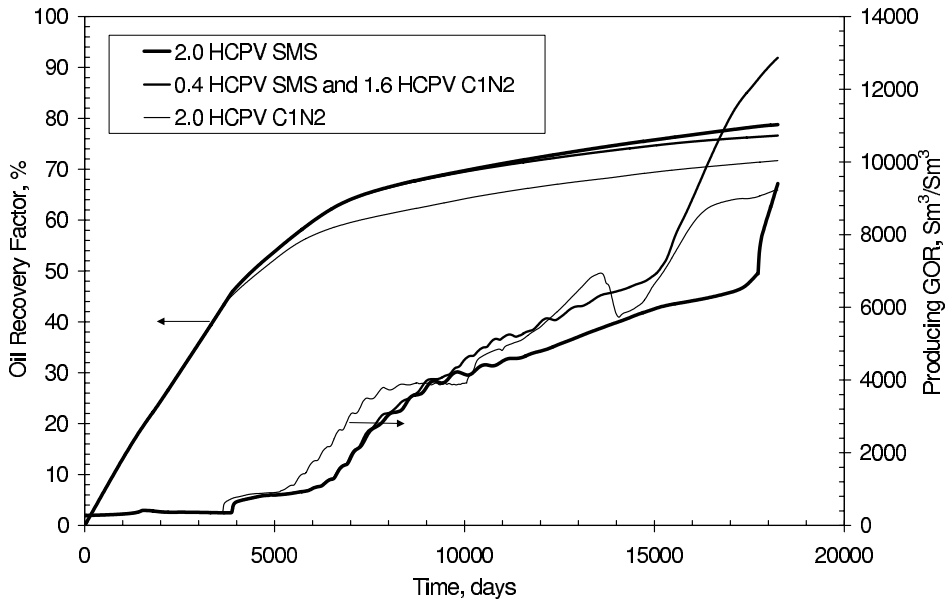

Figure 1.61: Comparison of oil recovery and GOR performance for different injection gases for the eight-layer dipping reservoir with varying permeabilities, p = 393 bara, N = 500. 3650 days corresponding to approximately 0.3 HCPV injected.

Injection Gas Composition

Slug injection also was simulated for the eight-layer model. This subsection presents the simulation results for slug injection for full pressure maintenance. Full vertical communication between Garn1 and Garn2 was allowed.

Three cases were simulated to compare recovery efficiencies:

1. 2.0 HCPV continuous SMS gas injection;

2. 0.4 HCPV SMS gas injection followed by 1.6 HCPV dry gas injection;

3. 2.0 HCPV continuous dry gas injection.

Figure 1.61 shows the oil recovery and GOR performance for these cases. Continuous SMS gas injection resulted in the ultimate oil recovery of 78.7%, 6% higher than that for continuous dry gas injection and 2% higher than for SMS gas slug injection. Increase in GOR occurred slightly earlier for continuous dry gas injection. Little difference was found

between the continuous SMS gas injection and the 0.4 HCPV SMS gas followed by 1.6 HCPV dry gas injection.

From 1D simulations, we would expect no difference in performance for these cases as the reservoir pressure was higher than the saturation pressure of the GOC mixture and any gas would have a system MMP equal to the maximum saturation pressure of the fluid system for 1D flow. The results shown here were clearly affected by the flow path caused by layer permeability distribution and the effect of gravity segregation. Vertical flow among the layers altered the first-contact miscible nature in the model and was believed to be responsible for the difference in performance for these three injection cases. In addition, sweep efficiency could also be affected by the density differences between the injection gases and the reservoir fluids.

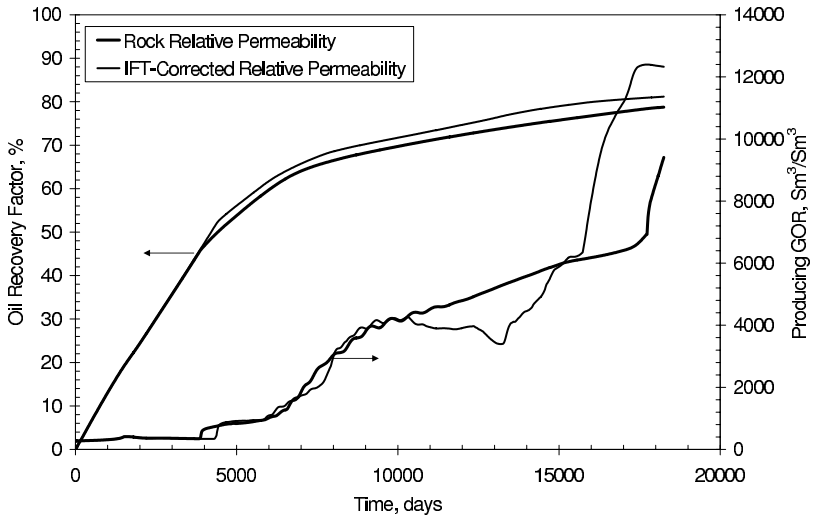

Figure 1.62: IFT effect on relative permeability and impact on oil recovery and GOR performance using SMS gas injection in the eight-layer model, p = 393 bara, N = 500.

Relative Permeability Treatment

All the 2D simulation results presented thus far have used the input rock curves without alternation of relative permeability due to reduced gas-oil IFT. The 3D full-field model (not presented here) showed significant difference in GOR and oil recovery from different treat-

ments of the relative permeabilities. Comparison was made for the effect of IFT reduction on oil recoveries for the 2D model and shown in Figure 1.62. Simulations were run at 393 bara using a 500x1x8 grid.

Gas breakthrough was delayed slightly for IFT-corrected relative permeability curves, resulting in an increase in recoveries of about 2% after 5000 days of production. This difference increased only slightly during the next 15 years, reaching a maximum difference of only 3%. It is clear that introducing IFT dependent relative permeability curves in the 2D model did not affect oil recovery significantly.

1.9 Conclusions

This section summarizes this chapter, presenting the most important conclusions from the study. We believe that the conclusions from 1D simulation study are general and applicable to any undersaturated gas-oil system for 1D flow. Contributions and recommendations for future research also are given in each subsection.

1.9.1 Conclusions

This study has led to the following conclusions:

1. The system MMP for an undersaturated gas-oil system was found to be in the limited range between the shallowest C/V MMP and the maximum saturation pressure of the fluid system, if C/V mechanism exists for an injection gas. If only VGD mechanism exists, the system MMP is defined by the maximum saturation pressure, which is the upper bound pressure for the system MMP.

2. When the reservoir pressure is maintained at/above the maximum saturation pressure in a 1D displacement, *any* injection gas will lead to system miscibility (near-100% oil recoveries at all depths). The main miscibility mechanism is first-contact miscible. Multi-contact miscibility might only be excepted at the point of injection.

Furthermore, oil recovery is independent of reservoir formation dip angles. Therefore, the optimal injection gas for full pressure maintenance is always the cheapest gas available for injection.

3. It is possible to achieve miscibility under partial pressure maintenance by enriched gas injection. The miscibility mechanism is predominately the multi-contact condensing/vaporizing mechanism.

4. The system MMP might be approximated by the shallowest C/V MMP for an undersaturated gas-oil system where the gas zone is relatively small, such as the fluid system used in this study. For an undersaturated gas-oil system where the gas zone is large and the VGD mechanism exists in the upper part of the gas zone, the system MMP tends to approach the maximum saturation pressure of the fluids system, which is the upper bound pressure for the system MMP. How much it will increase depends on the size of the gas zone where the VGD mechanism exists. In this case, the benefit of enriched gas injection might be very limited. Cheapest available injection gas operated at the upper bound for the system MMP might be more economically viable.

5. For an undersaturated gas-oil system, if the main recovery target is the grading oil zone, enriched gas injection at the undersaturated GOC might be considered.

6. For any 1D flow path (e.g. a streamline), once an injection gas develops multi-contact miscibility with a reservoir fluid and a leading-edge oil bank, this oil bank will first-contact miscibly displace any downstream oil – independent of whether the downstream oil is miscible or not with the injection gas. A leading-edge oil bank miscible displacement can result from either the VGD mechanism of gas displacing oil, or C/V mechanism (gas displacing reservoir gas or oil).

7. It was found that an oil bank still will develop at immiscible conditions if the C/V mechanism exists, but at a reduced size. The combined effects of the development of the C/V oil bank and gravity might represent a potential for improving (accel-

erating) oil recoveries for two-phase reservoirs at low pressures by enriched gas or CO_2 injection, preferentially for high vertical permeability and high structural relief reservoirs.

8. 2D cross-section studies showed that gravity segregation can be a very efficient recovery process in the development of undersaturated gas-oil reservoirs.

1.9.2 Summary of Contributions

1. We have demonstrated that it is possible to develop a miscible displacement by enriched gas injection for an undersaturated gas-oil system at pressures lower than its maximum saturation pressure.

2. Two pressure bounds for the system MMP have been identified, which can be calculated by a PVT simulator with an MMP option. We also have demonstrated the dynamic nature of the system MMP for an undersaturated gas-oil reservoir, which should be captured by numerical simulations.

3. Another contribution has been the finding that once an injection gas develops C/V mechanism and a leading-edge oil bank, the developed oil bank will miscibly displace any downstream oil.

1.9.3 Recommendation for Future Research

The reason why the system MMP was somewhat lower than the shallowest C/V MMP for CO_2-enriched gas injection is not clear. It could be because the oil saturation was too low to develop miscibility at the shallowest C/V MMP. At somewhat lower pressure, oil saturation increased for the downstream fluids. The downstream fluids had a C/V MMP equal to the reservoir pressure and thus developed miscibility. In Chapter 2, we show that some level of oil saturation prior to gas injection is required for the condensing/vaporizing mechanism to develop.

Another potential research topic following this work could be to investigate the immiscible recovery efficiency and the feasibility by CO_2 or other enriched gases injection in depleted oil and gas condensate reservoirs where vertical flow is expected to be strong (e.g. high vertical permeability and high structural relief reservoirs).

1.10 Nomenclature

AF	=	acentric factor of component
$C/VMMP$	=	condensing/vaporizing minimum miscibility pressure, bara
kh	=	flow capacity, product of layer thickness and permeability, m-md
k_h	=	horizontal permeability, md
MW	=	molecular weight of component, kg/kmol
N_c	=	name of component
p	=	reservoir pressure, bara
p_c	=	critical pressure of component, bara
$PCHOR$	=	parachor of component
p_s	=	saturation pressure, bara
RF	=	recovery factor, percent
T_c	=	critical pressure of component, K
Z_c	=	critical Z-factor of component
Δx	=	grid cell size in x-direction

1.11 References

1. Schulte, A.M.: "Compositional Variations within a Hydrocarbon Column due to Gravity," paper SPE 9235 presented at the 1980 SPE Annual Technical Conference and Exhibition, Dallas, Sept. 21-24.

2. Huang, W.W.: "Some Experiences with a Critical Reservoir Fluid," paper SPE 14415 presented at the 1985 SPE Annual Technical Conference and Exhibition, Las Vegas, September 22-25.

3. Broekers, M.P. and van Dorp, W.G.: "Miscible Gas Drive in Unit 1 of the Statfjord Reservoir," paper SPE 15876 presented at the SPE European Petroleum Conference, London, October 20-22.

4. Hoier, L. and Whitson, C.H.: "Compositional Grading - Theory and Practice," SPEREE, Dec. 2001, 535-545.

5. Riemens, W.G., Schulte, A.M., and de Jong, L.N.J.: "Birba Field PVT Variations Along the Hydrocarbon Column and Confirmatory Field Tests," JPT (Jan. 1988) 40, No. 1, 83-88.

6. Jaramillo, J.M. and Barrufet, M.A.: "Effects in the Determination of Oil Reserves Due to Gravitational Compositional Gradients in Near-Critical Reservoirs," paper SPE 71726 presented at the 2001 Annual Technical Conference and Exhibition, New Orleans, Sept. 30-Oct. 3.

7. Metcalfe, R.S., Vogel, J.L., and Morris, R.W.: "Compositional Gradient in the Anschutz Ranch East Field," paper SPE 14412 presented at the 1985 SPE Annual Technical Conference and Exhibition, Las Vegas, Sept. 22-25.

8. Takahashi, K., Fevang, O., and Whitson, C.H.: "Fluid Characterization for Gas Injection Study Using Equilibrium Contact Mixing," paper SPE 78483 presented at the

2002 the 10th Abu Dhabi International Petroleum Exhibition and Conference, Abu Dhabi, Oct. 13-16.

9. Smith, R.W., Bard, W.A., Lugo, C., Yemez, I. Guerini, A., Whitson, C.H. and Fevang, .: "Equation of State of a Complex Fluid Column and Prediction of Contacts in Orocual Field, Venezuela," paper SPE 63088 presented at the 2000 SPE Annual Technical Conference and Exhibition, Dallas, Oct. 1-4.

10. Stalkup, F.I.: "Displacement Behavior of the Condensing/Vaporizing Gas Drive Process," paper SPE 16715 presented at the 1987 SPE Annual Technical Conference and Exhibition, Dallas, Texas, Sept. 27-30.

11. Stalkup, F.I., Jr.: *Miscible Displacement*, Monograph Series, SPE, Richardson, TX (1984).

12. Whitson, C.H. and Brule, M.R.: *Phase Behavior*, Monograph Series, SPE, Richardson, TX (2000).

13. Zick, A.A.: "A Combined Condensing/Vaporizing Mechanism in the Displacement of Oil by Enriched Gases," paper SPE 15493 presented at the 1986 SPE Annual Technical Conference and Exhibition, New Orleans, Oct. 5-8.

14. Johns, R.T., Fayer, J.F. and Orr, F.M., Jr. "Analytical Theory of Combined Condensing/Vaporizing Gas Drives," paper SPE 24112 presented at the 1992 SPE/DOE Symposium on Enhanced Oil Recovery, Tulsa, April.

15. Hoier, L.: "Miscibility Variations in Compositionally Grading Petroleum Reservoirs," Thesis for Dr.ing, Norwegian University of Science and Technology, NTNU, Nov. 1997.

16. Seto, C.J., Jessen, K., and Orr, F.M., Jr.: "Compositional Streamline Simulation of Field Scale Condensate Vaporization by Gas Injection," paper SPE 79690, SPE Reservoir Simulation Symposium, Houston, TX, Feb. 3-5, 2003.

17. Hoier, L. and Whitson, C.H..: "Miscibility Variation in Compositionally Grading Reservoirs," SPEREE, Feb. 2001, 36-41.

18. Jessen, K., Orr, F.M., Jr.: "Gas Cycling and the Development of Miscibility in Condensate Reservoirs," paper SPE 84070 presented at the 2003 SPE Annual Technical Conference and Exhibition, Denver, Oct. 5-8.

19. Orr, F.M., Jr. et al: "Laboratory Experiments To Evaluate Field Prospects for CO_2 Flooding," JPT (April 1982) 888.

20. Cook, A. B., Johnson, F. S., Spencer, G. B., Bayazeed, A.F. and Walker, C. J.: "Effects of Pressure,Temperature, and Type of Oil on Vaporization of Oil During Gas Cycling, RI 7278, USBM(1969).

21. Cook, A. B., Johnson, F. S., Spencer, G. B., Bayazeed, A.F. and Walker, C. J.: "Realistic K Values of C_{7+} Hydrocarbons for Calculating Oil Vaporization During Gas Cycling at High Pressures, JPT (July 1969).

22. Zick, A.: Personal Communication.

23. Stalkup, F.I., Jr.: "Status of Miscible Displacement," paper SPE 9992 presented at the 1982 SPE International Petroleum Exhibition and Symposium, Beijing, China, March 18-26.

24. Johns, R.T. and Orr, F.M., Jr.: "Miscible Gas Displacements of Multicomponent Oils," SPEJ (March 1996) 39.

25. Wang, Y. and Orr, F.M., Jr.: "Calculation of Minimum Miscibility Pressure," paper SPE 39683 presented at the 1998 SPE/DOE Improved Oil Recovery Symposium, Tulsa, April 19-22.

26. Novosad, Z. and Costain, T.G.: "New Interpretation of Recovery Mechanisms in Enriched Gas Drives," J. Can. Pet. Tech. (March-April 1988) 21, No. 2, 54-60.

27. Zhou, D. and Orr, F.M., Jr.: “Analysis of Rising-Bubble Experments To Determine Minimum Miscibility Pressures,” SPEJ (March 1998) 19.

28. Montel F., Bickert J., and Le Goff C.: “Modeling the Effect of External Gas Flux on Reservoir Fluid Distribution,” paper SPE 77383 presented at the 2002 SPE Annual Technical Conference and Exhibition, San Antonio, Sept. 29-Oct. 2.

29. Chaback, J.J.: “Discussion of Treatment of Variations of Composition with Depth in Gas-Condensate Reservoirs,” SPERE, Feb. 1992, 157-158.

30. Zick A.: Zick Technologies, www.zicktech.com, PhazeComp model.

31. Coats K.H.: “Sensor Users Manual, March 2001,” Coats Engineering, Inc., Website: `www.coatsengineering.com`.

32. Soave, G.: “Equilibrium Constants for a Modified Redlich-Kwong Equation of State,” Chem. Eng. Sci. (1972), 27, 1197-1203.

33. Lohrenz, J., Bray, B. G., and Clark, C. R.: “Calculating Viscosities of Reservoir Fluids From Their Compositions,” J. Pet. Tech. (Oct. 1964) 1171-1176; Trans., AIME, 231.

34. Hearn, C.L. and Whitson, C.H.: “Evaluating Miscible and Immiscible Gas Injection in Safah Field, Oman,” paper SPE 29115 presented at the 1995 13th SPE Symposium on Reservoir Simulation, San Antonio, Feb. 12-15.

Chapter 2

Modeling Physical Dispersion of 1D Multi-Contact Miscible Processes

2.1 Introduction

Physical dispersivity represents one of the major concerns in miscible gas injection, chemical flooding and tracer test applications. Physical dispersion results in dilution of injectant concentrations and even the loss of designed miscibility, thus potentially leading to failure of the project. For oil reservoirs on field-scale, physical dispersion may not be important as the mixing zone is small relative to the distance between the injector and the producer and the oil saturations prior to gas injection usually are high. For lab-scale experiments, however, the effect of physical dispersivity can be crucial.

Physical dispersivity is a rock property that reflects pore-level irregularities of the porous media. Lab measurements reveal that physical dispersivity is in the order of 0.30 cm for consolidated rocks. Perkins and Johnston [1] reviewed physical dispersion for porous media and gave correlations for quantifying physical dispersivity.

For decades, many in the petroleum industry have mixed physical dispersivity with reservoir heterogeneity and too high (orders of magnitude) apparent dispersivities have been used and reported in the literature. Recently, Coats et al [2] pointed out that the

reported large apparent dispersivity is a reflection of reservoir conformance, not the true physical dispersivity of the rock. Under the assumptions made in their simulation study, they demonstrated that heterogeneities alone cause no mixing.

In reservoir modeling, the general approach to modeling physical dispersivity is to emulate it by numerical dispersivity in finite-difference numerical simulation models. Some reservoir simulators also allow direct input of physical dispersivity.

The first objective of this study was to develop an equation for calculating the optimum[1] number of grid cells to accurately emulate physical dispersion in reservoir simulations for 1D first-contact miscible processes. The developed method should be used for simulation models that use single-point upstream mobility weighting and IMPES (implicit in pressure and explicit in saturation) numerical formulation. The method is based on: (1) the analysis of Lantz's equation for numerical dispersion for a finite-difference numerical simulator, and (2) the number of timesteps required for defining the mixing zone where the injectant concentrations ranging from 0.1 to 0.9 at one pore volume (PV) injection. Notes on dispersion in 2004 by Coats [3] provides a starting point for this work.

This chapter first presents the proposed method for determining the optimum number of grid blocks and the verifications of the method by fine grid numerical simulations and analytical calculations.

The second objective of this study was to investigate the effect of oil saturation prior to gas injection on the development of multi-contact condensing/vaporizing miscibility when physical dispersion was included. Under the influence of physical dispersion, the minimum miscibility pressure (MMP) is no longer a pure thermodynamic property of the reservoir oil for the injection gas at the reservoir temperature. In addition, it will be affected by flow parameters such as phase mobilities. To what extent the minimum miscibility conditions are affected by current oil saturation in the presence of dispersion is an open question and has not been addressed in the literature. The effect may be important for designing miscible gas floods for gas condensate reservoirs and for oil reservoirs at the

[1]Optimum means that the minimum number of grid cells to be used in simulations still yielding accurate simulation results.

tertiary development phase, where the oil saturations usually are low prior to gas injection.

The equation for selecting grid block size (Δx) and timestep size (Δt) intended for first-contact miscible displacement was extended for 1D multi-contact miscible gas injection processes. A complication encountered has been the instability in the calculated oil production performance when the timestep size was too large. Therefore, a second equation for determining the number of grid cells was given based on a smaller value of the ratio of the product of timestep size and pore velocity (u = $\frac{v}{\phi}$) to grid block size – CFL [4,5] number (CFL = $\frac{\Delta t \cdot u}{\Delta x}$). We found that CFL = 0.1 generally avoided numerical instability for multi-contact displacement calculations in this study. The CFL number may vary from problem to problem. In this method, the number of grid cells is calculated based on the pre-selected CFL number, and the timestep size is then calculated based on the Δx and the CFL number.

Physical dispersivities were emulated using the second equation for Δx and Δt in the simulation models for 1D multi-contact displacement, which enabled us to study the impact of oil saturation on the development of miscibility with the inclusion of physical dispersion.

For a depleted petroleum reservoir where gas and oil coexist, we studied the impact of relative permeability on miscibility for the 1D near-miscible displacement.

Several authors [6, 7] have reported the development of an oil bank for gas condensate reservoirs undergoing miscible or near-miscible gas injection, when C/V miscibility mechanism [8] exists. As discussed in Chapter 1, we found that this is general for all saturated gas-oil reservoirs undergoing enriched gas injection.

As used for the study presented in Chapter 1, Sensor [9] also was used to perform numerical simulations in this study. IMPES formulation was selected.

Section 2.2 presents the proposed equation for determining the optimum number of grid cells for 1D first-contact miscible displacements and verifications of the proposed method by numerical simulations and analytical calculations.

Section 2.3 presents the simulation results showing the effect of oil saturation prior

to gas injection on the development of miscibility for a 1D multi-contact displacement. First, the equation for calculating grid block and timestep sizes for representing physical dispersivity is presented. Then, the simulation results are presented for simulation models initialized with different oil saturations at different levels of dispersivity.

Section 2.4 summarizes this chapter, presenting conclusions and recommendation from this study.

The derivations of the first proposed equation is given in Appendix B at the end of the thesis.

2.2 First-Contact Miscible Displacement

This section presents the equation for calculating the optimum number of grid cells for simulating 1D first-contact miscible displacements. The proposed equation was then verified by analytical calculations and fine grid simulations. Simulation runs using different grid cell and timestep sizes to represent the same value of physical dispersivity were performed. The produced tracer concentrations of the effluent were compared and analyzed. Analytical calculations also was conducted and the results were compared with simulation results.

2.2.1 Governing Equations

This subsection reviews governing equations quantifying numerical dispersion in numerical reservoir simulations using single-point upstream mobility weighting and IMPES formulation. We considered 1D unit-mobility single-phase displacements in this subsection. The two fluids (displacing and displaced) had equal viscosity and density and were assumed to be incompressible. Lantz [10] gives the following equation for numerical dispersion:

$$D_n = 0.5u(\Delta x - u\Delta t), \tag{2.1}$$

where D_n stands for numerical dispersion coefficient.

Numerical dispersivity α (= $\frac{D_n}{u}$) is defined by the following equation:

$$\alpha = 0.5(\Delta x - u\Delta t). \tag{2.2}$$

To ensure a positive timestep size, the following equation must be satisfied:

$$\Delta x > 2\alpha. \tag{2.3}$$

It is clear that, to obtain a dispersion-free displacement, the timestep Δt must equal $\frac{\Delta x}{u}$.

From Eq. (2.2), for a given pore velocity u and dispersivity α, timestep size Δt can be calculated by the following equation:

$$\Delta t = \frac{\Delta x - 2\alpha}{u}. \tag{2.4}$$

Conveniently, a dimensionless Peclet number often is used to represent dispersivity for a porous medium. Neglecting molecular diffusion, the Peclet number is defined as:

$$N_{pe} = \frac{L}{\alpha}, \tag{2.5}$$

where N_{pe} denotes Peclet number and L is the characteristic length of the porous medium – the distance from the injector to the producer.

From Eqs. (2.3) and (2.5), it follows that the upper limit on the number of grid cells is:

$$N_{max} = \frac{N_{pe}}{2}. \tag{2.6}$$

Sensor allows an input of CFL number for timesteping. Under the assumptions made in this subsection, the CFL can be expressed by:

$$CFL = \frac{u\Delta t}{\Delta x} = \frac{\Delta x - 2\alpha}{\Delta x}. \tag{2.7}$$

CFL number should not exceed unity because $\alpha \geq 0$ and CFL = 1 results in zero numerical dispersion.

The length of the mixing zone where injectant concentrations range from 0.1 to 0.9 is denoted by L_m. It is a function of the core length L, the Peclet number and pore volumes (PVs) injected [11]:

$$L_m = 3.625L\sqrt{\frac{PV}{N_{pe}}}. \tag{2.8}$$

2.2.2 Optimum Number of Grid Blocks

Eq. (2.2) implies that the grid block size could be chosen arbitrarily for an injection rate and an emulated dispersivity, and the timestep size can be calculated by this equation. In fact, if the grid block is too large, the timestep size must also be large based on Eq. (2.4). This may result in too few timesteps to properly describe the concentration profile[2], and the resulting concentration curve may not be physically correct. On the other hand, if the grid block size is chosen too small, the simulation will require too many timesteps that are unnecessary, and the computing resource will be wasted.

To properly predict the concentration curve of the produced injectant, it is important to allow a certain level of resolution of data points, especially for the dispersive front of the curve. Our method of obtaining the resolution is to request a certain number of timesteps for the mixing zone where the injectant concentrations range from 0.1 to 0.9 at *one* PV injected. As long as this portion of the curve is well-defined, a smoothly continuous concentration curve is guaranteed.

For a given n and a Peclet number, the number of grid cells N can be calculated using the following equation; the derivations of the equation are given in Appendix B.

$$N = \frac{1}{\frac{2}{N_{pe}} + \frac{3.625\sqrt{\frac{1}{N_{pe}}}}{n}}, \tag{2.9}$$

[2]The curve of the produced injectant concentrations versus pore volume injected.

where n denotes the number of timesteps for defining the mixing zone where injectant concentrations range from 0.1 to 0.9 at one PV injected. Note that when n approaches infinity, N approaches the upper limit N_{max}.

Δx is then calculated by:

$$\Delta x = \frac{L}{N}. \tag{2.10}$$

The constant timestep size Δt is determined by Eq. (2.4).

This approach finds the optimum number of grid blocks and timestep size for the simulation model, ensuring the desired resolution for defining the injectant concentration curve and optimal computing costs.

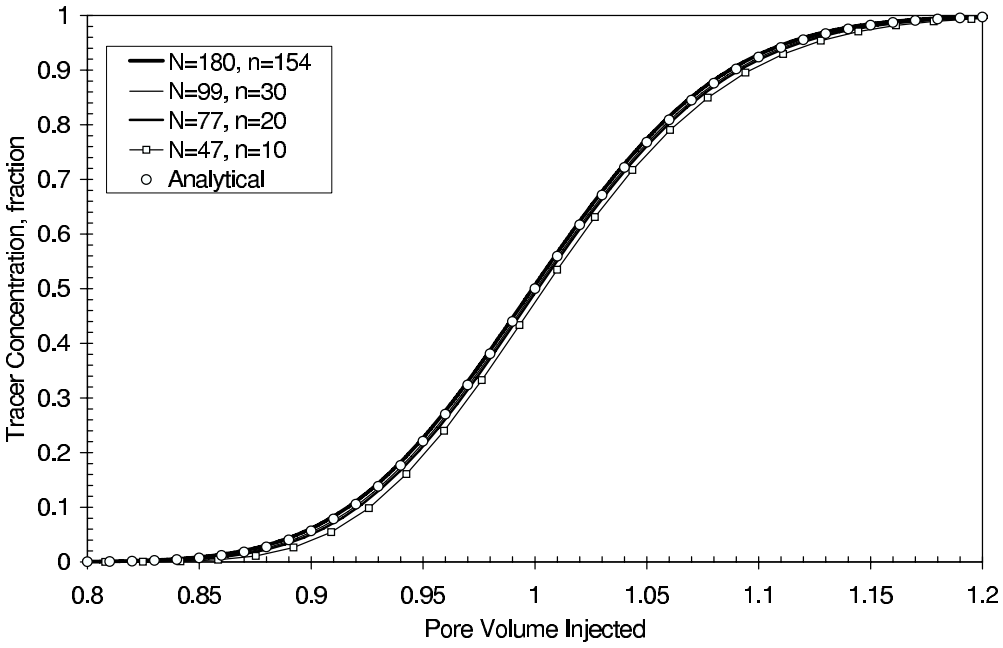

Figure 2.1: Comparison of the produced tracer concentrations of the runs emulating a physical dispersivity of 0.20 cm for a core of 90 cm long (N_{pe} = 450), 100% saturated with water, and undergoing water plus tracer injection.

2.2.3 Verification of the Proposed Equation

Analytical calculation and numerical simulation for a series runs for a core plug were performed to verify the proposed method. The simulated core initially was 100% saturated

Table 2.1: GRID BLOCK AND TIMESTEP SIZES AND CPU COMPARISON.

N	n	Δx cm	Δt days	CFL	CPU second
180	154	0.50	0.0328	0.20	0.95
99	30	0.91	0.0167	0.56	0.16
77	20	1.17	0.0252	0.66	0.12
47	10	1.91	0.0497	0.79	0.08

with water undergoing water (with tracer) injection. The water was assumed to be incompressible. The length of the core was 90 cm, Δy = Δz = 30.48 cm, porosity ϕ = 0.35, physical dispersivity α = 0.20 cm, and N_{pe} = 450. The pore velocity was set to 30.5 cm/d. The core was simulated using different numbers of grid cells ranging from 47 to 180, and the produced tracer concentration curves were compared and analyzed.

Analytical equation for calculating tracer concentrations as a function of pore volumes injected for such a system also exists, Coats et al [2]. We used Eq. (4) in that paper for the analytical calculations. The equation is:

$$C = \frac{1}{2} erfc(\frac{1 - PV}{2\sqrt{\frac{PV}{N_{pe}}}}), \tag{2.11}$$

where C refers to concentration, normalized to 1.0 for initial injected tracer concentration.

Figure 2.1 shows the tracer concentration curves of several simulation runs and the analytical results. The run with 99 grid cells generated 30 timesteps for concentrations from 0.1 to 0.9 at one pore volume injection. The run with 77 cells provided 20 timesteps for concentrations from 0.1 to 0.9 at one pore volume injection. The run using 47 cells resulted in 10 timesteps for tracer concentrations ranging from 0.1 to 0.9 at one pore volumes injected. These runs reproduced the results of the analytical calculations and the predictions of the fine-grid run using 180 grid cells, corresponding to 154 timesteps describing the mixing zone. The figure indicates that it is sufficient to use 47 grid cells (n = 10) in the simulation model for this problem. The CPU time of this run was less than one-tenth of that of the fine-grid run (using 180 grid cells) in this study, as shown in Table 2.1.

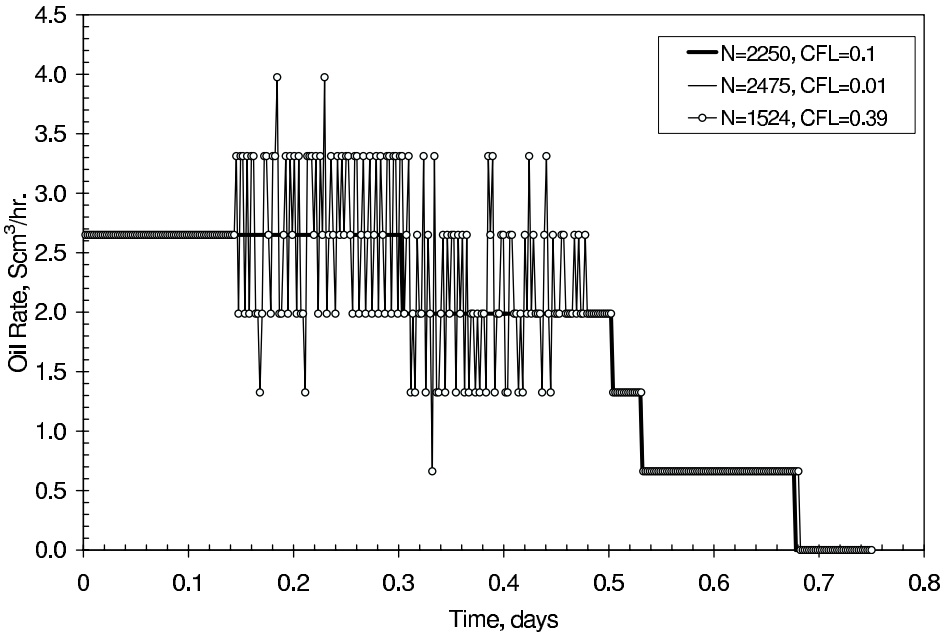

Figure 2.2: Performance of oil rate for the runs using different CFL numbers. Different CFL numbers imply different numbers of grid cells and different timestep sizes for a constant dispersivity of 0.3 cm.

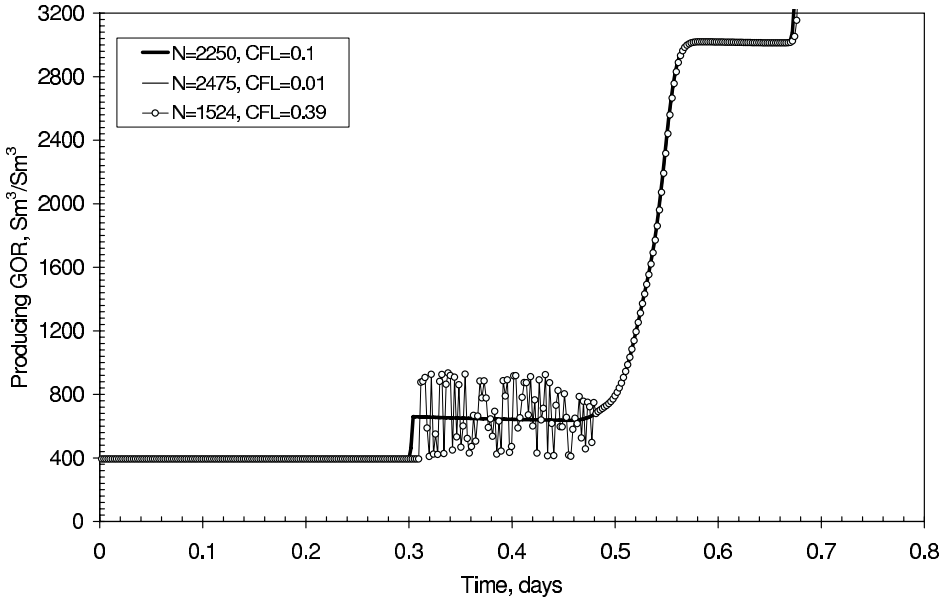

Figure 2.3: Performance of producing GOR for the runs using different CFL numbers. Different CFL numbers imply different numbers of grid cells and different timestep sizes for a constant dispersivity of 0.3 cm.

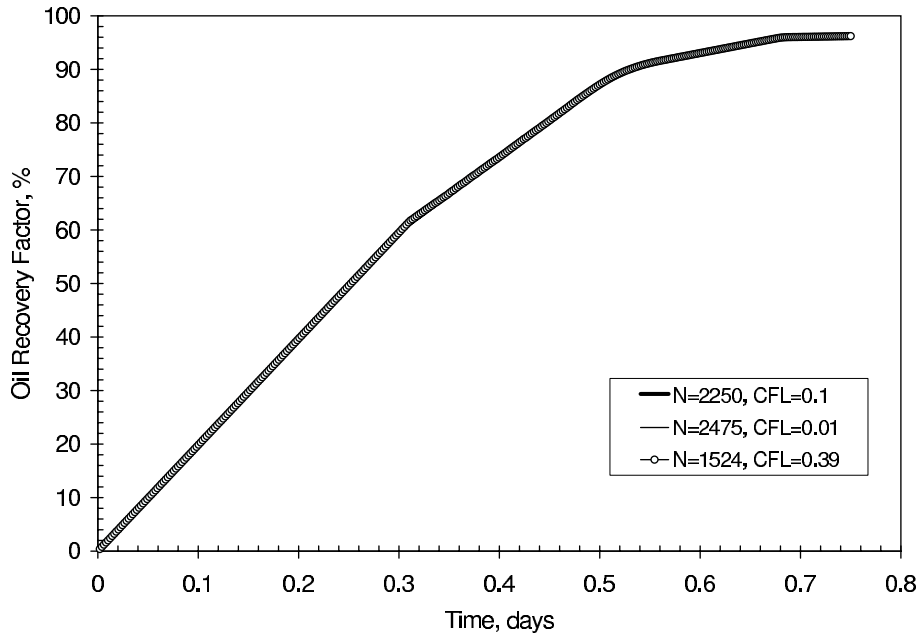

Figure 2.4: Performance of oil recovery for the runs using different CFL numbers. Different CFL numbers imply different numbers of grid cells and different timestep sizes for a constant dispersivity of 0.3 cm.

2.3 Multi-Contact Miscible Displacement

This section presents the equations for representing physical dispersion and simulation results for 1D multi-contact miscible displacement. For first-contact miscible displacement, equations Eqs. (2.9), (2.10), and (2.4) provide a basis for an accurate representation of the physical dispersivity through numerical simulations. For a multi-contact miscible process where a two-phase region exists, e.g. multi-contact oil displacement by gas, we assume that these equations still provide reasonable approximation[3] of dispersivity as the two-phase region usually is limited in size compared with the distance between the injector and producer.

For multi-contact miscible processes, when CFL = 0.39 (calculated bases on the equation for first-contact miscible for n = 200 and α = 0.3 cm, N_{pe} = 300) was used for the same core discussed in Subsection 2.3.2, but initialized with 100% oil undergoing gas

[3]To our knowledge, no accurate method exists for quantifying two-phase flow dispersivity. It therefore is impossible to verify the accuracy of the approximation.

injection, it was found that the performance of oil production rate and the producing gas-oil ratio were erratic, as shown in Figures 2.2 and 2.3. Figure 2.4 shows that the oil recoveries were not influenced.

To achieve a stable and smooth production performance, a reduction in the CFL number was required. We found that CFL = 0.1 normally resulted in non-erratic performance for the problem studied. In this study, we therefore used a constant CFL number of 0.1 for simulating the multi-contact process. We also are aware that this number may be problem dependent. Some investigators [12] have used a value of 0.05 in their studies.

2.3.1 Determination of Grid and Timestep Sizes

Again, starting with Eq. (2.2), if we divide the equation by Δx and multiply it by L on both sides, we will get the following equation after some simple manipulation:

$$N = \frac{L}{2\alpha}(1 - CFL). \tag{2.12}$$

CFL remains the same definition as defined in Eq. (2.7). The timestep size is calculated based on the pre-selected CFL number by:

$$\Delta t = \frac{\Delta x}{u} CFL. \tag{2.13}$$

2.3.2 Description of Simulation Models

Tests on a 1D multi-contact miscible gas-oil displacement were simulated for a 15.24 m long slimtube. The reservoir fluid was characterized by a 9-component SRK [13] equation of state (EOS) model. Viscosities were calculated by LBC [14] viscosity correlation. Tables 1.1 to 1.3 give parameters of the EOS model and the viscosity correlation coefficients. The four-stage separator conditions are given in Table 1.5.

An oil was chosen such that its bubblepoint pressure equals its dispersion-free condensing/vaporizing minimum miscibility pressure (C/V MMP) with the injection gas at the

Table 2.2: COMPOSITION OF THE RESERVOIR OIL AND INJECTION GAS.

N_c	Oil mol-fraction	SepGas mol-fraction
CO_2	0.03239	0.03956
C_1N_2	0.58706	0.73799
C_2	0.085194	0.10375
C_3C_4	0.082157	0.08911
C_5C_6	0.028004	0.01509
C_7C_9	0.055141	0.01294
$C_{10}C_{13}$	0.037048	0.00147
$C_{14}C_{29}$	0.069985	0.00009
C_{30+}	0.023012	0.00000
Sum	1.0	1.0

reservoir temperature of 141 °C. The dispersion-free C/V MMP was 381.3 bara at the reservoir temperature, calculated by a PVT program based on a multi-cell algorithm – PhazeComp [15]. Hoier [16] confirmed that this program is capable of calculating unbiased dispersion-free MMPs, provided that the EOS model describes key compositional effect properly. Composition of the reservoir oil is given in Table 2.2, together with the composition of the injection gas (SepGas). The reservoir pressure was kept at the dispersion-free C/V MMP during displacement.

Note that the dispersion-free C/V MMP is a *thermodynamic* property of the reservoir oil and independent of flow parameters such as relative permeability or fluid mobilities. However, when dispersion is included, we found that the oil saturation prior to gas injection affects the development of miscibility. In this study, we focused on the impact of oil saturation prior to gas injection on the developed miscibility with the presence of physical dispersivity.

Different values of dispersivity were assumed ranging from 15.2 to 0.03 cm and emulated in the numerical simulations. The number of grid cells and the size of the timesteps calculated by Eqs. (2.12) and (2.13) are given in Table 2.3.

The simulation models were initialized with different values of oil saturation and equilibrium gas prior to gas injection; no water was present in these models. Different rel-

Table 2.3: GRID AND TIMESTEP SIZES USED IN THE SIMULATIONS.

α cm	N_{pe}	N	Δx cm	Δt days	CFL
15.24	100	45	33.87	1.11e-3	0.1
3.00	500	225	6.77	0.22e-3	0.1
1.50	1000	450	3.39	0.11e-3	0.1
0.30	5000	2250	0.68	0.022e-3	0.1
0.15	10000	4500	0.34	0.011e-3	0.1
0.11	13333	6000	0.25	0.083e-3	0.1
0.03	50000	22500	0.07	0.002e-3	0.1

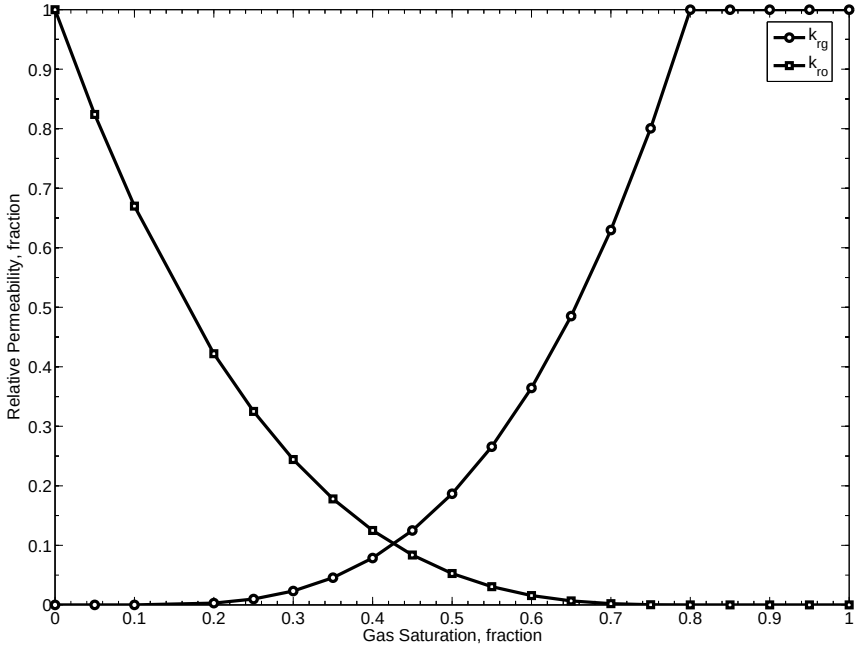

Figure 2.5: Gas-oil relative permeability curves.

ative permeability curves were used to evaluate the oil mobility effect on the development of miscibility. Fluid pore velocity was assumed to be 30.48 m/d, corresponding to 1 PV injection at 0.5 days.

The permeability of the slimtube was 10 Darcy, resulting in negligible pressure drop over the slimtube. The porosity of the slimtube was assumed to be 0.2. A set of Corey [17] type relative permeabilities (rock curves) was used with the saturation exponents for oil and gas of 3 and unity endpoint relative permeabilities. Figure 2.5 shows these relative permeability curves for gas-oil displacement. All the simulation runs used a residual oil saturation of 0.2 except otherwise stated. The critical gas saturation was assumed to be 0.1.

The gas injector was completed in the first grid cell (1, 1, 1) and the producer was put in the last grid cell (N, 1, 1). A fixed injection rate was used and the producer was put on bottom-hole flowing pressure (BHFP) control, so that a constant reservoir pressure was always maintained.

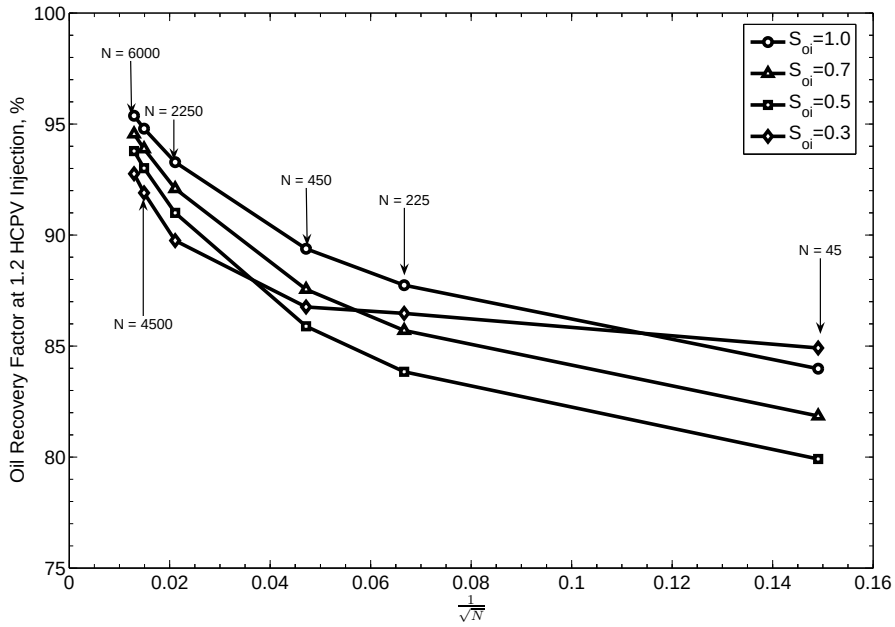

Figure 2.6: Simulated oil recovery factors at 1.2 PV of separator gas injected. Rock curves with S_{org} = 0.2 were used in the simulations. For the corresponding Peclet numbers, refer to Table 2.3.

2.3.3 Effect of Oil Saturation on Developed Miscibility

This subsection presents simulation results for models with different initial[4] oil saturations at different levels of dispersion.

Figure 2.6 shows the oil recovery factors at 1.2 PV injection for models initialized with S_{oi} = 1.0, 0.7, 0.5 and 0.3. These initializations represent different degrees of mobility for the liquid phase. The figure shows a common feature, i.e. all the curves are upward-concave. Meaningful linear extrapolation should start from N = 2250 ($\frac{1}{\sqrt{N}}$ = 0.021) for these initializations. Then a near-100% dispersion-free oil recovery can be obtained at the thermodynamic C/V MMP for all these cases, regardless the value of initial oil saturation. This figure also shows that linear extrapolation based on recoveries of runs with too high (e.g. $\alpha > 0.30$ cm, $\frac{1}{\sqrt{N}} > 0.021$) dispersivity can easily lead to an overestimate of MMP.

The oil recoveries of the runs N $<$ 2250 ($\frac{1}{\sqrt{N}} > 0.021$) and S_{oi} = 0.3 are higher than those of the runs $S_{oi} > 0.3$ are simply because the oil recovery from the vapor phase dominated when an immiscible displacement was predicted.

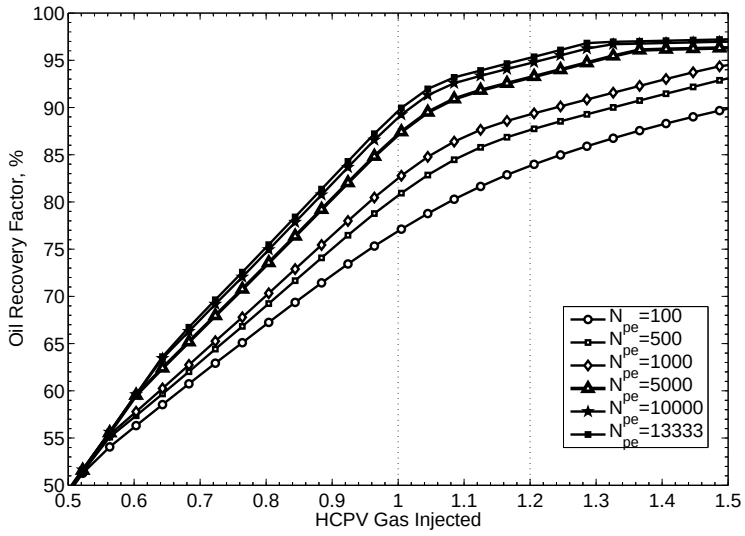

Figure 2.7: Simulated oil recovery factors versus pore volumes injected. S_{oi} = 1.0; rock curves with S_{org} = 0.2 were used in the simulations. For the number of grid cells used, refer to Table 2.3.

[4]Initial in this chapter refers to oil saturation prior to gas injection.

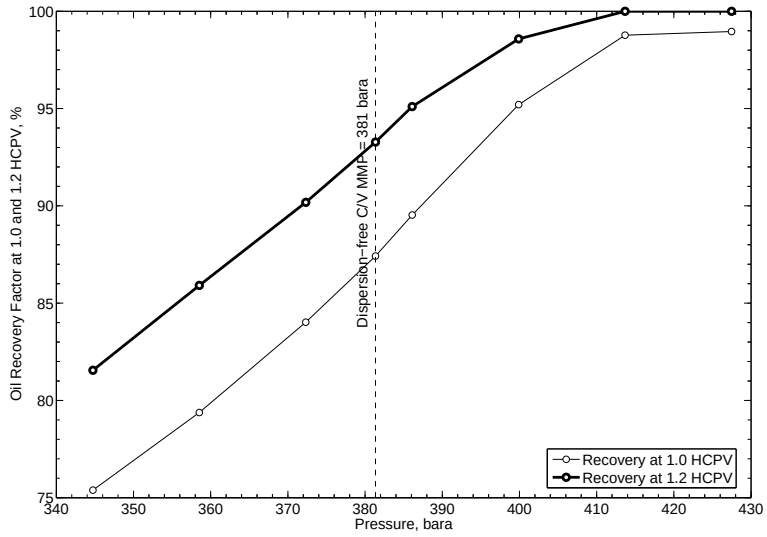

Figure 2.8: Simulated oil recoveries at 1.0 and 1.2 PV injected versus displacement pressure. The emulated physical dispersivity was 0.3 cm. N =2250, S_{oi} = 1.0, and S_{org} = 0.2. Rock curves were used in the simulations.

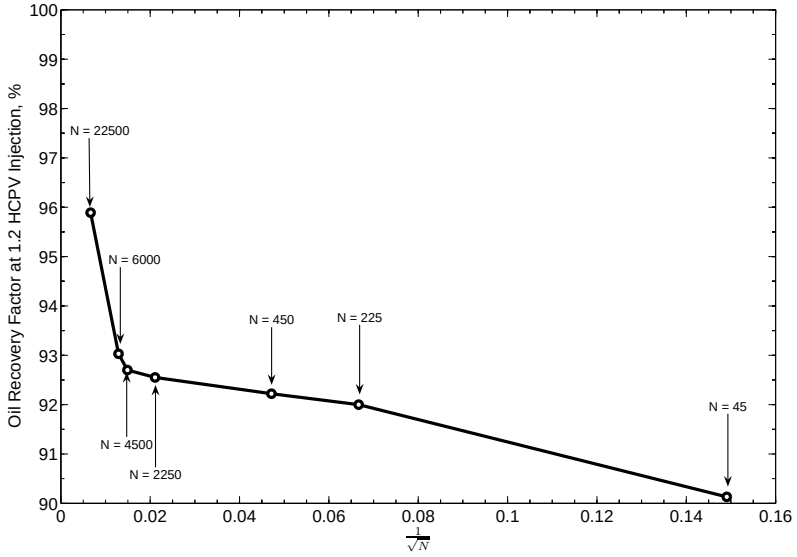

Figure 2.9: Simulated oil recovery factors at 1.2 PV of separator gas injection. S_{oi} = 0.2 = S_{org}. Rock curves were used in the simulations. For the corresponding Peclet numbers, refer to Table 2.3.

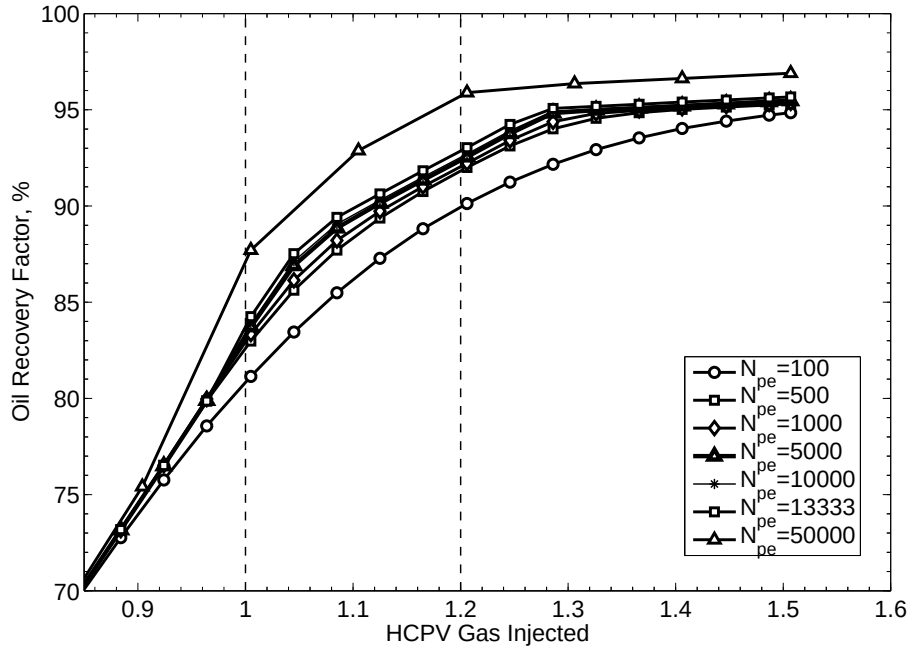

Figure 2.10: Simulated oil recoveries versus PV injected. S_{oi} = 0.2 = S_{org}. Rock curves were used in the simulations. For the number of grid cells used, refer to Table 2.3.

Figure 2.7 shows the simulated oil recoveries versus pore volumes injected for the model initialized with 100% oil. The oil recovery increases with increasing Peclet number or decreasing dispersivity. In the lab, for a 100% oil-saturated slimtube with a realistic level of physical dispersivity of 0.30 cm or N_{pe} = 5000, the expected recovery at 1.2 pore volumes injected will be about 93% at the thermodynamic MMP.

Figure 2.8 shows simulated oil recoveries at 1.0 and 1.2 PV of gas injected for a slimtube having a physical dispersivity of 0.3 cm and initialized with 100% oil. The number of grid cells used was 2250. Oil recoveries continue to increase at displacement pressures higher than the dispersion-free C/V MMP.

Figure 2.9 shows the simulated oil recoveries at 1.2 PV of gas injected of the runs initialized with S_{oi} = 0.2, equal to the residual oil saturation of the gas-oil relative permeability curves. It indicates that the starting point for a meaningful linear extrapolation may be N = 6000 ($\frac{1}{\sqrt{N}}$ = 0.013 and α = 0.11 cm) for this system. Then the extrapolated dispersion-free recovery will be 100% at the C/V MMP. In the lab, however, for a slimtube

experiment with a physical dispersivity of $<$ 0.30 cm, the expected oil recovery at 1.2 PV would only be 92.5%. Figure 2.10 shows the simulated oil recoveries versus PV injected for these initializations. Even for the run with N_{pe} = 50000, the recovery curve has yet to flatten out at 1.2 PV injected.

For the model initialized with 5% oil saturation, i.e. $S_{oi} < S_{org}$, the overall oil recoveries of all the simulation runs were close to 100% even at high dispersivity levels. The curve (recovery versus $\frac{1}{\sqrt{N}}$ curve) did not show the upward-concave feature. Oil recoveries from the vapor phase dominated the behavior of the recovery curve. However, the near-100% overall recovery did not imply a miscible displacement of oil by injection gas in these cases.

Due to the fact that the simulated oil recoveries were overall recoveries from both liquid and vapor phases, the overall oil recovery at 1.2 PV injected might not be a clear indication of developed miscibility between the injection gas and reservoir oil. Difference in densities of liquid and vapor at reservoir conditions might be more indicative for assessing miscibility.

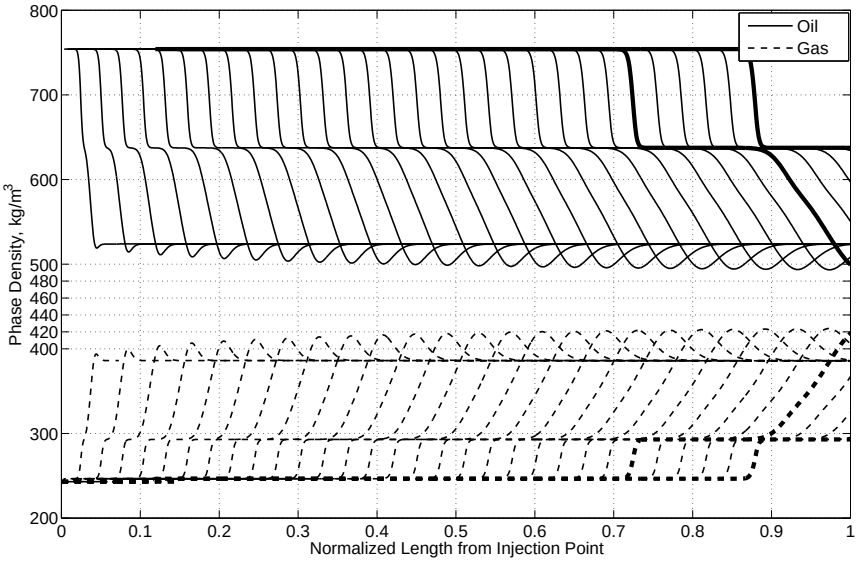

Figure 2.11: Snapshot of phase densities at different pore volumes injected for the run S_{oi} = 1.0 and N = 2250. Rock curves with S_{org} = 0.2 were used in the simulations.

For a fixed level of dispersion, e.g. N_{pe} = 5000 (α = 0.30 cm and N = 2250), runs initialized with different oil saturations showed different closeness to miscibility during the displacement. Figure 2.11 shows the snapshots of phase densities at different pore volumes of gas injected for the case that the initial oil saturation was unity. The snapshots were taken at every 0.04 PV injected. The thick lines represent phase densities at 1.0 and 1.2 PVs. Phase densities tended to converge during the first 0.5 PV injected and then stayed more-or-less constant.

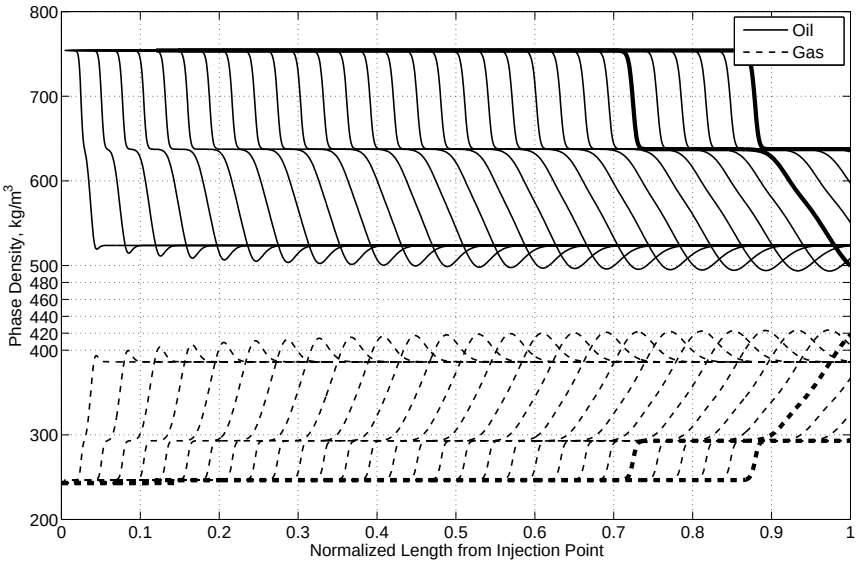

Figure 2.12: Snapshot of phase densities at different pore volumes injected for the run S_{oi} = 0.5, N = 2250. Rock curves with S_{org} = 0.2 were used in the simulations.

Figures 2.12 to 2.14 show the density snapshots for the runs initialized with 0.5, 0.3 and 0.2 oil saturations, respectively. The closeness to miscibility for the runs with S_{oi} = 1.0 and down to S_{oi} = 0.3 was quite similar though the difference in phase densities increased slightly for the run with S_{oi} = 0.3. For the run initialized with S_{oi} = 0.2, shown in Figure 2.14, the difference in phase densities was clearly greater than those of the above cases, indicating a less miscible displacement.

When we further reduced the oil saturation prior to gas injection to 5% in the model, immiscible displacement resulted at the same dispersion level. Figure 2.15 shows that the

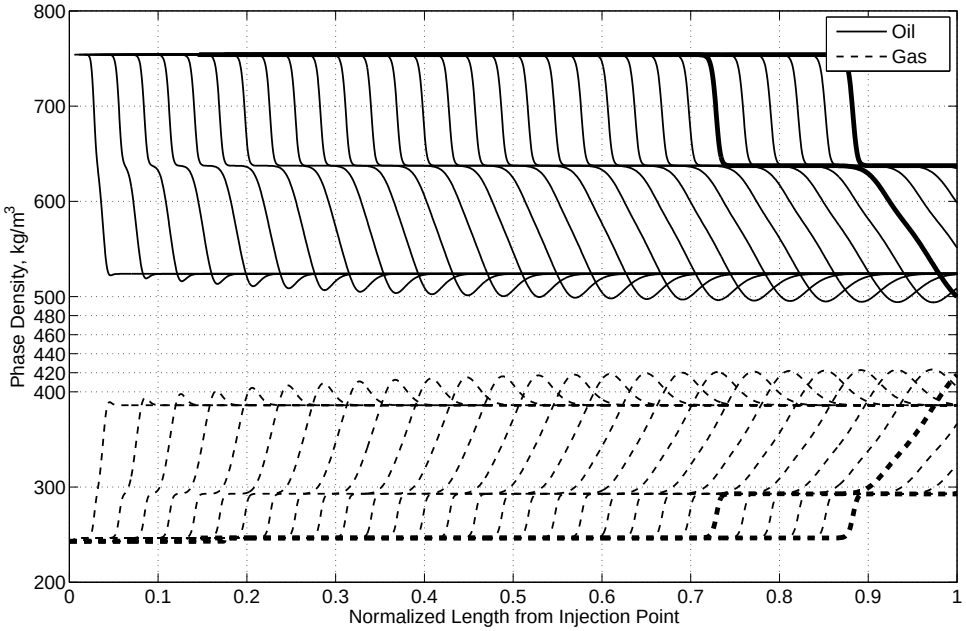

Figure 2.13: Snapshot of phase densities at different pore volumes injected for the run S_{oi} = 0.3, N = 2250. Rock curves with S_{org} = 0.2 were used in the simulations.

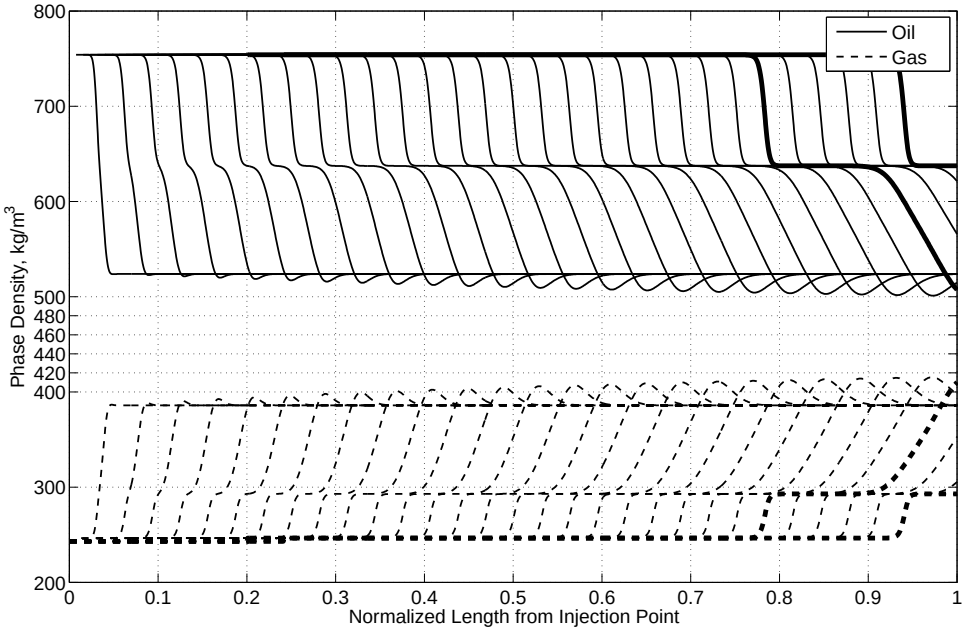

Figure 2.14: Snapshot of phase densities at different pore volumes injected for the run S_{oi} = 0.2, N = 2250. Rock curves with S_{org} = 0.2 were used in the simulations.

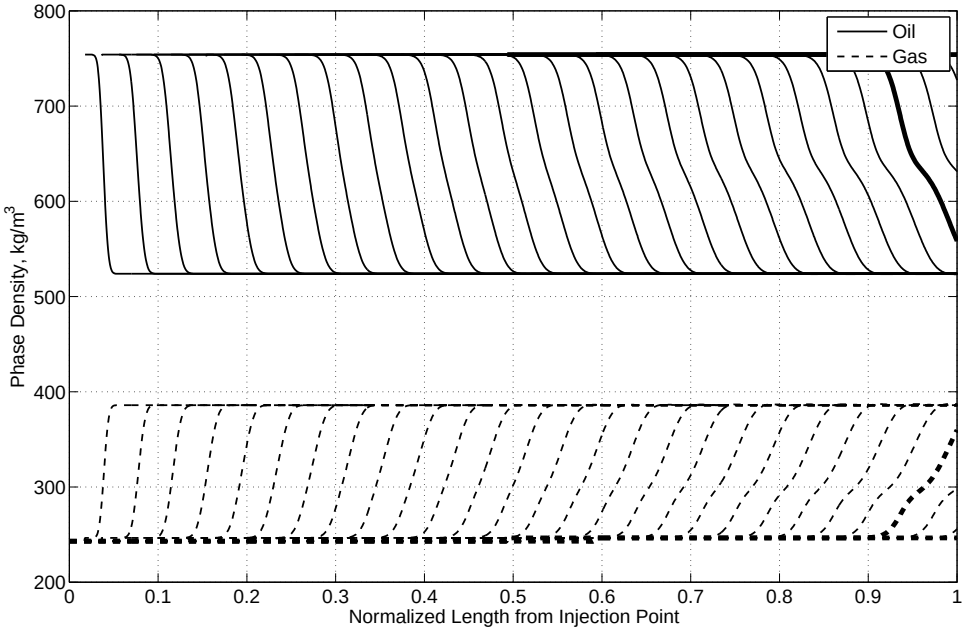

Figure 2.15: Snapshot of phase densities at different pore volumes injected for the run S_{oi} = 0.05, N = 2250. Rock curves with S_{org} = 0.2 were used in the simulations.

difference in densities remained the same as the initial equilibrium phase density difference. This also was observed for all the initializations at high levels of dispersivity. For example, When α = 15.24 cm and 45 grid cells ($\frac{1}{\sqrt{N}}$ = 0.149) were used, all the runs initialized with different oil saturations indicated an immiscible displacement. The difference in phase densities remained the same as that between the initial equilibrium phases. This also is indicated on the recovery curve in Figure 2.6.

The above figures of snapshots may only provide qualitative illustration on changes in phase densities along the slimtube during the displacement. Figure 2.16 shows the minimum difference in phase densities at 0.44 PV injected for the runs initialized with different values of oil saturations and gridded with different numbers of grid cells. The minimum difference in phase densities increased with increasing dispersivity for a fixed oil saturation prior to gas injection. For a fixed level of dispersivity, the minimum value of phase density difference decreased with increasing oil saturation up to 0.3. When the model initially

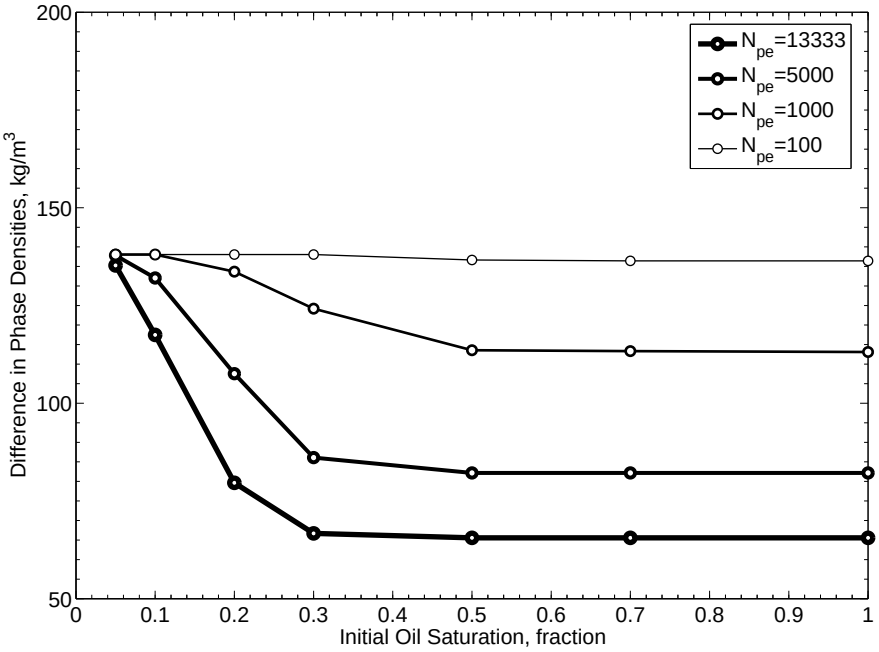

Figure 2.16: Minimum difference in phase densities at 0.44 PV injected for the runs initialized with different values of oil saturation and at different dispersivity levels. Rock curves with S_{org} = 0.2 were used in the simulations.

contained more than 30% oil prior to gas injection, the minimum difference in phase densities tended to be constant for a value of dispersivity. Miscibility becomes insensitive to oil saturation prior to gas injection.

2.3.4 Dispersion Effect on the Development of Oil Bank

A persistent feature for miscible gas injection in 1D models of gas condensate reservoirs is that an oil bank will build up during the displacement. The magnitude of the oil bank is greatly influenced by dispersion involved.

We show simulation results of cases that were initialized with 20% oil saturation and the oil initially had no mobility. These may be simulating a depleted gas condensate reservoir undergoing miscible or near-miscible gas injection. Figures 2.17 and 2.18 show the developed oil bank and the difference in phase densities for four runs at dispersion levels of 1.52, 0.30, 0.11, and 0.03 cm. At lower level of dispersion, the oil bank was more

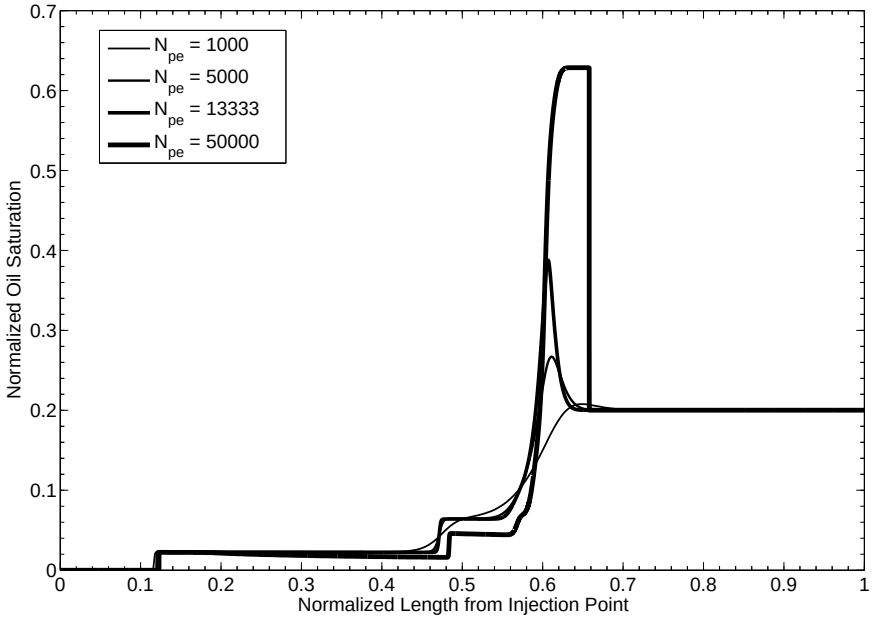

Figure 2.17: Oil bank development and magnitude of the oil bank at 0.6 PV for displacements with difference degrees of dispersion. S_{oi} = 0.2, S_{org} = 0.2, rock curves. For the number of grid cells used, refer to Table 2.3.

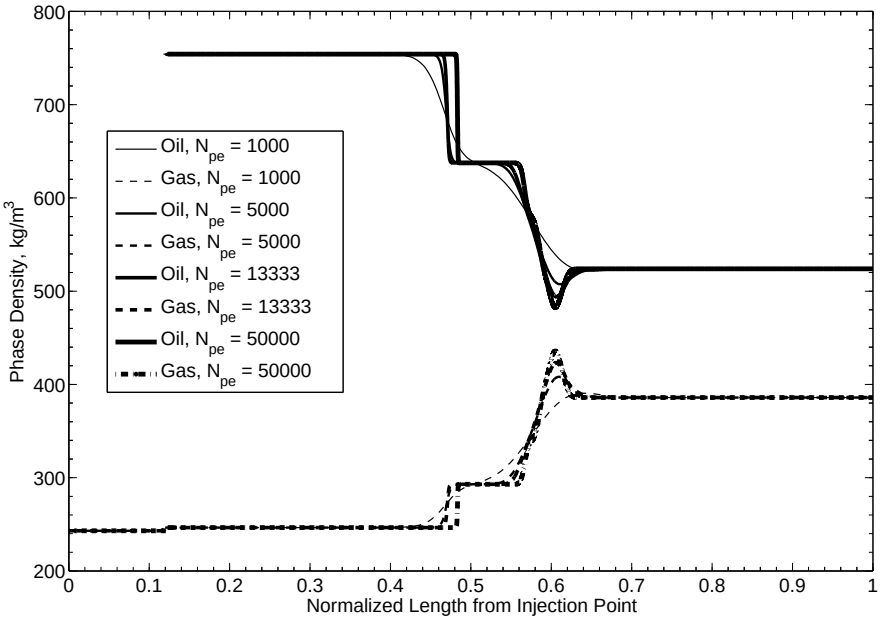

Figure 2.18: Difference in phase densities at 0.6 PV for runs with different degrees of dispersion. S_{oi} = 0.2, S_{org} = 0.2, rock curves. For the number of grid cells used, refer to Table 2.3.

developed in size and the difference in densities was small. It also is observed that the oil bank developed earlier. Oil recoveries also were higher when dispersivity was smaller.

2.4 Conclusions and Recommendation

To summarize, this study has led to the following conclusions:

1. A method for the optimum number of grid cells and timestep size for numerical simulation models has been proposed and verified for 1D first-contact miscible displacements. It ensures a smooth curve of recovery versus pore volumes injected at minimum computing cost.

2. For a 1D multi-contact displacement of oil by enriched gas where C/V mechanism exists:

   - Liquid phase composition dictates the C/V MMP. As long as the oil initially has certain mobility, initializations with different oil saturations should result in the same dispersion-free thermodynamic C/V MMP, provided that the extrapolation of recovery versus $\frac{1}{\sqrt{N}}$ is conducted properly.
   - Initializations with different oil saturations might require different starting points for a meaningful linear extrapolation for an estimate of dispersion-free recovery for defining an unbiased MMP on the recovery-pressure curve. Low initial oil saturation cases require low degree of dispersion as a starting point for linear extrapolation.
   - For a multi-contact miscible displacement to develop, some level of initial oil saturation and mobility might be required. Miscibility may never develop if initial oil saturation is too low even at very low dispersivities.

3. For the readiness of defining C/V MMP for gas condensate reservoirs undergoing miscible gas injection, we recommend that the reservoir be initialized with 100% oil. This might involve least work for a proper estimate of a dispersion-free C/V MMP.

2.5 Nomenclature

D_n	=	numerical dispersion coefficient
k_{rg}	=	relative permeability to gas, fraction
k_{ro}	=	relative permeability to oil, fraction
L	=	distance from the injector to the producer, m
N	=	number of grid cells
N_c	=	name of component
N_{max}	=	maximum number of grid cells
N_{pe}	=	Peclet number, dimensionless
PV	=	pore volume, dimensionless
S_{oi}	=	oil saturation prior to gas injection, fraction
S_{org}	=	residual oil saturation to gas, fraction
u	=	pore velocity, m/day
v	=	superficial velocity or Darcy velocity, v=uϕ, m/day
α	=	dispersivity, cm
Δt	=	timestep size, days
ϕ	=	porosity, fraction
Δx	=	grid block size in x direction, m
Δy	=	grid block size in y direction, m
Δz	=	grid block size in z direction, m

2.6 References

1. Perkins, T.K., and Johnston, O.C.: “A Review of Diffusion and Dispersion in Porous Media,” SPEJ (March 1963) 70-84.

2. Coats, K.H., Whitson, C.H. and Thomas, L.K.: “Modeling Conformance as Dispersion,” paper SPE 90390, presented at the 2004 SPE Annual Technical Conference and Exhibition, Houston, TX, Sept. 26-29.

3. Coats, K.H.: “Notes on Dispersion 2004,” Personal communication.

4. Coats, K.H.: “IMPES Stability: The Stable Step,” paper SPE 69225, presentation at the 2001 SPE Reservoir Simulation Symposium, Houston, TX, Feb. 11-14.

5. Coats, K.H.: “IMPES Stability: The CFL Limit,” paper SPE 66345, presentation at the 2001 SPE Reservoir Simulation Symposium, Houston, TX, Feb. 11-14.

6. Hoier, L. and Whitson, C.H.: “Miscibility Variation in Compositionally Grading Reservoirs,” SPEREE, Feb. 2001, 36-41.

7. Jessen, K., Orr, F.M., Jr.: “Gas Cycling and the Development of Miscibility in Condensate Reservoirs,” paper SPE 84070 presented at the 2003 SPE Annual Technical Conference and Exhibition, Denver, Oct. 5-8.

8. Zick, A.A.: “A Combined Condensing/Vaporizing Mechanism in the Displacement of Oil by Enriched Gases,” paper SPE 15493 presented at the 1986 SPE Annual Technical Conference and Exhibition, New Orleans, Oct. 5-8.

9. Coats K.H.: “Sensor Users Manual, March 2001,” Coats Engineering, Inc., website: `www.coatsengineering.com`.

10. Lantz, R.B.: “Quantitative Evaluation of Numerical Dispersion (Truncation Error),” SPEJ (Sept. 1971) 315.

11. Coats K.H.: Personal communication.

12. Johns, R.T., Fayers, F.J., and Orr, F.M. Jr.: “Effect of Gas Enrichment and Dispersion on Nearly Miscible Displacements in Condensing/Vaporizing Drives,” SPE ATS (1993) 2, No. 2,26-34.

13. Soave, G.: “Equilibrium Constants for a Modified Redlich-Kwong Equation of State,” Chem. Eng. Sci. (1972), 27, 1197-1203.

14. Lohrenz, J., Bray, B. G., and Clark, C. R.: “Calculating Viscosities of Reservoir Fluids From Their Compositions,” J. Pet. Tech. (Oct. 1964) 1171-1176; Trans., AIME, 231.

15. Zick A.: Zick Technologies, PhazeComp model, Website: `www.zicktech.com`.

16. Hoier, L.: “Miscibility Variations in Compositionally Grading Petroleum Reservoirs,” Thesis for Dr.ing, Norwegian University of Science and Technology, NTNU, Nov. 1997.

17. Brooks R.H. and Corey A.T.: “Properties of Porous Media Affecting Fluid Flow,” Journal of Irrigation and Drainage Division, 6, 1966.

Appendix A: SPE 90379 Miscible Gas Injection in Under-saturated Gas-Oil Systems

Is not included due to copyright

Appendix B: Derivation of Equation 2.9 for Optimum Number of Grid Cells

Based on Eq. 2.8, length of mixing zone in which injectant concentrations range from 0.1 to 0.9 at one PV injected:

$$l_{m1} = 3.625L\sqrt{\frac{1}{N_{pe}}}. \tag{B-1}$$

It can also be expressed as:

$$l_{m1} = nu\Delta t = n(\Delta x - 2\alpha). \tag{B-2}$$

Combining equations Eq. (B-1) and Eq. (B-2) and divided by L on both sides,

$$3.625\sqrt{\frac{1}{N_{pe}}} = n(\frac{\Delta x}{L} - \frac{2\alpha}{L}) = n(\frac{1}{N} - \frac{2}{N_{pe}}). \tag{B-3}$$

Solving for N, we will get the final equation:

$$N = \frac{1}{\frac{2}{N_{pe}} + \frac{3.625\sqrt{\frac{1}{N_{pe}}}}{n}}. \tag{B-4}$$